DISSERTATION

AN INVESTIGATION OF SYNAPTIC VESICLE DOCKING AND PRIMING AND A PROPOSED METHOD FOR QUANTITATIVELY MEASURING BOTH IN *DROSOPHILA* USING ELECTRON TOMOGRAPHY

Submitted by

Jasmin A. Twiggs

Department of Biomedical Sciences

In partial fulfillment of requirements

For the Degree of Doctor of Philosophy

Colorado State University

Fort Collins, Colorado

Fall 2023

Doctoral Committee:

Advisor: Noreen Reist

Frederic Hoerndli
Kim Hoke
Michael Tamkun

ABSTRACT

AN INVESTIGATION OF SYNAPTIC VESICLE DOCKING AND PRIMING AND A PROPOSED METHOD FOR QUANTITATIVELY MEASURING BOTH IN *DROSOPHILA* USING ELECTRON TOMOGRAPHY

The nervous system, as the body's command center, plays a crucial role in cellular communication within the brain and between the brain and other body systems. Neurons, the individual cellular units, transmit electrical information and communicate with other cells through neurotransmitter release in response to electrical stimuli. Chapter 1 introduces the foundational concepts of neuronal structure and function and delves into the mechanisms underlying neurotransmitter release. Special attention is given to the neuromuscular junction (NMJ), a well-studied chemical synapse crucial for muscle movement. The synaptic vesicle cycle is introduced, with particular emphasis on docking and priming. The significance of active zones, specialized sites for efficient signal transmission, and their associated structural components are underscored. Synaptotagmin, a pivotal protein in calcium-triggered vesicle fusion, is discussed with emphasis on its C_2B polylysine motif. Throughout the chapter, the utility of *Drosophila* as a model system for studying synaptic processes, particularly at the NMJ, is emphasized. In sum, Chapter 1 provides the foundational knowledge essential for comprehending the intricate cellular and molecular facets of synaptic communication within the nervous system, serving as a precursor to subsequent chapters' investigations.

Chapter 2 examines synaptotagmin's C_2B polylysine motif and its role in synaptic vesicle docking at the *Drosophila* NMJ. It explores the polylysine motif’s potential involvement in

endocytosis, demonstrates an unaffected interaction with AP-2, and uses electron microscopy to find no significant changes in vesicle distribution. The findings suggest that the reduced neurotransmitter release in the polylysine mutant is likely due to an impairment in vesicle priming.

Chapter 3 introduces a method for studying synaptic vesicle docking and priming in *Drosophila*, using electron tomography. I address the limitations of conventional electron microscopy and underscore the need for higher-resolution techniques to assess molecular structures that mediate physiological processes. Chapter 3 also emphasizes the significance of the contact area between docked vesicles and the presynaptic membrane as a correlate of vesicle priming. The protocol, expected results, and key considerations are discussed. The methods presented in Chapter 3 offer a promising approach for understanding synaptic processes.

In Chapter 4, I discuss key considerations for when standard electron microscopy can be used for assessing vesicle docking. Then, I discuss how the electron tomography method presented in Chapter 3 could not only confirm the results found in Chapter 2, that the synaptotagmin C_2B polylysine motif is not implicated in vesicle docking but could also be used to directly test the mutant's role in priming. Specific aims for future studies on the synaptotagmin polylysine mutation in *Drosophila* are presented, potential results and interpretations are discussed. Finally, I showcase interesting, unpublished findings from electron tomograms I have taken at the *Drosophila* NMJ and discuss their potential significance.

Keywords: synaptic vesicle, docking, priming, electron microscopy, electron tomography, synaptotagmin, polylysine motif, active zone, ultrastructure, active zone material

ACKNOWLEDGMENTS

As my time at Colorado State University comes to a close, I have thought about the many people who have impacted my life and made it possible for me to achieve this doctorate. First and foremost, I would like to thank my parents. Now that I am a parent myself, I appreciate the sacrifices you endured to provide the best life you could for me. Your sacrifices enabled me to succeed in school from a young age, develop ambitions not possible for yourselves, and, most importantly, taught me to lead life with my heart. I thank you for all the love and support you've provided over the years and hope this dissertation, and my love, serve as evidence that your sacrifices weren't for nothing.

Second, I would like to thank my advisor, Dr. Noreen Reist. You accepted me into your lab with open arms and allowed me to pursue a project that I found exciting. During difficulties with research, the pandemic, or life in general, you remained a source of encouragement. I am happy to have found a lab family.

Thank you to my committee: Dr. Fred Hoerndli, Dr. Kim Hoke, and Dr. Michael Tamkum for your time and feedback throughout my graduate career. You all have been a source of knowledge and advice throughout the past 7 years.

I would also like to thank the past and present members of the Reist Lab. Mallory Shields, you took me under your wing and mentored me during my early years of grad school. I will always appreciate our bachelor nights, the adventure that was Cold Spring Harbor, and the numerous laughs we shared. Matt Bowers, you were a constant source of support and always a pleasant, easy-going comrade. Morgan Litchford, Kaitlin Reed, Vincent Elias, and Andrew Bollegar, you all have made the lab environment feel less like work and, overall, a more

enjoyable place to be.

A special thanks to Brittany Runyan for doing all that you do. You have helped me navigate through graduate school, encouraged me to persevere even when it felt impossible, provided reassurances countless times, given advice on all things from school and career to life and motherhood. You have significantly enriched my time at CSU, and I am forever grateful for you.

My friends and family have provided unwavering love and support throughout my graduate career. Of note, my Grandma Maria, Grandma Sandra and Papa Ray, cousin D'Armani, and best friends Escarolyn, Steve, Laura. You've helped me realize my goal of obtaining a PhD and have inspired me throughout. I love you all immensely. Kayla, Sebastian, Landon, and Mimi are friends who've become family. Thank you for your love. Tyler W., Lauren Y., Taylor Z., Alice M., Jane T., Emily C., Amy J., your friendship has been nourishing in ways I could never fully describe.

Thank you to my funding sources that made all this work possible. My time as a graduate student has been supported by a National Science Foundation Bridge to Doctorate Fellowship and a National Science Foundation Graduate Research Fellowship Program Fellowship. I would also like to thank the Molecular, Cellular and Integrative Neurosciences program for supporting me throughout my first year and the Department of Biomedical Sciences for supporting me throughout my time at CSU.

Finally, to my husband Aaron, thank you for loving and supporting me over the last 5 years. Starting a family while working towards my doctorate has not been easy. However, the family that we've created and the dream that we share is my biggest motivator in life. I love you.

DEDICATION

I dedicate this dissertation to my children, Quinn and Joey. Nothing in life will ever be more fulfilling than getting to love you unconditionally. I hope that one day you will recognize this accomplishment for what it is: a demonstration that with some ambition, hard work, support from loved ones, and perseverance, you can do anything you set your mind to. I can't wait to witness all the things you accomplish in life.

I love you always. - Mommy

TABLE OF CONTENTS

LIST OF FIGURES

CHAPTER 1: INTRODUCTION

Nervous System Overview

The nervous system is the body's command center, it is responsible for cellular communication not just within the brain but also between the brain and the rest of the bodies' systems. The neuron is the individual cellular unit whose function is to transmit electrical information and to communicate with other cells by releasing a neurotransmitter in response to an electrical stimulus. Neuronal function is supported by a canonical cellular structure comprising a cell body, dendrites, an axon, and axon terminals. The neuronal cell body is the metabolic center of the neuron and contains the typical organelles (e.g., nucleus, mitochondria, etc.). The cell body and dendrites together comprise the main input region of the neuron that receive electrical or chemical signals from other neurons. The axon of a neuron is a long, tail-like structure that protrudes from the cell body at a location called the axon hillock. Axons are responsible for the propagation of electrical information from the cell body toward the next cell in the circuit. Axon terminals are the site at which a neuron transmits electrical or chemical signals with a nearby cell.

A synapse is a specialized contact site where a neuron communicates with the next cell in circuit. Of the two predominant types of synapses in the nervous system, electrical and chemical, my work focuses on chemical synapses. Chemical synapses are comprised of a presynaptic neuron, a post-synaptic cell and a synaptic cleft or space between the two cells. At a chemical synapse, neurotransmission utilizes small, diffusible chemicals, called neurotransmitters, that are packaged into synaptic vesicles to relay signals from the pre- to the post-synaptic cell. Depolarization of the presynaptic axon terminal of a neuron opens voltage-gated Ca^{2+} channels

causing an influx of Ca^{2+}. This increase in Ca^{2+} triggers synaptic vesicles to fuse with the presynaptic membrane at specialized sites called active zones (Couteaux & Pecot-Dechavassine, 1970; Dreyer et al., 1973; Südhof, 2012). Vesicle fusion releases the neurotransmitter into the synaptic cleft where it binds to receptors on the post-synaptic cell. Transmitter binding to the receptors results in an electrical signal in the postsynaptic cell, thus propagating intercellular communication.

Neuromuscular Junction

The neuromuscular junction (NMJ) is a well characterized, easily accessible chemical synapse between the nerve and the muscle. Without this specialized synapse, nerves and muscles would fail to communicate with the speed and efficiency required for movement. During this fast and efficient communication, the muscle is activated by a Ca^{2+}-dependent release of neurotransmitters from nerve terminals. In most NMJs, acetylcholine (ACh) is the primary neurotransmitter. However, *Drosophila* NMJs utilize the neurotransmitter glutamate. The neuromuscular junction is a fail-safe synapse. Its stability and reliability ensure the continuation of neurotransmission. This is especially remarkable given that only 2-5% of docked synaptic vesicles fuse given a stimulus. Due to their fail-safe nature and ease of accessibility, the NMJ is has been studied extensively in several species, including frogs and *Drosophila*, using light-microscopy, electron microscopy and electrophysiology (Slater, 2015; Atwood and Karaunanithi, 2002). The NMJ is therefore one of the (if not the) most highly characterized synapses in the nervous system.

The Synaptic Vesicle Cycle Overview

Following vesicle fusion, the vesicle membrane and associated proteins must be retrieved to refill the synaptic vesicle pool. This cycle is diagramed in Figure 1-1. Synaptic vesicles are

actively loaded with neurotransmitters (Fig. 1-1a) and trafficked to the presynaptic membrane where they are docked, or held in contact with the presynaptic membrane, at active zones by specific molecular interactions (Figs. 1-1b–d) (Sudhof, 2004; Szule and Coorssen, 2003, Bennet et al., 1992). The synaptic vesicles are held in contact with the presynaptic membrane by the Soluble NSF-Attachment protein REceptor complex, commonly referred to as the SNARE complex (Zhang et al., 2022; Sutton et al., 1999). The SNARE complex comprises a vesicle-associated SNARE protein (vSNARE) and target-membrane associated SNARE proteins (tSNAREs) (Schiavo et al., 1997; Sauvola and Littleton, 2021). At the synapse, the vSNARE is synaptobrevin while the tSNAREs are SNAP-25 and syntaxin (Schiavo et al., 1997; Szule and Coorssen, 2003). When the synaptic vesicle is trafficked to the presynaptic membrane, synaptobrevin winds together with SNAP-25 and syntaxin on the target membrane to form a coiled-coil structure (Sutton et al., 1998; Karmaker et al., 2019). The extent of contact between a docked vesicle and the presynaptic membrane is postulated to be mediated by the force generated by the SNARE complex (Jung et al., 2016; Szule and Coorssen, 2003; Szule et el., 2003; Zhou et al., 2015; Zhou et al., 2017). The forces generated by the SNARE complex will be elaborated upon later in this chapter. A vesicle is considered to be fusion-competent or maximally-primed (Fig. 1-1d) when its area of contact with the presynaptic membrane is largest (Jung et al., 2016). At the active zone, voltage-gated calcium channels open upon depolarization allowing an influx of calcium along its electrochemical gradient into the nerve terminal (Atlas, 2022; Chapman, 2018; Sudhof, 2013) (Fig. 1-1e). The calcium then binds to the synaptic vesicle protein, synaptotagmin, which triggers the fusion of maximally primed vesicles with the presynaptic membrane (Fig. 1-1f) (Brose et al., 1992; Bommert et al., 1993; Geppert et al., 1994; Desai et al., 2000; Mackler et al., 2002), releasing their neurotransmitter contents into the synaptic cleft.

Following fusion, the vesicle membrane merges with the presynaptic membrane (Fig. 1-1g), before clathrin mediated endocytosis retrieves the vesicle membrane and associated proteins back into the presynaptic terminal (Fig. 1-1h) (Heuser and Reese, 1973; Jorgensen et al., 1995; von Poser et al., 2000; Haucke at el., 2000; Sudhof, 2004; Littleton, 2006). Newly endocytosed vesicles are then either directly reloaded with neurotransmitter (Fig. 1-1a) or trafficked to endosomes for recycling (Fig. 1-1i) (Barker et al., 1972; Ceccarelli et al., 1973; Heuser and Reese, 1973; Koenig and Ikeda, 1996; Pyle et al., 2000; Richards et al., 2000; Sudhof, 2004), thus completing the synaptic vesicle cycle. It is important to note that deficits anywhere in the synaptic vesicle cycle could result in synaptic dysfunction. As this dissertation investigates specific interactions postulated to mediate synaptic vesicle docking, priming, and recycling, these steps are described in more detail below.

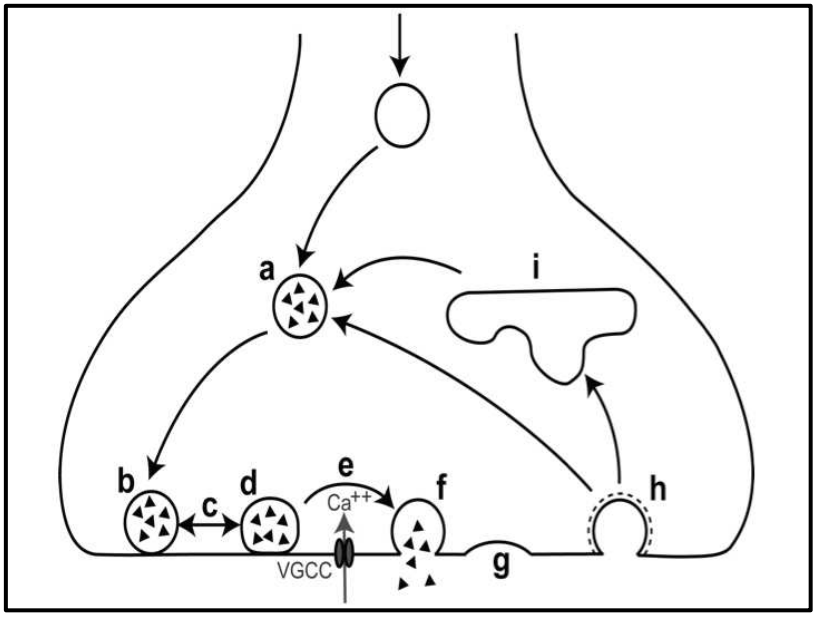

Figure 1-1. *Illustration of the Synaptic Vesicle Cycle*

Each highly-orchestrated step is represented by a letter: vesicles are loaded with neurotransmitter (a), then trafficked to the presynaptic membrane where they dock (b–d) and undergo a reversible process of synaptic vesicle priming (c) with some vesicles minimally-primed (b) and some maximally-primed (d). Then, when Ca^{2+} influx via voltage-gated Ca^{2+} channels (VGCC) occurs (e), maximally-

primed vesicles then fuse with the presynaptic membrane (f). After fusion, the vesicular membrane collapses (g) into the plasma membrane, is then endocytosed (h) and either refilled (a) or trafficked to endosomes (i). Figure adapted, with permission, from Bowers, 2020.

Synaptic Vesicle Docking and Priming

Formation of the SNARE complex is required for synaptic vesicle docking and priming. Vesicle trafficking to the presynaptic membrane, brings vSNAREs and tSNAREs close enough to form an energetically favorable coiled-coil structures that pull the vesicle closer and closer to the presynaptic membrane as the SNAREs zipper together (Abdulreda et al., 2009; Bai et al., 2004; Maximov et al., 2009; Sauvola and Littleton, 2021). The steps following the assembly of the SNARE complex, particularly vesicular docking and priming, are currently debated in the field.

In recent literature, the definition of synaptic vesicle docking varies. Some authors define a docked vesicle as any vesicle that is tethered to the presynaptic membrane by an electron-dense filament (Chang et al., 2018; Neher and Brose, 2018; Fernandez-Busnadiego et al., 2013; Sudhof, 2013, Slater, 2015). In contrast others define a docked vesicle as any vesicle whose membrane is in contact with the presynaptic membrane (Tan et al., 2022; Jung et al., 2016; Szule et al., 2012; Hammarlund et al., 2007; Slater, 2015). This distinction primarily differs between imaging techniques and is usually defined within articles. For the purposes of this dissertation, docked vesicles will generally be considered to be those whose membrane is in physical contact with the presynaptic membrane. However, close attention should be paid to Chapter 2, wherein the definition of docking differs slightly based on limitations in the microscopic techniques used.

Synaptic vesicle priming is typically defined as the point at which a vesicle becomes "fusion competent" or is most likely to fuse upon a calcium influx (Szule and Coorssen, 2003; Sudhof, 2004). However, the morphological nature of vesicular priming is unclear. Some

researchers hypothesize that priming is a stepwise process where irreversible molecular interactions form to stabilize the SNARE complex and further reduce the energy threshold for fusion (Sudhof, 2013; Imig et al., 2014). Using this logic, only those vesicles that have undergone tightly-regulated priming steps would fuse upon calcium influx. On the other hand, recent work conducted in the McMahan lab suggests that synaptic vesicle priming is a dynamic equilibrium, or reversible process, between force-generating interactions among the fusion machinery and repulsive forces between molecular components (Jung et al., 2016; Lin et al., 2022). Under the McMahan lab's "variable priming hypothesis", the priming state of any given docked vesicle can vary; and only vesicles with the highest area of contact between the vesicle and plasma membrane are considered to be in a "maximally-primed" state that can fuse upon a calcium influx. Bernard Katz had originally described a similar hypothesis in which "synaptic vesicles undergo frequent transient collisions with the axon membrane" during his Nobel Lecture in 1970. However, the notion was mostly abandoned by the field for a two-step docking-priming hypothesis (Sudhof, 2004; Slater, 2015). I will expand on the variable priming hypothesis later in this chapter, after I address ultrastructural analysis. In Chapter 3 of this dissertation, I present methods to assess vesicle docking and priming in *Drosophila* using the electron tomography techniques established by the McMahan lab in frog (Ress et al., 1999; Ress et al., 2004; Jung et al., 2016; Jung and Szule, 2017). Additionally, the methods I present in Chapter 3 could be used to directly test the function of a putative priming mutant of synaptotagmin, which I present later in this chapter and again in Chapter 2.

Synaptic Vesicle Endocytosis

Following exocytosis, synaptic vesicles are recycled through endocytosis, or the retrieval of vesicle membranes and their associated proteins into the synaptic terminal. This process of

continuous recycling of synaptic vesicles is essential for sustained neurotransmission (Hueser and Reese, 1973; Koenig and Ikeda, 1989; Gan and Watanabe, 2018). Endocytosis was first identified in the early 1970s (Barker et al., 1972; Ceccarelli et al., 1973, Heuser and Reese, 1973) and has been studied extensively using electron microscopy biochemistry and electrophysiology, in multiple model organisms (Sudhof, 2004; Littleton, 2006; Watanabe and Boucrot, 2017; Gan and Watanabe, 2018). To date, multiple modes of endocytosis have been identified: clathrin-mediated endocytosis, fast compensatory endocytosis, activity-dependent bulk endocytosis, ultrafast endocytosis, and kiss-and-run (Sudhof, 2004; Slater, 2015; Gan and Watanabe, 2018). However, clathrin-mediated endocytosis is thought to be the predominant mechanism of synaptic vesicle recycling. For that reason, I will only discuss clathrin-mediated endocytosis here.

During clathrin-mediated endocytosis, clathrin and its accessory proteins coat the membrane forming a vesicular invagination; dynamin then pinches off the neck of the invagination to cleave the newly-formed vesicle. In synapses, this process is highly regulated to ensure vesicles are specific in nature and contain all the lipids and proteins required for neurotransmission. For example, the clathrin adaptor protein, AP-2, has been proposed to retrieve synaptotagmin 1 during synaptic vesicle endocytosis (Zhang et al., 1994; Mizutani et al., 1997; Haucke et al., 2000; Jarousse et al., 2001). Synaptotagmin 1's role in endocytosis, through its interaction with AP-2, is elaborated upon later in this chapter, and assessed using standard electron microscopy in Chapter 2.

Active Zones

The term "active zone" was first coined in 1970 when scientists Couteaux and Pécot-Dechavassine identified a small, specialized portion of the presynaptic membrane, where electron-dense material could be seen directly adjacent to omega profiles of fusing synaptic

vesicles, captured by fixing frog neuromuscular junctions during stimulation (Couteaux and Pécot-Dechavassine, 1970). At typical synapses, the docking, priming, and fusion steps of the synaptic vesicle cycle occur at these specialized, active zone regions along the presynaptic membrane. Accordingly, the proteins required for the docking, priming and fusion steps of the synaptic vesicle cycle are highly concentrated at the active zone (Walter et al., 2018; Cano and Tabares, 2016; Sigrist and Schmitz, 2011). Further, the active zone region, within presynaptic terminals, precisely opposes post-synaptic specializations that permit post-synaptic cells to respond to the released neurotransmitter (Landis et al., 1988; Gundelfinger et al., 2000; Zhai and Bellen, 2004). The area surrounding the active zone is called the peri-active zone and is the location of synaptic vesicle endocytosis (Heuser and Reese, 1973; Cano and Tabares, 2016; Ackermann et al., 2015; Sudhof, 2012; Brodin and Shupliakov, 2006).

Although active zone structure varies depending on the organism and synapse type (see Active Zone Material below), active zones can almost universally be identified by their three distinct features: 1. the aggregation of electron dense material at the presynaptic membrane; 2. a tight cluster of synaptic vesicles; and 3. the presence of intramembranous particles.

The localization of intramembranous particles is a key attribute of active zones because they are generally believed to include the voltage-gated calcium channels which mediate calcium-triggered neurotransmitter release. Immunolabeling of voltage-gated calcium channels, at the NMJ of frogs and *Drosophila*, demonstrates that at least some of the intramembranous particles are voltage-gated calcium channels (Feeney et al., 1998; Fouquet et al., 2009). Notably, the proximity of voltage-gated calcium channels to synaptic vesicles that are closely associated with the presynaptic membrane: 1. explains the spatial-temporal efficacy of neurotransmission at the neuromuscular junction; and 2. could be used to identify the subpopulation of vesicles which

are fusion competent. For instance, at the *Drosophila* NMJ, intramembranous particles are present underneath the electron-dense T-bar where voltage-gated calcium channels have been localized by immunolabeling (Bruckner et al., 2017). If the intramembranous particles are in fact voltage-gated calcium channels, the docked synaptic vesicles located at the pedestal of the T-Bar, closest to the calcium-channels, are likely a part the primed vesicle population.

Active Zone Material

The electron-dense material localized at active zones, in association with docked synaptic vesicles, has been called "Active Zone Material" (AZM, Harlow et al., 1998; Ress et al., 2004; Nagwaney et al., 2009; Szule, 2021). It has also been referred to as presynaptic density or cytomatrix assembled at the active zone (CAZ, Gundelfinger and Dieck, 2000; Sigrist and Schmitz, 2011; Bruckner et al., 2012). Herein, the preferred term will be AZM.

The shape of the AZM varies depending on the organism and synapse type and can present as: (a) disc-like structures, as in the central synapses of vertebrates and the NMJ of *C. elegans*; (b) elongated structures resembling railroad ties as in the NMJ of frogs; (c) ribbon-like structures, as in some sensory neurons of vertebrates; and (d) specialized T-bar structures, as in the NMJ of *Drosophila* (Atwood and Karaunanithi, 2002; Hammarlund et al., 2007; Slater, 2015; Bruckner et al., 2015; Szule, 2022). For the purposes of this dissertation, the focus will primarily be on the elongated active zones in frog and the specialized T-bar active zones in *Drosophila* NMJs.

Despite the differences in AZM size and shape, presynaptic proteins that mediate docking, priming and fusion are highly conserved. However, experiments to identify protein components within the AZM have been limited to localization using antibodies, functional assessments based on genetic mutations, and protein-protein interactions (reviewed by Rizo and

Rosenmund, 2008; Sudhof and Rizo, 2011; Rizo and Sudhof, 2012; Sudhof, 2014; Rizo and Xu, 2015; Szule, 2021). The AZM comprises multiple classes of proteins required for protein scaffolding, vesicle trafficking, and coupling signal detection with vesicle fusion (see chapter 4).

Ultrastructural Analysis

Since physical interactions among presynaptic proteins are required for neurotransmitter release, determining the distribution of these proteins, and localizing specific protein-protein appositions within the AZM is required to test functional hypotheses regarding the molecular mechanisms of vesicle fusion. Due to the small size of the functional complexes (e.g., SNARE complexes are only ~12 nm in length, Sutton et al., 1998; Ernst and Brunger, 2003; Grushin et al., 2019) and the AZM structures connecting docked synaptic vesicles to the presynaptic membrane (e.g., pins are only ~13 nm in length, Jung et al., 2016), the resolution of standard electron microscopy (several 10's of nanometers in the z plane) is not sufficient to visualize the functionally significant structures. It is only with the relatively recent application of electron tomography that the ultrastructural organization of the macromolecular complexes within the AZM are beginning to be elucidated. Electron tomography involves taking many high-resolution micrographs, at varying degrees of tilt, of a single region-of-interest, within a single thin plastic section. The resulting tilt-series is then aligned, combined by averaging back-projections, and then reconstructed into a 3D virtual volume. In a 3D reconstructed volume, a given "virtual slice" within the volume can be between 2-3 orders of magnitude thinner than the "real" plastic section containing the tissue sample. For example, by applying electron tomography to 70 nm thin sections of a frog NMJ, the McMahan lab was able to obtain 3D reconstructions made up of "virtual" slices which were each only 0.5 nm thin. By doing so, they were able to obtain a spatial resolution of 2-3 nm within each reconstruction (Ress et al., 2004; Szule et al., 2015). This

increase in resolution allows for a much more detailed analysis of the synaptic ultrastructure than was ever previously possible. In Chapter 3 of this dissertation, I present methods of electron tomography at *Drosophila* NMJs, as established by the McMahan lab in frog. Within Chapter 3, I address the method's significance and potential implications. Below, the history and a current overview of AZM ultrastructural analysis using electron tomography will be presented.

The ultrastructural characterization of macromolecular complexes using electron tomography was initiated at the frog NMJ by the McMahan lab in 1998 (Harlow et al., 1998). By 2001, the McMahan lab was able to describe the architecture of the active zone within 15 nm from the presynaptic membrane at the frog's NMJ (Harlow et al., 2001). Within their tomograms, they characterize an active zone defined by two docked synaptic vesicles with AZM, protruding from the presynaptic membrane, between the docked vesicles. Harlow et al., 2001 further described the arrangement of the AZM which includes (a) A "beam" which runs along the presynaptic membrane between the two parallel rows of docked vesicles; (b) "ribs" which run parallel to, but separated from the presynaptic membrane, and connect the "beam" to vesicles on each side; and (c) "pegs" that connect "ribs" to macromolecules within the presynaptic membrane. Lastly, Harlow et al., 2001 describe their extended hypothesis which highlights that structural components of the AZM likely correspond to proteins such as calcium channels ("pegs"), SNAREs, syntaxin, and synaptotagmin ("ribs" and ""beams"). Their hypothesis that synaptic macromolecules comprise the beams, ribs, and pegs should be testable by combining their electron tomography methods with well-established procedures for localizing specific proteins. However, frogs are not amenable to genetic tagging, and immuno-tags introduce too much distance between the structure and the tag, so protein identification has not been possible.

In 1999 and then 2004, the McMahan lab published methods on automatic acquisition

and alignment of tilt images for electron microscopy and methods for generating high-resolution electron tomographic datasets, respectively (Ress et al., 1999; Ress et al., 2004). Using their established methods, the McMahan lab characterized the ultrastructure of the AZM, within 15 nm of the presynaptic membrane, at the mouse neuromuscular junction (Nagwaney et al., 2009). They found that although active zones at the mouse NMJ are much smaller than frog, there are similar structural components including beams, ribs and pegs which are localized adjacent to docked synaptic vesicles (Nagwaney et al., 2009). Although mice are a genetic model, further investigation to identify protein components of the AZM structures, in conjunction with electron tomography, has not been completed.

Since 2004, the McMahan lab has greatly expanded on their 3D renderings of frog NMJs, showing the structure of the AZM at 2 nm spatial resolution (see Fig. 1-2A). The structural characterization of the frog's AZM was expanded to include all discernable electron-dense material. Additional structures such as a "step", "spar", "mast", "boom", and "topmast" were identified as distinguishable, repeating structures that comprise the AZM [(See Fig. 1-2A,Szule et al., 2012) Note: lacking any information on the molecular constituents of each structure, they were assigned nautical names due to their association with "docked" vesicles]. Notably, they counted the occurrence of these structures within the AZM, and in relation to the vesicle face, and measured the average length and diameter of each structure. Further, Szule et al., 2012, identified the AZM structures at activated active zones and found that they were connected to omega figures, figures which are consistent with a vesicle fixed during fusion. This finding is vitally important to the hypothesis that the AZM is comprised of the synaptic proteins involved in vesicle exocytosis such as SNAREs, syntaxin, calcium channels and synaptotagmin.

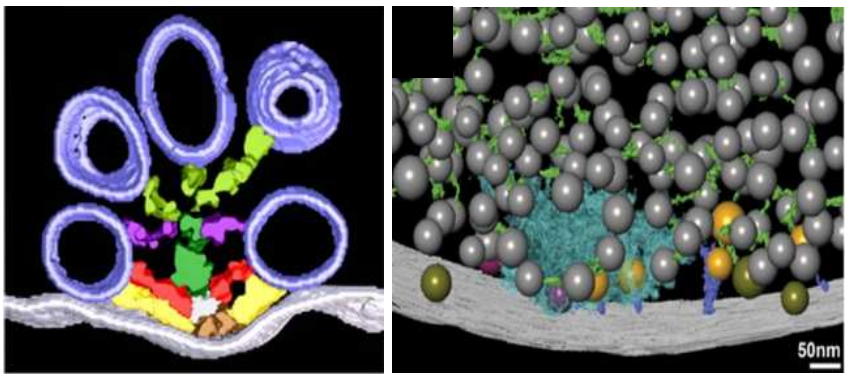

Figure 1-2. *Schematic 3D Reconstructions of the AZM at the Frog NMJ and Drosophila NMJ by Electron Tomography*

(A.) Frog: vesicles (blue spheres) and AZM (yellow, brown, white, green, red, and purple structures). (B.) *Drosophila*: vesicles (gray and gold spheres) are shown surrounding a convoluted AZM (light blue). Adapted from Szule et al., 2012 and Bruckner et al., 2017, respectively.

Many views of synaptic vesicles by standard electron microscopy and electron tomography rarely show electron-dense material within the vesicle lumen. By staining in acetone with freeze-substitution, Harlow et al., 2013, discovered intra-luminal densities within synaptic vesicles with a distinct, asymmetric, stereotyped appearance of macromolecular assemblies. Additionally, the stereotyped assembly of macromolecules assigns a polarity to the vesicles which revealed a systematic orientation of vesicles during trafficking, docking, priming and exocytosis (Harlow et al.,2013).

Unlike in the frog, synaptic electron tomography in other model organisms is not as advanced. As aforementioned, the ultrastructural analysis in mouse has defined similar macromolecular complexes within 15 nm of the presynaptic membrane using electron tomography. Conversely, electron tomography at the NMJ of *C. elegans* and *Drosophila* remains in its infancy. An extremely limited number of studies have accomplished high-resolution (<1 nm/pixel) electron tomography at the NMJ of *C. elegans* or *Drosophila*. For example, Stigloher et al., 2011 has examined the active zone material at the NMJ of *C. elegans* using electron

tomography. Their tomography revealed the AZM as a central dense projection within the active zone that connected to synaptic vesicles up to 100nm away from the presynaptic membrane (Stigloher et al., 2011). Although they were able to reconstruct high resolution tomograms, they were only able to achieve a spatial resolution of 4-5 nm: almost half the level of spatial resolution achieved in frog (2-3 nm, Ress et al., 2004; Szule et al., 2012; Harlow et al., 2013; Jung et al., 2016).

In *Drosophila*, Bruckner et al., 2017, have used electron tomography of NMJ active zone in 250 nm plastic sections. They were able to achieve virtual slices of 0.7 nm, however they did not comment on their spatial resolution, nor did they achieve sufficient resolution to render a clear 3D reconstruction of the active zone and its macromolecular structures (see comparison of Fig. 1-2B to Fig. 1-2A). They were able to segment, or outline the shape of, the AZM and surrounding synaptic vesicles in three-dimensions. However, the AZM segmentations present as an amorphous blob, with no discernable structural components (see Fig. 1-2B, Bruckner et al., 2017). As tomography in *Drosophila* is not yet as advanced as in frog, the organization of macromolecules comprising the AZM remains unknown. In Chapter 3, I present a method of electron tomography developed specifically to prepare *Drosophila* synapses for electron tomography with the 2-3 nm spatial resolution necessary to assess morphological relationships at the neuromuscular junction.

Morphological Docking and Priming

As aforementioned, the definition of docking varies depending on imaging techniques as well as the definition assigned by the lab in each study (Jung et al., 2016; Hammarlund et al., 2007; Reist et al., 1998; Stigloher et al., 2011; Kusick et al., 2023; Szule, 2022, Slater, 2015). Using standard electron microscopy, docked synaptic vesicles have been primarily defined as

those with little to no discernable gap between the vesicle and presynaptic membrane. Further, some studies define docked vesicles as only those which are in direct contact with the AZM and have no discernable gap between the vesicle and the presynaptic membrane. The definition of vesicle docking likely varies so much due to the resolution limitations of standard electron microcopy, varying thickness of plastic sections, and ultrastructure at a given AZ. I discuss key considerations, when using standard electron microscopy, to assess vesicle docking more in detail in Chapter 4.

More recently, the use of high-resolution electron tomography has provided an arguably more reliable assessment, and therefore a more consistent definition, of docked synaptic vesicles. This has been accomplished due to the high (down to as little as 2-3 nm) spatial resolution which allows for the characterization of structures within a sub-volume of tissue. In 2016, Jung et al., used a novel assessment of vesicle docking by measuring and comparing 1. the vesicle's membrane thickness (VM) away from the area of contact with the presynaptic membrane; 2. the presynaptic membrane's thickness (PM) away from the area of contact; and 3. the combined membrane thickness of the VM and PM (VM-PM) at the area of contact. Using these measures, Jung et al., 2016 were able to confirm whether vesicles in contact with the AZM were in physical contact with the presynaptic membrane or "docked". Further, Jung et al., 2016, demonstrate that only when frog NMJs are fixed *during* nerve stimulation, did they find that some docked vesicles possess a combined VM-PM membrane thickness that was less than the simulated sum of the VM and PM away from the contact site. In other words, the vesicle and plasma membranes were in a state of hemifusion at the area of contact. This study not only provided the first quantitative measure of vesicle docking but also morphological captured membranes in the process of fusing at the NMJ.

Using the same methods of electron tomography, Jung et al., 2016 also established a novel way to morphologically assess vesicle priming by measuring the area of contact between the vesicle and plasma membrane. When terminals were fixed at rest, they found that the extent of VM-PM contact area, for docked SVs, exhibits a normal frequency distribution (330 ± 150 nm^2). Moreover, when terminals were fixed during stimulation, there was, (a) A leftward shift in the normal distribution of the VM-PM contact area (230 ± 120 nm^2), and (b) a new population of vesicles that exhibited an even larger contact area (750- 850 nm^2) which was not observed at rest. Notably, some vesicles with a VM-PM contact areas >450 nm^2, and all vesicles with a VM-PM contact areas >650 nm^2, exhibited hemifusion as described above (Jung et al., 2016).

Lastly, to analyze whether variation in the extent of contact was attributable to variable force exerted towards the presynaptic membrane in resting terminals, Jung et al., measured the eccentricity of docked and undocked vesicles, and the length of AZM filaments (ribs, pins, pegs) in relation to their associated docked vesicle. When analyzing eccentricity, they found that docked vesicles exhibited an increase in eccentricity compared to that of undocked vesicles, and the long axis of docked vesicles was preferentially oriented to the AZM and presynaptic membrane, whereas undocked vesicles did not exhibit any common orientation (Jung et al., 2016). The orientation and eccentricity of docked vesicles is consistent with the hypothesis that force is being applied to docked vesicles to pull them toward the presynaptic membrane. In addition, the orientation and eccentricity of docked vesicles in Jung et al., 2016, supports the findings of vesicle orientation assessed by intra-luminal structures by Harlow et al. 2013. After analyzing AZM filament lengths, Jung et al., found that proximal rib and pin

lengths, and the distance from the rib-VM and pin-VM connection sites to the presynaptic membrane, all negatively correlated with VM-PM contact area and eccentricity consistent with the hypothesis that the ribs, pegs and pins are the structures supplying the force to pull docked vesicles toward the presynaptic membrane (Jung et al., 2016).

Taken together, the work done by the McMahan lab outlines a variable priming hypothesis that suggests how variable AZM-mediated forces could regulate synaptic vesicle docking and priming. Under this hypothesis, once a vesicle is docked, or held in contact with the presynaptic membrane, forces generated by macromolecular components of the AZM (such as ribs, pegs and pins) impose variable fusion probability on each vesicle. In other words, vesicles are in a state of dynamic equilibrium and can be minimally-primed, maximally-primed, or anywhere in between. Maximally-primed vesicles would be those which exhibit a large VM-PM contact area, are eccentric, oriented towards the AZM and presynaptic membrane and have the greatest amount of force generated from AZM (assessed by AZM length and distance correlations). Thus, the McMahan Lab has provided a morphological way to measure variable priming.

Now, using high resolution electron tomography, a quantitatively confirmed definition of docking, and new way to think of and measure priming, we can start assessing functional relationships at the NMJ. In Chapter 3, I combine all these methods, for the first time in *Drosophila*, and set the groundwork necessary to test a putative priming mutant, a synaptotagmin C_2B polylysine mutant, which I discuss below and later in Chapter 2.

Synaptotagmin

Synaptotagmin was first identified in 1981 as a 65kDa protein, or p65, localized to synaptic vesicles in neurons and neuroendocrine cells (Matthew et al. 1981). Shortly after its

identification, p65 was sequenced and renamed to synaptotagmin. The primary protein sequence revealed an N-terminal intravesicular domain, a transmembrane domain, and two cytoplasmic C2 domains: C_2A and C_2B connected by a linker domain (Perin et al., 1990 & Perin et al. 1991). C2 domains are highly-conserved calcium and phospholipid-binding domains found in a variety of proteins that consist of an eight-stranded beta-sandwich with a calcium-binding pocket and membrane-binding loops at one end (Sutton et al., 1995, Sutton et al., 1999, Nalefski et al., 1996, Nalefski et al., 2001).

There are 17 isoforms of synaptotagmin that have been identified. However, most studies focus on synaptotagmin 1 and 2, because they are the isoforms responsible for triggering fast, synchronous neurotransmitter release (Wolfes and Dean 2020). Synaptotagmin 1 and 2 are located on synaptic vesicles and are low-affinity Ca^{2+} sensors with fast membrane disassembly kinetics (Hui et al., 2005 & Wolfes and Dean, 2020). Ca^{2+} binding to both C_2A and C_2B domains of synaptotagmin 1/2 is required to trigger fast, synchronous, SNARE-mediated synaptic vesicle fusion events (Jorgensen et al., 1995; Nonet et al., 1993; Ullrich et al., 1994; Fukuda et al., 1995; Nalefski and Faulke, 1996; Mackler et al., 2002; Nishiki et al., 2004; Llinas et al., 2004; Shin et al., 2009). In mammals, synaptotagmin isoform expression varies depending on the location in the nervous system. Synaptotagmin 1 is predominantly expressed in the cerebral hemispheres. Whereas synaptotagmin 2 is predominantly expressed in the brainstem and spinal cord (Ullrich et al., 1994, & Marqueze et al., 1995). In *Drosophila*, which lacks synaptotagmin 2, synaptotagmin 1 is responsible for fast, synchronous synaptic vesicle fusion events throughout the nervous system (DiAntonio et al., 1993; Littleton et al., 1993; Lloyd at al., 2000; Chapman, 2008; Mackler et al., 2002; Yoshihara and Littleton, 2002). For the purposes of this dissertation, I will focus on the function of synaptotagmin 1 and will refer to synaptotagmin 1 simply as

synaptotagmin, unless otherwise noted.

Due to synaptotagmin's localization to synaptic vesicles, and its calcium and phospholipid binding properties, it was postulated to be involved in vesicle docking and exocytosis (Perin et al., 1991; Brose et al., 1992; Nalefski et al., 2001). In 1993, the Bellen and Schwarz labs published the first measurements of evoked synaptic transmission in synaptotagmin null mutants (DiAntonio et al., 1993; DiAntonio, Burgess et al., 1993; Littleton et al., 1993). Synaptotagmin null mutants show a dramatic decrease in evoked neurotransmitter release (90-95%), are exceptionally slow and uncoordinated, and die as first-instar larvae unless special husbandry is employed to promote their survival (DiAntonio et al., 1993; Littleton et al., 1993; Loewen et al., 2001; Mackler et al., 2002). Synaptotagmin null mutants also show an increase in spontaneous vesicle fusion (Littleton et al., 1993; Mackler et al, 2002). These genetic experiments demonstrate synaptotagmin's importance in synaptic transmission. The results from Littleton et al. (1993) and DiAntonio et al. (1993) were the first to reveal that synaptotagmin was essential for fast, synchronous evoked neurotransmitter release. Since then, synaptotagmin's role in calcium-dependent exocytosis has been studied extensively in multiple model organisms (Yoshihara and Littleton, 2002; Mackler et al., 2002; Fernandez-Chacon et al., 2002; Nishiki and Augustine 2004; Lui et al., 2009; Shin et al., 2009; Lee et al., 2013; Chapman, 2018). The two calcium-binding domains, C_2A and C_2B, of synaptotagmin have been identified as the functional domains mediating its role as a calcium-sensor. Mutations within either of the C2 domain Ca^{2+} binding motifs results in varying degrees of synaptic impairment ranging from slight decreases in evoked transmitter release to lethality (Fukuda et al., 1995; Littleton et al., 2001; Mackler et al., 2002; Bai and Chapman, 2004; Fernandez-Chacon et al., 2002; Shin et al., 2009; Lee et al., 2013; Bowers and Reist, 2020). Such studies have demonstrated that Ca^{2+}-binding by the C_2B

domain and the resulting Ca^{2+}-dependent membrane penetration by the C_2B domain is the most critical effector interaction coupling Ca^{2+} binding to vesicle fusion (Littleton et al., 2001; Mackler et al., 2002; Paddock 11). In addition to its role in synaptic vesicle fusion, synaptotagmin is also involved in several other steps of the synaptic vesicle cycle, including endocytosis, docking, and priming.

Synaptotagmin's role in endocytosis was first postulated due to the depletion of synaptic vesicles observed in syt^{null} mutants (Jorgensen et al. 1995; Reist et al., 1998; Littleton et al., 2001; Loewen, Royer et al., 2006; Liu et al., 2009). Synaptotagmin's ability to bind the clathrin-adaptor protein, AP-2, and associated proteins, which are required for clathrin-mediated endocytosis, also suggested a role in endocytosis (Zhang et al., 1994; Haucke & De Camilli, 1999; Haucke et al., 2000; von Poser et al., 2000; Jarousse et al., 2001; Fergestad and Broadie, 2001). In 2003, Poskanzer et al. tagged the synaptic vesicle protein, synaptobrevin, with a PH-sensitive green fluorescent protein (synapto-pHluorin) to measure the kinetics of endocytosis using quantitative live imaging at the NMJ in *Drosophila*. By stimulating release at the non-permissive temperature in dynamin mutants ($shibire^{ts}$) which blocks endocytosis, they were able to trap synaptic vesicle membranes in the plasma membrane (Koenig & Ikeda, 1989). They then used fluorescein-assisted light inactivation (FlAsH-FALI) after exocytosis to photoinactivate transgenic syt1 tagged with a tetracysteine motif. Upon returning preparations to the permissive temperature, they showed that endocytosis of synaptic vesicle membranes resumed in controls but not in preparations where synaptotagmin was photoinactivated. Thus, by combining the synapto-pHlourin and FlAsH-FALI techniques, Poskanzer et al. were able to experimentally uncouple the exocytic and endocytic functions of synaptotagmin *in vivo*. This set of experiments revealed, for the first time, that synaptotagmin (or a closely associated protein) is necessary for

compensatory endocytosis. The mechanism by which synaptotagmin is involved in clathrin-mediated endocytosis of synaptic vesicles has remained unclear, although synaptotagmin's documented interactions with AP-2 provide a good candidate for this mechanism.

Synaptotagmin's role in vesicle docking was first postulated due to its molecular interactions with SNARE proteins and other membrane bound synaptic proteins (Petrenko et al., 1991; Bennett et al., 1992; Schiavo et al., 1997; Broadie, 1996). In 1998, Reist et al. used electron microscopy to demonstrate that syt^{null} mutants in *Drosophila* have a decrease in morphologically docked synaptic vesicles. Their findings support the hypothesis that synaptotagmin is involved in vesicle docking. However, the molecular mechanism by which synaptotagmin mediates vesicle docking remained unclear. Synaptotagmin's interactions with the SNARE complex, complexins, and PIP2 led to hypotheses that synaptotagmin participated in the docking and/or priming of vesicles (Z. Wang et al., 2011; Sudhof, 2013; Chang et al. 2018; Zhou et al., 2017; Bouazza-Arostegui et al., 2022). However, the putative role in vesicle priming remains the least understood of all its postulated roles.

C_2B Polylysine Motif of Synaptotagmin

The C2 domains of synaptotagmin contain a highly-conserved polylysine motif that creates a positively-charged region along the side of the eight-stranded beta-sandwich. In the C_2B domain of synaptotagmin 1, two or three lysine residues (located at amino acid positions 379, 380, and 384 in *Drosophila* or 326, 327 with or without 331 in mammals, see Fig. 2-1 comprise this motif (Fukuda et al., 1995; Jorgensen et al., 1995; Haucke et al., 2000; Mackler and Reist, 2001; Jarousse et al., 2001; Llinas et al., 2004; Borden et al., 2005; Loewen, Lee et al., 2006; Chang et al., 2018;). Research in the Reist lab was the first to show that mutation of these lysine residues resulted in an ~40% decrease in the evoked junction potential (EJP) compared to

a WT control at the *Drosophila* NMJ *in vivo* (Mackler and Reist, 2001). This result was later replicated at mammalian hippocampal synapses *in vitro* (Haucke et al., 2000; Borden et al., 2005; Chang et al., 2018). Although this was the first synaptotagmin mutation shown to disrupt efficient synaptic transmission, two decades later, the mechanism disrupted by this mutation is still unclear.

Early biochemical work indicated that a calcium-independent interaction between the C_2B polylysine motif and the clathrin adapter protein, AP-2, may mediate synaptotagmin's role in endocytosis (Chapman et al., 1998; Haucke & De Camilli, 1999; Haucke et al., 2000; Littleton et al., 2001; Zhang et al., 1994, see however Ubach et al 2001). In 2006, Loewen, Lee et al., use a polylysine motif mutant in *Drosophila* to test the role of this motif in endocytosis *in vivo*. They found that the polylysine motif mutant was able to rescue the vesicle depletion observed in the syt^{null} mutants which is inconsistent with a deficit in endocytosis. As a direct test, they used an FM1-43 assay (Betz and Bewick, 1992) and found that the rate of endocytosis was unchanged in the polylysine mutant compared to controls. Thus, the decrease in evoked transmitter release caused by the C_2B polylysine mutation is not due to a disruption of endocytosis (Loewen, Lee et al., 2006).

To verify that the C_2B polylysine motif did not result in a developmental disruption of postsynaptic function, Loewen, Lee, et al. (2006) used immunostaining of glutamate receptors (GluRIII) and active zones (nc82). They found no difference in the area of staining in mutants compared to controls, indicating that the pre- and post-synaptic regions at the NMJ were intact (Loewen, Lee, et al., 2006). Additionally, Mackler and Reist (2001) found no differences in the amplitude of spontaneous fusion events in the polylysine motif mutants. Taken together, these results indicate that the decrease in EJP amplitude is not due to a deficit in the post-synaptic

cell's ability to respond to neurotransmitter release but rather is due to a presynaptic deficit somewhere in the synaptic vesicle cycle.

Calcium-dependent interactions of the C_2B polylysine motif have been postulated to mediate aspects of vesicle fusion. Specifically, synaptotagmin oligomerization (Chapman 98, Wu 03); synaptotagmin simultaneously binding two membranes (Araç et al., 2006); and synaptotagmin binding negatively charged phospholipids (Li et al., 2006) have been proposed to regulate fusion pore opening, dilation, or stability (Wang et al., 2001, Bai and Chapman, 2004, Li et al., 2006). To investigate the calcium dependent function for the C_2B polylysine motif, Loewen, Lee, et al. looked at the EJP amplitude in increasing calcium concentrations. They found that although EJP amplitudes in the polylysine mutant were smaller at all Ca^{2+} concentrations, the Ca^{2+}-dependence of release was not different when compared to the control (no change in Hill coefficient). Since, the calcium cooperativity of release is unchanged in the polylysine mutant, the decrease in evoked release is most likely due to a deficit in a Ca^{2+}-independent step of the vesicle cycle. Indeed, when Loewen, Lee et al., looked at the rate of recovery following high frequency stimulation, they found that the polylysine mutants recovered more slowly than the controls. Since recovery is a Ca^{2+}-independent phase of the vesicle cycle, these findings also indicate that the polylysine motif must function during a calcium-independent vesicle targeting step, such as docking and/or priming.

The polylysine motif's calcium-independent interactions with phosphatidylinositol 4,5-bisphosphate (PIP_2) containing membranes, and t-SNAREs, may mediate synaptic vesicle docking and/or priming (Bai and Chapman, 2004; Li et al., 2006; Wang et al., 2017). However, the molecular mechanisms mediating synaptotagmin's role in docking and priming are not well understood. In Chapter 2 of this dissertation, we reassess the polylysine motif's interaction with

AP-2 by testing this interaction specifically in *Drosophila*. We found, while C_2B does indeed bind AP-2 in *Drosophila*, this interaction is not disrupted by the C_2B polylysine mutation. This finding is consistent with the finding that the C_2B polylysine motif does not disrupt the rate of endocytosis (Loewen, Lee et al., 2006). In Chapter 2, I also assess the polylysine motif's role in vesicle docking using electron microscopy methods that have previously identified docking deficits in syt^{null} *Drosophila* mutants (Loewen, Royer et al., 2006). In Chapter 3, I propose a method to measure morphological vesicle priming in *Drosophila* using high resolution electron tomography. The methods I propose in Chapter 3 enable the first direct test of a putative priming mutant and can be used to investigate the polylysine motif's role in vesicular docking and priming using the higher resolution of electron tomography.

Drosophila as a Model System

The previous experimentation to characterize the synaptic ultrastructure at the NMJ has primarily been done in frogs by the McMahan lab. While partial AZM renderings have been generated at the mouse NMJ (Nagwaney et al., 2009), the entire AZM has not been segmented. Additionally, there are limitations to using the frog or mouse as model organisms for elucidating the morphological arrangement molecular components at synapses, which is the ultimate goal of electron tomographic analyses. Frog is not a genetic model, which limits the ability to tag and identify individual proteins to understand the relationship between structure and function. Mouse, though amenable to genetic manipulation, is costly and time-consuming. *Drosophila*, on the other hand, provides an ideal, inexpensive, genetic model organism with an exceedingly rapid life cycle of just 10 days. Further, an extensive amount of research on synaptic transmission, synaptic proteins, and active zones at the NMJ has been conducted in *Drosophila* (Koenig and Ikeda, 1989; Koenig and Ikeda, 1989; DiAntonio et al., 1993; Broadie, 1996; Lloyd

et al., 2000; Owald and Sigrist 2009; Slater, 2015; Gan and Watanabe, 2018; Sauvola and Littleton, 2021). Combined, this makes *Drosophila* an ideal model organism for conducting synaptic structure and function studies at the NMJ. Yet, electron tomography of the *Drosophila* AZM is in its infancy and has yet to be done with sufficient resolution to render a clear 3D reconstruction of the AZM (for example, Jiao et al., 2010; Leitinger et al., 2012; Zhan et al., 2016; Bruckner et al., 2017;). By extending the McMahan lab's 2-3 nm-resolution tomography to *Drosophila* synapses, we will provide a new protocol that will permit the structural measurements necessary for the first direct test of a molecular motif hypothesized to enhance vesicle priming. In addition, since *Drosophila* are amenable to transgenic tagging, segmenting the AZM connecting docked vesicles, presynaptic membrane, and T-bars at the level of resolution the McMahan lab has attained in frog, has the potential to open a whole new field of structural identification of synaptic molecules critical for intercellular communication in the nervous system.

Chapter Summary

Chapter 1 provides a comprehensive introduction to the nervous system's fundamental elements, focusing on the structure and function of neurons and the mechanisms underlying synaptic communication. Neurons, comprising cell bodies, dendrites, axons, and axon terminals, serve as the primary units for electrical signal propagation. The chapter introduces chemical synapses, with particular emphasis on neurotransmitter release mechanisms. The neuromuscular junction (NMJ) is highlighted as a fail-safe, chemical synapse essential in muscle control. Detailed attention is devoted to the synaptic vesicle cycle, elucidating the sequence of events in neurotransmitter release and vesicle recycling, with particular emphasis on the docking and priming steps. The significance of active zones, specialized sites for efficient signal transmission,

and their associated components are underscored, with a focus on synaptotagmin, a required protein for calcium-triggered vesicle fusion. Synaptotagmin's C_2B polylysine motif and its role in vesicle docking and priming are specifically highlighted. Throughout the chapter, the utility of *Drosophila* as a model system for studying synaptic processes, particularly at the NMJ, is emphasized. In sum, Chapter 1 provides the foundational knowledge essential for comprehending the intricate cellular and molecular facets of synaptic communication, within the nervous system, serving as a precursor to subsequent chapters' investigations.

Chapter 2 of this dissertation investigates the role of synaptotagmin's C_2B polylysine motif in synaptic vesicle docking at the *Drosophila* NMJ. Initially, the chapter explores the motif's potential involvement in endocytosis by testing its controversial interaction with AP-2. A pull-down assay from the Reist Lab is presented, indicating that mutating the polylysine motif to glutamines, which disrupts the synaptic vesicle cycle, does not disrupt AP-2's interaction with the C_2B domain of synaptotagmin. This is consistent with previous finding by Loewen et al., 2006 which demonstrates that the deficit in evoked transmitter release in the C_2B polylysine mutant is not due to impaired endocytosis. Their work suggests the deficit may instead be related to vesicle docking and/or priming. Accordingly, electron microscopy is then used in chapter 2 to assess vesicle docking. My analysis of synaptic vesicle distributions at *Drosophila* active zones found no significant changes in the polylysine mutant compared to the wild-type control, demonstrating the C_2B polylysine mutant does not disrupt vesicle docking. To demonstrate that these measurements would detect a docking deficit if one were present, I conducted a direct comparison of vesicle docking data in synaptotagmin-null mutants and polylysine motif mutants. My comparison showed that a docking deficit would have been detected with our standard electron microscopy techniques if present. These results collectively suggest that the observed

deficit in evoked neurotransmitter release in the polylysine mutant likely arises from impaired vesicle priming.

Chapter 3 presents a detailed adaptation to *Drosophila* of the McMahan group's groundbreaking method for studying synaptic vesicle docking and priming by morphological measurements. It addresses the limitations of conventional electron microscopy and expands on the power of electron tomography to obtain 2-3 nm spatial resolution. This method combines *Drosophila*'s genetic advantages with high-resolution imaging to investigate the molecular processes underlying neurotransmitter release. The chapter outlines the protocol, covering sample preparation and data analysis tools. Results show the first tomograms to achieve 2-3 nm resolution in *Drosophila* and show the protocol's effectiveness in generating tomograms with high enough resolution for measuring critical parameters like membrane thickness and VM-PM contact area in *Drosophila*. The discussion section highlights specific considerations such as maintaining osmolarity during sample prep and software limitations. In summary, Chapter 3 offers an innovative approach that marries *Drosophila* genetics and high-resolution imaging which has the potential to unlock deeper insights into synaptic mechanisms through ultrastructural mapping and protein identification.In Chapter 4, I discuss how the synaptotagmin polylysine motif mutant may mediate vesicle priming through molecular interactions with inositol phosphates. I then discuss key considerations when assessing vesicle docking using standard electron microscopy and how electron tomography is a superior method to assess vesicle docking. I discuss how the electron tomography method presented in Chapter 3 could not only confirm the results found in Chapter 2, that the synaptotagmin C_2B polylysine motif is not involved in vesicle docking but could also be used to directly test the mutant's potential role in priming. Specific aims for future studies on the synaptotagmin polylysine mutation in

Drosophila are presented. The potential results and interpretations for the specific aims are discussed. Lastly, I showcase interesting, unpublished findings from electron tomograms I have taken at the *Drosophila* NMJ and discuss their potential significance.

CHAPTER 2: THE C_2B POLYLYSINE MOTIF OF SYNAPTOTAGMIN IS NOT REQUIRED FOR DOCKING OF SYNAPTIC VESICLES

Overview

Chemical synapses are specialized contact sites that regulate cell to cell communication in the nervous system through neurotransmitters. Neurotransmitters are packaged in synaptic vesicles, which mediate the release of neurotransmitters into the synapse. Upon the arrival of an action potential at the pre-synaptic cell, calcium enters the cell and binds to intercellular proteins evoking vesicle fusion and releasing neurotransmitters onto the post-synaptic cell. The synaptic vesicle protein, synaptotagmin, is known to be a Ca^{2+} sensor which mediates synaptic vesicle fusion. Synaptotagmin has four distinct domains, two of which are Ca^{2+} binding domains (C_2A and C_2B). In addition to sensing Ca^{2+} via its C_2 domains, synaptotagmin is also hypothesized to mediate the docking of vesicles to the pre-synaptic membrane and/or the priming of vesicles to a ready-releasable state. Previous literature has identified a particular polylysine motif in the C_2B domain of synaptotagmin. Electrophysiological analysis of these polylysine mutants revealed decreased evoked transmitter release, which could be a result of disrupting Ca^{2+}-triggered vesicle fusion, endocytosis or vesicle docking and/or priming. Previous literature has demonstrated that the polylysine mutant still acts in a calcium-cooperative manner and does not affect vesicle endocytosis. This suggests that the polylysine mutant acts on the vesicle cycle somewhere after endocytosis and before vesicle fusion, possibly at the step of vesicle docking and/or priming. The present study uses electron microscopy to investigate the role of synaptotagmin's C_2B polylysine motif in vesicle docking at the *Drosophila* neuromuscular junction (NMJ). The distance of synaptic vesicles from the presynaptic membrane was measured. We found no differences

between controls and the polylysine mutants in the distance of synaptic vesicles from the plasma membrane of active zones. Thus, our results rule out the hypothesis that the polylysine motif is required for docking of vesicles at the presynaptic membrane. This finding suggests that the polylysine motif has implications in the priming of synaptic vesicles at the neuromuscular junction. Future studies will aim to elucidate the polylysine motif's role in vesicle priming and how this relates to the overall function/interactions of synaptotagmin.

Introduction

Fast and efficient intercellular communication at the NMJ is orchestrated through the release of neurotransmitter from presynaptic nerve terminals onto a muscle fiber. Neurotransmitter filled synaptic vesicles fuse with the presynaptic membrane at "active zones," specific presynaptic specialization, that mediate fast and efficient transmitter release required for movement. Synaptic vesicles must first be docked and primed at the presynaptic membrane prior to fusion. Immediately following vesicle fusion, synaptic vesicles are replenished though clathrin-mediated endocytosis (CME). These recycled synaptic vesicles are then loaded with neurotransmitter and trafficked to the presynaptic membrane, thus completing the synaptic vesicle cycle. Deficits anywhere in the synaptic vesicle cycle could result in synaptic dysfunction.

At the active zone, vesicular and target membrane SNARE proteins mediate the fusion event (Bennet et al., 1992; Schiavo et al., 1992; Schiavo et al., 1997; Weber et al., 1998; Rizo and Xu, 2015; Sauvola and Littleton, 2021) while the synaptic vesicle protein, synaptotagmin, is the Ca^{2+} sensor that triggers fast, synchronous neurotransmitter release (Geppert et al., 1994; Mackler et al., 2002; Chapman, 2018). Synaptotagmin is composed of an N-terminal intravesicular domain, a transmembrane domain, and two cytoplasmic C_2 domains, C_2A and C_2B

(Perin et al., 1990 & Perin et al. 1991, Sutton et al., 1995, Sutton et al. 1999). C_2 domains are evolutionarily conserved calcium-binding domains found in many proteins that consist of an eight-stranded beta sandwich with a calcium binding pocket at one end. The crystal structure of the C_2B domain of synaptotagmin is shown in Figure 2-1B. Ca^{2+} binding to both C_2A and C_2B is required to trigger fast, synchronous, SNARE-mediated vesicle fusion events (Mackler et al., 2002; Nishiki and Augustine, 2004; Striegel et al., 2012; Bowers and Reist, 2020, Bai and Chapman, 2004). However, synaptotagmin is also hypothesized to play roles in other steps of the vesicle cycle, including endocytosis and Ca^{2+}-independent docking and/or priming of synaptic vesicles (Z. Wang et al., 2011, Sudhof 2013, Chang et al. 2018, Zhou et al., 2017, Bouazza-Arostegui et al., 2022).

Synaptotagmin's role in endocytosis was first postulated due to the depletion of synaptic vesicles observed in *syt*^{null} mutants and due to synaptotagmin's interaction with the clathrin adaptor protein AP-2 (Jorgensen et al. 1995, Reist et al., 1998, Littleton et al., 2001, Loewen, Royer et al., 2006, Liu et al., 2009, Zhang et al. 1994, Haucke & De Camilli, 1999, Haucke et al. 2000, von Poser et al., 2000, Jarousse et al., 2001, Fergestad et al., 2001). In a set of experiments using synapto-Phlourin and fluorescein-assisted light inactivation (FlAsH-FALI) after exocytosis, Poskanzer et al., were able to experimentally uncouple exocytic and endocytic functions of synaptotagmin in vivo, which revealed that the C_2B domain of synaptotagmin, or an associated protein, are necessary for clathrin-mediated endocytosis.

The C_2B domain of synaptotagmin contains an evolutionarily conserved polylysine motif (Fig 1, cyan and *). Early biochemical work indicated that the polylysine motif interacts with AP-2 (Chapman et al., 1998; Haucke & De Camilli, 1999; Haucke et al., 2000; Littleton et al., 2001; Zhang et al., 1994, see however Ubach et al 2001) leading to the hypothesis that the C_2B

polylysine motif may mediate synaptotagmin's role in endocytosis. Mutations in the polylysine motif decrease synaptic transmission; the amplitude of evoked transmitter release is decreased by ~40% (Mackler & Reist, 2001, Lui et al., 2009, Niskiki & Augustine, 2004, Schiavo et al., 1992), consistent with deficits in any of the synaptic vesicle steps listed above, including endocytosis.

To directly test for a functional role in endocytosis, Loewen, Lee, et al. (2006) measured the rate of endocytosis in C_2B polylysine motif mutants using FM1-43 and found that it was unchanged compared to controls. In addition, the polylysine motif mutant was able to rescue the synaptic vesicle depletion seen in syt^{null} mutants, again inconsistent with a role in endocytosis. To probe for other deficits in the synaptic vesicle cycle, they tested the rate of recovery following high-frequency stimulation. Importantly, they found that polylysine motif mutants recovered more slowly than controls.

The findings that: 1) the polylysine motif displayed no change in the rate of endocytosis, 2) rescued synaptic vesicle depletion, yet 3) exhibited delayed recovery from high-frequency stimulation, implicate a role in Ca^{2+}-independent vesicle trafficking. Synaptotagmin has been hypothesized to mediate the docking of vesicles to the pre-synaptic membrane and/or the priming of vesicles to a ready-releasable state. Synaptotagmin's documented interactions with PIP_2 (phosphatidylinositol 4,5-bisphosphate) pose a possible mechanism to synaptotagmin's role in docking and/or priming. Calcium-independent binding of PIP_2 to synaptotagmin's polylysine motif is postulated to facilitate exocytosis by facilitating the close apposition of vesicle and target membranes (Bai et al., 2004; Wang et al., 2017).

This study reassesses the synaptotagmin C_2B polylysine motif's interaction with AP-2 and investigates the motif's role in vesicle docking at the *Drosophila* neuromuscular junction to

directly test the hypothesize that this polylysine motif is required to dock synaptic vesicles at the active zone.

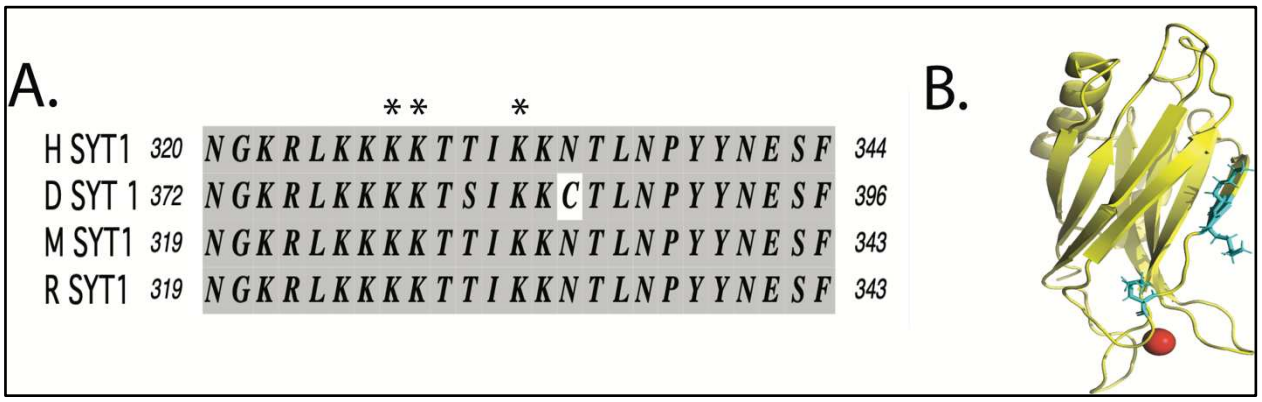

Figure 2-1. *The Three Lysine Residues of the Second C_2B Polylysine Motif*

Three highly conserved lysine residues within the second C_2 domain of synaptotagmin that constitute the C_2B polylysine motif are shown. (A.) ClustalW protein sequence alignments of the portion of the C_2B domain containing the polylysine motif (*) of synaptotagmin 1 from Human, *Drosophila*, Mouse, and Rat. (B.) Crystal structure of the C_2B domain of synaptotagmin made using PyMOL (pdb 1K5W). The three lysine residues are shown in cyan. Yellow arrows indicate β sheets; yellow spiral indicates an α helix; the red circle indicates a Ca^{2+} atom bound to the calcium binding pocket of C_2B.

* = evolutionarily conserved lysine residues

Materials and Methods

Fly Lines

Mutant and wild type control synaptotagmin were each expressed as a UAS-driven transgene in a synaptotagmin null mutant (sytAD4, DiAntonio & Schwarz, 1994) background such that the only synaptotagmin expressed was from the transgenes. Expression of the UAS-driven transgene was localized to the nervous system using elavGAL4, a pan-neuronal source of Gal4 (Brand & Perrimon, 1993; Robinow & White, 1988). The fly lines utilized were: *yw;sytAD4/CyO GFP; P[UASsytwt]*, *yw;sytAD4/CyO GFP; P[UASsytK379,380,384Q]*, and *yw;sytAD4 P[elavGal4]/CyO GFP* (Mackler and Reist, 2001). The transgenic *Drosophila* used

had the genotypes: yw;syt^{AD4} P[elav-Gal4]/syt^{AD4};P[UAS syt^{K379,380,384Q}]/+ (referred to as P[syt^{KQ}]) and yw;syt^{AD4} P[elav-Gal4]/syt^{AD4};P[UAS syt^{wt}]/+ (referred to as P[syt^{WT}]). OregonR *Drosophila* (true wild type, +/+) were used in one comparison.

Molecular Modeling

Since the crystal structure of *Drosophila* syt1 has yet to be solved and the C_2B domains of *Drosophila* syt1 and rat syt1 are virtually identical, we utilized rat syt1 for our model. Specifically, for this study, the crystal structure of Rat syt1 C_2B domain (PDB File 1K5W) was obtained from the Protein Data Bank. Next, we generated a model of the polylysine mutation using the mutagenesis wizard in the molecular graphics system PyMOL (Version 1.8; Schrödinger, LLC & DeLano, 2020). In the model, rat syt1 C_2B residues 326, 327, and 331 were mutated to glutamines, to represent the homologous polylysine mutant residues 379, 380, and 384 in *Drosophila* syt1.

Recombinant Proteins

Drosophila cDNA for C_2A (residues 191-317), C_2B (323-474), and C_2AB (191-474) was obtained by PCR amplification of *syt I* cDNA that was either wild-type or that contained a C_2B polylysine motif mutation with lysine residues 379, 380, and 384 mutated to glutamines (Mackler and Reist, 2001). They were subcloned into the expression vector pET 28a(+) (Novagen, Madison, WI) and transformed into *E. coli* BL21 Rosetta to express recombinant proteins with a C-terminal six-histidine tag. The transformants were grown to the log phase (optical density (O.D.) at 600 nm of 0.5) at 37 °C in Luria-Bertani (LB) broth with 50 μg/ml kanamycin. Expression of recombinant proteins was induced by adding 0.2-0.5 mM IPTG. The cells were cultured at 25 °C for overnight. The cultured cells were harvested by centrifugation at 4°C and frozen at -70 °C. His6-tagged recombinant proteins were purified using a Ni-NTA

agarose column chromatography (Qiagen, Valencia, CA) according to the manufacturer's instructions (Qiagen, Valencia, CA) with the addition of DNase I/RNase A incubations to aid the removal any nucleic acid contaminants. Briefly, bacterial pellets were resuspended in 300 mM NaCl, 50 mM Tris-HCl, pH=8.0, 1% Triton X-100, containing 0.5 mg/ml Lysozyme (Sigma, St. Louis, MO) and a protease inhibitor cocktail (P8340, Sigma, St. Louis, MO; 1ml/4g of *E. coli* (wet weight)), sonicated (5 cycles, 20 sec on/90 sec off), incubated with 10 μg/ml DNase I and RNase A and 0.5 mM $MgCl_2$ for 1 hr, spun at 12,000 rpm 2 X 20 min and the supernatant was applied to Ni-NTA resins (1 ml of resin/2 L of cultured cells). Column was washed with 300 mM NaCl, 20 mM Tris-HCl pH gradient pH=8.0 to 6.8 (10 column volumes at each pH) and then incubated in 1 mg/ml DNase I and RNase A, 300 mM NaCl, Tris-HCl, pH=6.8 overnight followed by two high salt washes (1 M NaCl, 20 mM Tris-HCl, pH=6.8, 10 volumes each). His6-tagged proteins were eluted with a step gradient of imidazole (5 mM-200 mM) and dialyzed against HBS (150 mM NaCl, 50 mM HEPES, pH=7.6). Removal of nucleic acid contaminants was verified by UV spectral analysis on a Hewlett Packard 8425A spectrophotometer. *E. coli* BL21 Rosetta containing pET28 vector was induced with 2mM IPTG, resuspended with HBS and lysed by sonication. The resulting lysates were used for the negative control in the binding assay.

Detergent extraction

Drosophila heads (OrR) were sonicated (4 cycles, 60 sec on/90 sec off) in 280 mM sucrose containing a protease inhibitor cocktail (P8340, Sigma, St. Louis, MO; 100ul/100mg of *Drosophila* head) and spun at 5000 rpm for 2 min (Eppendorf 5417C microcentrifuge). The supernatant was spun at 11,000 rpm for 12 min and membranes remaining in the supernatant were extracted for 45 min at 4°C in 10 volumes of extraction buffer (1% Triton X-100, 100 mM

NaCl, 50 mM HEPES, pH=7.6, Protease Inhibitor; 1ml/10ml of total volume of protein mixture). Extraction mix was spun at 100,000 X g for 1 hr at 4°C.

Binding assay

100 μg of His6-recombinant proteins in 500ul of HBS were applied to 10 μl Ni-NTA resin, washed 3 X with 500 ul of HBS to remove unbound proteins. 1ml of Detergent extracts (1 mg/ml) of *Drosophila* were adjusted to 1 mM $CaCl_2$ or 2 mM EGTA respectively and subjected to recombinant protein-resin mixes and incubated for 2 hrs at 4°C. The resulting proteins-resin complexes were washed 3 X with 1 ml HBS and boiled in 20 μl SDS sample buffer (2% SDS, 2 mM dithiothreitol, 4% glycerol, 40 mM Tris-HCl, pH6.8, 0.01% bromophenol blue) and separated by SDS-PAGE. Bound AP-2 was detected by Western blot analysis using an antibody directed against *Drosophila* alpha-adaptin (Gonzalez-Gaitan & Jackle, 1997) diluted 1:4,000 in PBS containing 0.05% Tween and 10% NGS (PBS-Tw-NGS) and an HRP-conjugated donkey anti-rabbit IgG (Jackson ImmunoResearch Labs, West Grove, PA) diluted 1:20,000 in PBS-Tw-NGS, which was visualized using a chemoluminesent signal detection system, a Supersignal West Dura Extended Duration Substrate kit (Pierce, Rockford, IL) in an Epichemi3 Darkroom (UVP, Upland, CA). Amounts of bound recombinant proteins on the Ni-NTA resin was examined by Ponceu-S (0.1% Ponceu-S in 5% acetic acid) staining of the blot to ensure equal loading.

Electron Microscopy

Third instar larvae were dissected in cold, Ca^{2+}-free HL3 saline, and then embedded, sectioned, and stained as previously described (Loewen, Royer, et al., 2006). Briefly, immediately following dissection, third in stars were fixed for 1 hr in ice-cold primary fixative (1% acrolein, 2.5% glutaraldehyde in 0.1 M cacodylate buffer, pH 7.2), rinsed in 0.1 M

cacadylate buffer, post-fixed for 1 hr in secondary fixative (0.5% OsO_4, 0.8% KFeCn in 0.1 M cacodylate buffer, pH 7.2), incubated in 5% uranyl acetate for 1 hr to overnight at 4 °C, and then dehydrated and embedded in Embed-812 (Electron Microscopy Sciences). Thin plastic sections of 70 nm were taken and poststained in 5% uranyl acetate and Reynold's lead citrate. Electron micrographs of neuromuscular junctions on muscle fiber number 6 from abdominal segments 3 and 4 were taken at 15,000X magnification on a JEOL 2000 EX-II transmission electron microscope operated at 100 keV. Images were scanned using an Agfa DuoScan T2500 and adjusted for contrast using Adobe Photoshop software.

Analysis

Only electron micrographs of active zones containing clearly visible T-bars and presynaptic membranes were selected for analysis. Micrographs of experimental and control groups were randomized and blinded. To analyze the distribution of synaptic vesicles, the parameters to define the active zone were set and applied to each micrograph. The active zone region was defined as 150 nm from either side of the T-bar (see yellow lines on Fig. 2-3C) and within 200 nm from the presynaptic membrane. To ensure there were no differences between the region of active zone analyzed for the experimental and control lines, the cumulative length of active zone membrane analyzed on either side of the T-bar was compared (see Fig. 2-3D. If the middle of a synaptic vesicle was more than 200 nm from the presynaptic membrane, it was not included in the analysis. The average diameter of small clear vesicles (35 ± 5 nm SD) from similar specimens was previously documented in Loewen, Royer, et al. (2006). Only small, clear vesicles that were < 50 nm in diameter were included in the synaptic vesicle distribution. Any dense core vesicles and large vesicles that were > 50 nm were left out of the analysis. To ensure the number of synaptic vesicles per active zone analyzed was not different between experimental

and control lines, the total count of synaptic vesicles per active zone were compared (see Fig. 2-3E. To measure the distribution of synaptic vesicles, a line was drawn from the middle of the vesicle lumen to the nearest surface of the presynaptic membrane, which are shown by the black lines on Figure 2-3C. This was done for every small clear vesicle within the active zone parameters defined above. The length of the line drawn for each vesicle was recorded as that vesicle's distance from the presynaptic membrane. The data was pooled into 12 nm bins starting from the first 0-23 nm bin. Docked vesicles were defined as those whose center was within 23 nm from the presynaptic membrane (Loewen, Royer et al., 2006). Thus, all vesicles in the 0-23 nm bin were defined as docked. Seventy-three active zones from the experimental polylysine motif mutant (P[syt^{KQ}]) and 74 active zones from the WT control (P[syt^{WT}]) were used in the analysis.

Results and Discussion

AP-2 Binding Is Not Mediated by C_2B Polylysine Motif

To determine whether the synaptotagmin/AP-2 interaction in *Drosophila* is mediated by the C_2B polylysine motif, a pull-down assay was performed (Fig. 2-2). Ponceu-S stain shows that approximately equal amounts of recombinant protein were used in paired control and mutant lanes (Fig. 2-2A). Immunolabeling demonstrates that AP-2 binds specifically to the C_2B domain of synaptotagmin (Fig. 2-2B, compare C_2A vs. C_2B and C_2AB lanes) and that this interaction is calcium independent (Fig 2B, - vs + lanes). Importantly, AP-2 binds equally across all C_2B containing lanes, including the polylysine motif mutant lanes, C_2B-KQ and C_2AB-KQ (Fig. 2-2B). These results demonstrate that AP-2 binds to the C_2B domain of synaptotagmin in *Drosophila*, as seen previously in *Drosophila*, mouse, rat, and liposomes (Littleton et al., 2001; Mizutani et al., 1997; Zhang et al., 1994; Chapman et al., 1998; Hauke et al., 2000). However,

the polylysine mutation does *not* affect this interaction with AP-2 (Fig. 2-2B, C_2B-KQ and C_2AB-KQ). These results are consistent with the findings of Ubach et al. 2001. Thus, the decrease in EJP amplitude in the C_2B polylysine mutant is independent of AP-2 function during endocytosis, consistent with the findings of Loewen, Lee, et al. (2006).

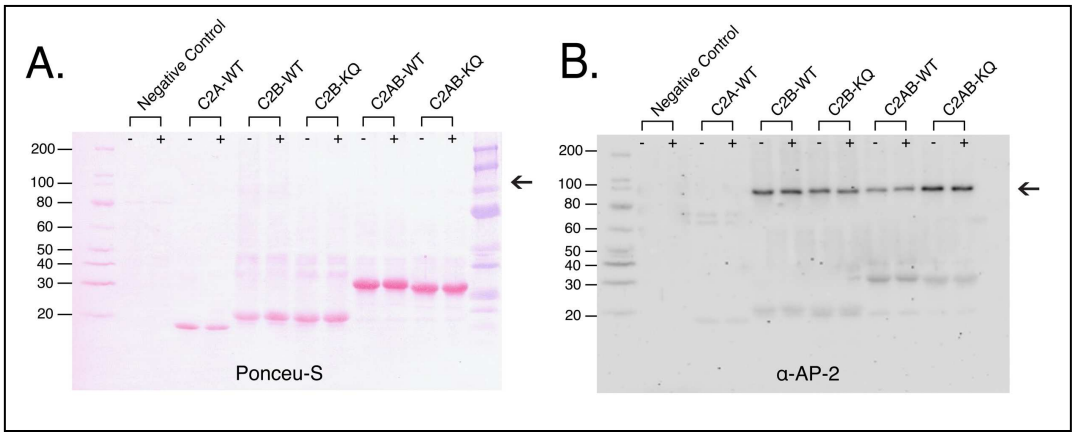

Figure 2-2. *AP-2 Binding is Intact in the C_2B Polylysine Motif Mutant*

A pull-down assay using 6-His recombinant synaptotagmin peptides was performed both in the presence and absence of calcium: 2 mM EGTA (-) or 1 mM CaCl2 (+). For negative control, the 50 amino acid peptide from pET 28a(+) was expressed with IPTG in E. coli. (A.) SDS-PAGE assay stained with Ponceu-S showing approximately equal amounts of recombinant peptides were used to compare mutants and controls. (B.) SDS-PAGE assay immunolabeled with anti-AP-2 antibody. Recombinant WT control peptides C_2B and C_2AB bind AP-2 in a Ca^{2+}-independent manner. The C_2A peptide does not bind AP-2. The polylysine motif mutation, C_2B-KQ and C_2AB-KQ, does not affect the interaction with AP-2.

Measuring Vesicle Docking by Electron Microscopy

Electron microscopy was used to analyze whether the polylysine motif mutant causes a disruption in synaptic vesicle docking. Electron micrographs showing active zones at the *Drosophila* NMJ were taken of the polylysine mutant and WT controls (see Fig. 2-3). To analyze docking, the synaptic vesicle distribution was assessed specifically in the active zone region immediately surrounding the T-bar (Fig. 2-3C, and see methods). The total plasma membrane

length and synaptic vesicle count included per active zone region were calculated as a control to ensure there were no differences in the length of active zones or the number of synaptic vesicles being analyzed (Fig. 2-3 D-E, respectively). Synaptic vesicles were then grouped into bins based on their distance in nm from the presynaptic membrane.

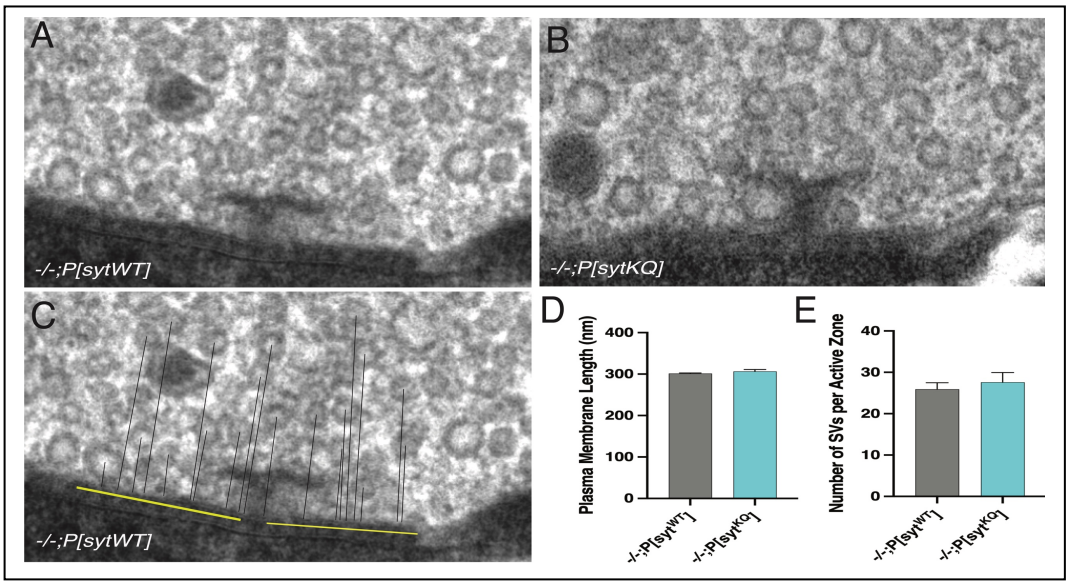

Figure 2-3. *Electron Micrographs of Drosophila Neuromuscular Junctions*

Neuromuscular junctions in 70 nm sections of chemically-fixed and stained third instar larva. (A.–B.) Active zones and the vesicle cloud for the transgenic control and polylysine mutant, respectively. (C.) Control with overlay of example measurements used to determine vesicle distributions. Black lines represent measurement from center of a small clear vesicle to the cytoplasmic leaflet of the plasma membrane. Yellow lines mark a 150 nm region of presynaptic membrane on either side of the T-bar that we defined as the active zone regions (Loewen, Lee at al., 06). Synaptic vesicle distribution measurements were obtained from this region. Only vesicles whose centers lay within 200 nm from the marked active zone membrane were included in measurements. (D.) Total plasma membrane length and (E.) total number of SVs analyzed per active zone is shown for WT control and polylysine mutant.

C_2B Polylysine Motif Does Not Affect Synaptic Vesicle Docking

The distribution of synaptic vesicles in the vicinity of active zones reveals that there is no difference between the polylysine motif mutant and WT control across all distances from the

presynaptic membrane (Fig. 2-4). More specifically, analysis of the 0-23 nm bin demonstrated that there was no difference between the wildtype and polylysine mutants in the number of vesicles that were immediately adjacent to the plasma membrane ("docked" vesicles, $p = 0.49$). This result establishes that the polylysine motif is not required for docking of vesicles at the presynaptic membrane.

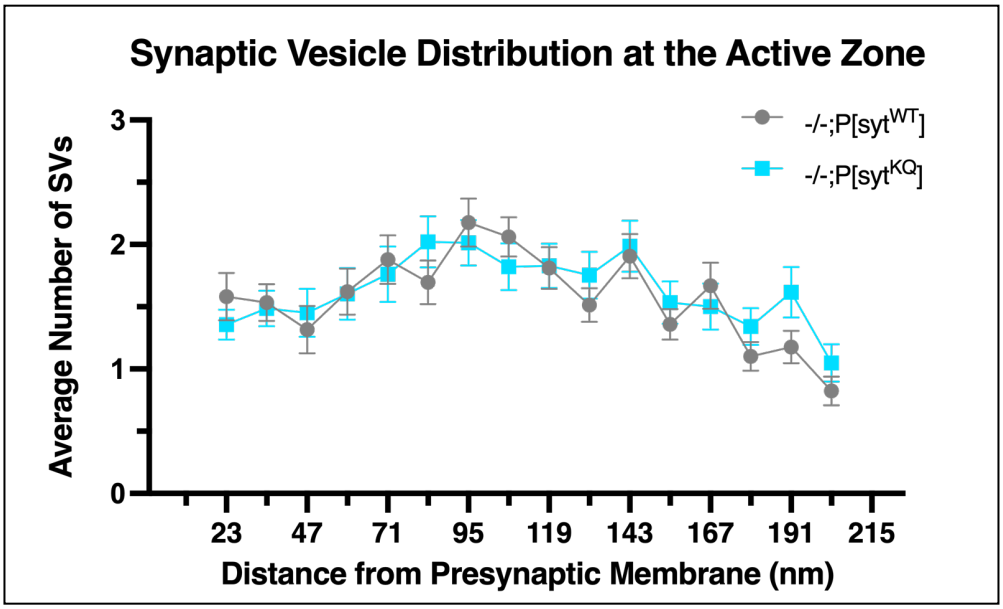

Figure 2-4. *Synaptic Vesicle Distribution at the Drosophila NMJ Active Zone*

Comparison of small clear synaptic vesicle distribution at active zones for WT control versus polylysine mutant. The distance of the small clear synaptic vesicles from the presynaptic membrane was binned for both genotypes. No significant differences were found (P-value range 0.49-0.62).

C_2B Polylysine Motif Likely Plays a Role in Synaptic Vesicle Priming

In the present study, we build on previously-established characterizations of the synaptotagmin C_2B polylysine motif in *Drosophila*. Loewen, Royer, et al. (2006) demonstrated that when the polylysine motif is mutated to glutamines, there is an ~40% decrease in evoked neurotransmitter release. Originally, this decrease in evoked release was thought to result from a disruption in synaptic vesicle endocytosis based on the finding that the C_2B polylysine motif

interacted with the clathrin adapter protein, AP-2 (Chapman et al., 1998; Haucke & De Camilli, 1999; Haucke et al., 2000; Littleton et al., 2001; Zhang et al., 1994). However, Loewen, Lee et al. (2006) demonstrated that the polylysine mutant did not affect the rate of vesicle endocytosis. Additional biochemical analyses from the Südhof lab suggested that the apparent interaction between the C_2B polylysine motif and AP-2 may be an artifact caused by nucleic acid contamination (Ubach et al., 2001). Yet a different lab still found AP-2 binding was disrupted by the C_2B mutation (Jarousse & Kelly, 2001). To address this controversy, we analyzed AP-2 binding to synaptotagmin C_2 domains and found that AP-2 does bind to the C_2B domain of synaptotagmin, but this interaction was not disrupted by mutating the polylysine motif (see Fig. 2-2B). Thus, we confirm, at least in *Drosophila*, that the C_2B polylysine motif does not bind AP-2 consistent with the finding that this motif does not play a role in vesicle endocytosis (Loewen 2006).

Further, Loewen, Royer, et al. (2006) demonstrated that the C_2B polylysine motif does not disrupt the Ca^{2+} cooperativity of release. Yet it does slow the rate of recovery to baseline levels of evoked release following high frequency stimulation. Together, these data suggest that the polylysine motif functions during a Ca^{2+} independent stage of the vesicle cycle somewhere after endocytosis and before Ca^{2+}-dependent vesicle fusion, leaving vesicle docking and priming as likely candidates.

Here we demonstrate that synaptic vesicle docking is not impacted because the number of docked vesicles at the active zones of the polylysine mutant did not differ from that found in the active zones of the WT control. This is in direct contrast to a recent study in mice where the authors found that in <u>both</u> syt^{null} mutants and in C_2B polylysine mutants there was an ~50% decrease in the number of docked vesicles (S. Chang et al., 2018). Since it has been suggested

that a rapid freeze/freeze substitution preparation is necessary to measure synaptic vesicle docking (Fouquet et al., 2009; Rostaing et al., 2006), we wanted to address any concern regarding the chemical fixation used in this study.

Docking Deficits are Detectable using Chemical Fixation Electron Microscopy

To demonstrate that our fixation protocol is appropriate for measuring docking, we compared our docking results to the data from a previous publication, Loewen, Royer, et al. (2006) [Fig. 2-5 black bars and cross-hatched bars], where vesicle docking in syt^{null} mutants was assessed using the same chemical fixation procedure. In both studies, docked synaptic vesicles were defined as those whose centers were within 23 nm from the cytoplasmic leaflet of the presynaptic membrane. We normalized the data from Loewen et al. 2006 to either the true wild type control (Fig. 2-5A, +/+) or the transgenic wild type control (Fig. 2-5B, P[syt^{WT}]) to permit a direct comparison with the current results. At the *Drosophila* neuromuscular junction, Loewen, Royer, et al. found an ~50% decrease in the number of docked synaptic vesicles in syt^{null} mutants (Fig. 2-5A, white cross-hatched bars, -/-) compared to both true wild type (Fig. 2-5A, black bars, +/+) and transgenic wild type (Fig. 2-5A, grey cross-hatched bars P[syt^{WT}]) controls. This result is approximately equivalent to the docking deficit found by S. Chang et al. (2018) at synapses in cultured hippocampal neurons from wild type and syt^{null} mutant mice. Importantly, a side-by-side comparison of the data from Loewen, Royer, et al. and the present study normalized to the transgenic control demonstrates that our fixation protocol does reveal a significant decrease in vesicle docking in the syt^{null} mutant (Fig. 2-5B, white to grey cross-hatched columns, 0-23 nm bins) that is not observed in the polylysine mutant (Fig. 2-5B, blue to grey columns, 0-23 nm bins).

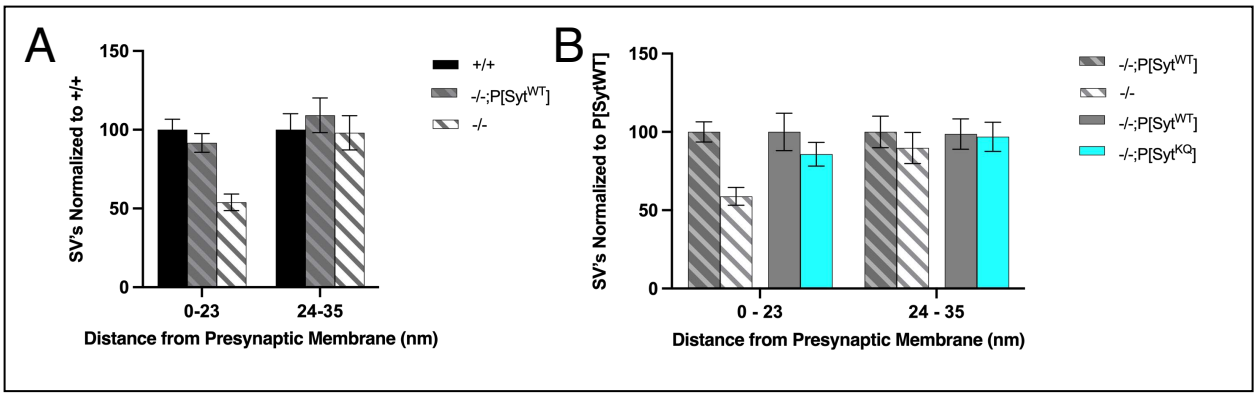

Figure 2-5. *Detection of Docking Deficits Using Chemical Fixation*

(A.) *Data re-graphed from Loewen et al 2006 show that our fixation protocol detected an ~50% decrease in the number of synaptic vesicles (SVs) within 0–23 nm from the presynaptic membrane in synaptotagmin null mutants (-/-) compared to both a true wild type control (+/+) and a transgenic wild type control (-/-;P[syt^{WT}]). Data were normalized to the true wild type control. (B.) Side-by-side comparison of data from Loewen, Royer, et al. (2006) and the present study normalized to the transgenic wild type control (-/-;P[*syt^{WT}*]) showing the percentage of SVs in the two bins closest to the presynaptic membrane. A 46% decrease in vesicle docking (0–23 nm bin) is clearly seen in synaptotagmin null mutants *(-/-) when normalized to the transgenic wildtype *(-/-;P[syt^{WT}], P =0.001), and yet is *not* seen in the polylysine mutants (-/-;P[Syt^{KQ}]) when normalized to the transgenic wildtype (-/-;P[syt^{WT}], P = 0.49).

*Data adapted from Loewen, Royer, et al. (2006).

Therefore, our chemical fixation methods are reliable for detecting docking deficits and we can be confident that we would be able to detect a docking deficit if one were present. Additionally, since 70 nm thin plastic sections were used for imaging, and the average diameter of larval synaptic vesicles is 35 ± 5 nm (Loewen, Lee et al., 2006), it is likely that many vesicle profiles do not capture the entire vesicle within the electron micrograph. Instead, it is likely that many profiles only represent a portion of the vesicle. Accordingly, our method of measuring from the presynaptic membrane to the center of each vesicle avoids any error that might be caused due to partial vesicle profiles. Since the results from Loewen, Lee et al., 2006, suggest a deficit in a Ca^{2+}-independent vesicle trafficking and we show here that docking is not disrupted, we

hypothesize that the decrease in evoked transmitter release reported for the C_2B polylysine mutant is due to a deficit in vesicle priming at the active zone.

Synaptotagmin's documented interactions with PIP2 pose a likely mechanism to synaptotagmin's role priming (Bai et al., 2004; Li et al., 2006, Madziva et al., 2005, Osborne et al., 2007, Voleti et al., 2017; Wang et al., 2017, Zhu et al., 2022). Additionally, some of the lysine residues within the C_2B Polylysine series have been shown to bind calcium channels *in vitro*, suggesting the motif plays a role in localizing synaptotagmin closely to calcium channels (Charvin et al., 1997; Sheng et al., 1997), which could affect the rate at which vesicles fuse with the membrane following calcium influx. Thus, if this physical interaction localizing calcium with the C_2B domain of synaptotagmin were impaired, evoked transmitter release could be as well.

CHAPTER 3: A METHOD TO QUANTITAVELY MEASURE SYNAPTIC VESICLE DOCKING AND PRIMING USING ELECTRON TOMOGRAPHY IN *DROSOPHILA*

Introduction

Significance of the Protocol

Until very recently, there has not been a way to directly measure morphological vesicle priming because the three-dimensional (3D) resolution limitations (~50 nm in the Z-plane) of standard electron microscopy has limited our ability to identify the spatial relationships between docked vesicles and the presynaptic membrane. A method to assess synaptic vesicle docking and priming using electron tomography has been established at frog neuromuscular junctions (Jung et al., 2016). However, frogs are not amenable for the genetic experimentation that has proven to be extremely valuable for determining the molecular mechanisms of biological processes. *Drosophila melanogaster*, on the other hand, is a widely-used model system for genetic manipulations. The protocol outlined herein presents a unification of *Drosophila* as a genetic model system, with the ultra-high spatial resolution of electron tomography developed in frog for the assessment of synaptic vesicle docking and priming.

Background

Neurotransmitters are stored in synaptic vesicles that fuse with the presynaptic membrane at "active zones," sites specialized to mediate this fusion event (Couteaux and Pecot-Dechavassine, 1970; Dryer et al., 1973; Zhai and Bellen, 2004; Sudhof, 2012, 2013; Szule, 2021). Synaptic vesicles must first be docked and primed with the presynaptic membrane prior to fusion (Sudhof, 2004; Sudhof and Rizo, 2011; Szule and Coorssen, 2003, Bennet et al., 1992). Proteins required for each of these steps are highly concentrated at the active zone and

specifically organized into active zone material ([AZM]; see Fig. 3-2; Rizo, 2022; Szule, 2021; Slater, 2015;). Previous experimentation has revealed some of the functional roles of several proteins concentrated at active zones. The SNARE proteins mediate the vesicle fusion event (Schiavo et al., 1997; Sauvola and Littleton, 2021; Szule and Coorssen, 2003; Sutton et al., 1998; Karmaker et al., 2019), while synaptotagmin is the essential Ca^{2+} sensor for triggering fusion (Brose et al., 1992; Bommert et al., 1993; Geppert et al., 1994; Desai et al., 2000; Mackler et al., 2002). Determining the precise location and morphological relationships of each AZM protein is prerequisite to deciphering the molecular mechanisms mediating docking, priming and fusion of synaptic vesicles (Slater, 2015; Szule, 2021; Rizo, 2022). Unfortunately, the location of these essential proteins within the AZM remains unknown partially due to the three-dimensional (3D) resolution limitations of standard electron microscopy (~50 nm in the Z-plane, due to thickness of the tissue section). Electron tomography is a technique that capitalizes on the powerful magnification and resolution of the electron microscope combined with 3D tomographic reconstructions (Ress et al., 1999; Harlow et al., 2001, Ress et al., 2004; Lucic et al., 2005; Barcena and Koster, 2009; Szule et al., 2015). Recent advances in electron tomography permit the analysis of 0.5 nm virtual slices through a single 50-70 nm sample, enabling a 3D rendering of the sample in all three planes (Szule et al., 2012; Harlow et al., 2013; Jung et al., 2016). However, the methods of sample preparation, data acquisition and data analysis for high-resolution electron tomography are extremely intricate (see Fig 3-1) and must be optimized for the materials involved (see discussion).

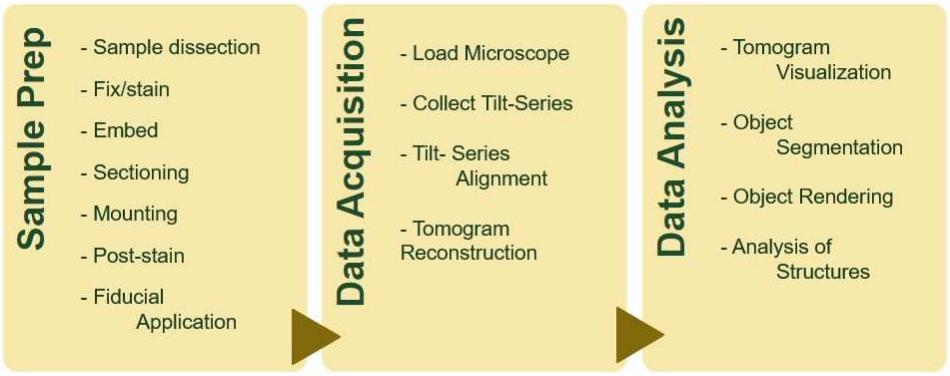

Figure 3-1. *Overarching methodology phases for high-resolution electron tomography*.

Electron tomography involves sample preparation, data acquisition and data analysis. Careful attention needs to be taken at every step of the methodology to successfully reconstruct high-resolution electron tomograms.

Only recently, using high-resolution electron tomography, has the 3D active zone ultrastructure of mouse and frog been determined at a sufficient level of spatial resolution (2-3 nm) to begin assessing functional relationships (Szule et al., 2012; Harlow et al., 2013; Jung et al., 2016). Nevertheless, there remain major limitations to protein identification because frogs are not amenable to genetic tagging, while mice are costly, time consuming, and less thoroughly developed for electron tomography as compared to the frog. The fruit fly, *Drosophila melanogaster*, is an extensively utilized genetic model system that is also relatively inexpensive and rapid. However, tomography in the fruit fly is in its infancy and has yet to be done with sufficient resolution to render a clear 3D reconstruction of the active zone and its macromolecular structures (compare Fig. 3-2B to Fig. 3-2A; Szule et al., 2012; Bruckner et al., 2017).

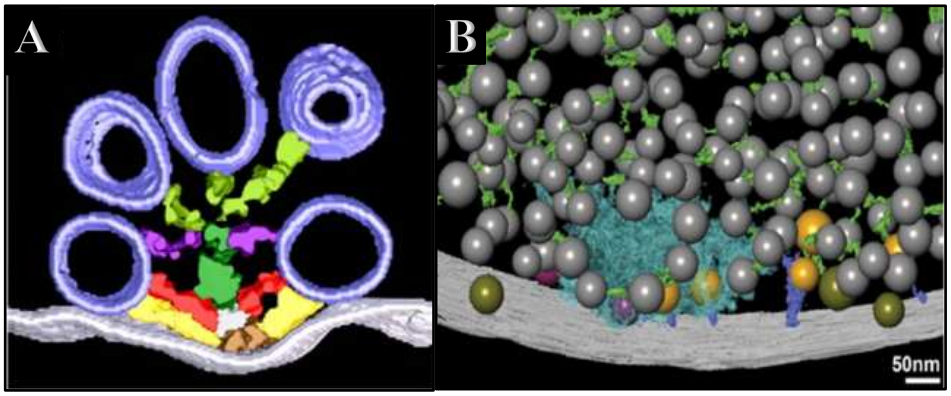

Figure 3-2. *Schematic 3D Reconstructions of the AZM at the Frog and Fly NMJs by Electron Tomography*

(A.) Frog: vesicles (blue spheres) and AZM (yellow, brown, white, green, red, and purple structures). (B.) *Drosophila*: vesicles (gray and gold spheres) surrounding a convoluted AZM (light blue). Images used are from Szule et al. (2012) and Bruckner et al. (2017), respectively.

The protocol presented here was developed specifically to prepare *Drosophila* larval neuromuscular junctions (NMJs) for electron tomography with the 2-3 nm spatial resolution necessary to assess morphological relationships at the neuromuscular junction. Within this protocol, I outline the intricate steps of sample preparation specific to NMJs in *Drosophila* L3 larvae (see Supplemental-1) and discuss key considerations during tissue preparation (see Discussion). Data acquisition methods are highlighted, and challenges related to microscope capability, image file size/type, and tilt-series alignment are addressed. The methods presented here used the software package, EM3D, for tilt-series alignment, tomogram reconstruction, and object segmentation/rendering. Strengths and challenges of EM3D are addressed in the discussion.

Materials and Methods

See Supplemental-1 for sample preparation, fixation, sectioning, and post-staining protocols. See Supplemental-2 for ImageJ, Excel, and Mathematica macros.

Tilt Series Acquisition

Datasets consisting of a series of tilt-images were collected using one of three electron microscopes designed for automatic data acquisition, which were: (a) an FEI Tecnai G2 F20 TEM with a 2048x2048 Gatan Tridiem GIF-CCD; (b) an FEI Tecnai F20 FEG-TEM equipped with a Gatan K3 4k direct electron detector and Gatan US4000 CCD cameras; and (c) an FEI Tecnai F30 FEG-TEM equipped with a Gatan K2 Summit 4k direct electron detector and Gatan OneView IS 4k CCD cameras.

Electron microscopes must be equipped with a beam blanker. Beam blanking occurred for 0.4-0.8 seconds per image, just before image capture. The beam blanking duration was adjusted for higher tilt ranges based on amount of drift appearance. Beam blanking is an absolutely essential step, generally not mentioned in methods sections, that is required to reduce the appearance of drift within individual images. Without beam blanking, projection images within a tilt-series appeared blurry, as if the section was drifting in the microscope. By beam blanking, energy absorbed by the plastic section from the electron beam was given time to dissipate before image capture, thus reducing the appearance of drift. To reduce shrinkage of the plastic sections due to electron beam exposure, the stage/specimen holder/specimen in each microscope was cooled to liquid nitrogen temperatures.

A tilt-series, for a given dataset, was composed of projection images taken in a dose-symmetric manner at 1° tilt intervals (i.e., 0°, -1°, +1°, -2°, +2°, etc.) to ±60° along a single tilt axis. Dual axis tilt-series were collected but were not used in reconstructions (see Chapter Summary). Electron dosage per tilt-series collected ranged from 30e-/tilt image to 89e-/tilt image, depending on contrast of staining within the sample. An upper limit of electron dosage of 100e- per tilt image was used (see discussion). The tilt-series were collected at magnifications

ranging from 32,000X to 120,000X, depending on the size, location, and appearance of the active zone. Tilt-series acquisition was restricted to active zones that had a clearly visible, electron dense T-bar and good visibility of the plasma membrane leaflets. If the T-bar or plasma membrane were not clearly visible, the site was not imaged. Only neuromuscular junctions on muscle fiber 6 in muscle segments 3 and 4 were imaged, as is NMJs on muscle fiber 6 are the standard in neuromuscular junction studies in *Drosophila*.

Reconstruction of Electron Tomograms Using EM3D

To enable this phase of the methodology, 5 nm or 10 nm gold colloid beads were applied to grids prior to tilt series acquisition (see Supplemental-1 for application). Images within a tilt-series were automatically aligned using the gold colloid as fiducial markers (see Fig. 3-3, left panel for individual projection image showing the 5 nm gold beads). Once images had gone through automatic alignment, the alignment error was recorded. If the alignment error was greater than 1 px, it was reprocessed until a suitable alignment error of $\leq$ 1 px was obtained. If an alignment error of $\leq$ 1 px could not be obtained, the dataset was not used.

Following alignment, reconstructions were created in EM3D using a weighted back-projection method. Both the automatic alignment and reconstruction algorithms are in the unified software package for electron tomography, EM3D (em3d.org; Jung et al., 2016; Ress et al., 2004; Szule et al., 2012). Spatial resolution of datasets was 2–3 nm, as previously calculated in Ress et al. (2004).

Segmentation of Structures Using EM3D

Reconstructions were composed of 1 voxel thick virtual slices through the tissue section (see Fig 3-3 right panel, for example virtual slice from a tomogram). The virtual slice thickness is equivalent to the pixel size within the tilt series images (unless the images were decimated),

which varied depending on the magnification used. Using these methods, the virtual slice thickness we obtained per dataset ranged from 0.116–0.63 nm.

Stained structures within the tissue section appear as electron dense, or dark, structures within the reconstruction (see Supplemental-1 for more information on sample fixation and staining). Heavily-stained structures within the reconstructions were segmented to define volumes-of-interest (VOIs) using both manual and semi-automatic methods in EM3D (Ress et al., 2004). VOIs were segmented, throughout the volume, based on their greyscale within all three spatial planes (XY, ZY, YZ). EM3D was designed specifically for segmentation of objects at the neuromuscular junction of frog. Accordingly, the manual and semi-automatic segmentation tools in EM3D have features suited specifically for structures within active zones (membranes, filaments). For example, the segmentation tools include a closed loop tool ideal for segmenting vesicles, an open loop tool ideal for segmenting plasma membranes and a manual tool for structures with more complex/unknown geometry. Further, the segmentation tools use anchor points, an adjustable search area and adjustable grey scales which enable the user to match the size, shape and staining of a particular object. Careful attention must be paid to the size of the segmentation search area and the minimum and maximum greyscale settings of the segmentation search areas to maximize the amount of staining included while minimizing noise. The presynaptic membrane and vesicles are heavily stained and have a simple geometry, so the semi-automatic segmentation method was used most frequently. The presynaptic membrane and vesicles adjacent to the membrane were carefully segmented as individual VOIs. Special attention was paid to vesicles in contact with the presynaptic membrane to ensure the VOIs were not significantly overlapping within the virtual slices. Attention was also paid to ensure the segmentation followed the staining of an object in all 3 cardinal planes. This prevented the

segmentation of artifacts, for example, “shadows” cast from objects within the plastic section during imaging.

Visualization of VOIs for Measurements

Once VOIs were segmented, an overlay of the segmentation could be visualized over the virtual slice. This method of visualizing the segmentations was used to take measurements of the segmented structures (see Fig. 3-5B). EM3D has a simple line tool that can provide the length for a line drawn. However, there is no way to record multiple length measurements within EM3D. Therefore, the virtual slices with the segmentations overlayed were exported as an image stack and then imported into FIJI (an Image Processing package of ImageJ; https://fiji.sc) for making and recording measurements. The pixel size from EM3D was recorded for each dataset and set as the scale in FIJI. In FIJI, simple macros that record measurements on consecutive images within a stack were utilized (see Supplemental-2).

Measurements to Assess Vesicle Docking and Priming

To quantitatively assess the spatial relationship of docked synaptic vesicles with the presynaptic membrane, we measured vesicle membrane (VM) thickness, presynaptic membrane (PM) thickness, the combined thickness of the VM and PM (VM-PM) throughout the contact site, and the length of the VM-PM contact site in each virtual slice throughout the volume (see Fig. 3-5B). Vesicles were defined as docked if the VM and PM segmentations were in direct contact with each other at any point through the volume's depth (Jung et al., 2016).

Once image stacks of the virtual slices with overlaid segmentations were imported into FIJI, measurements were taken using the line tool. Membrane thickness measurements were made by drawing a line from the outer edge of the segmentation to the inner edge of the segmentation, perpendicular to the membrane angle. (see Fig. 3-5B, red lines – one thickened for

easier viewing) This was done for the VM and PM beyond the area of contact. At the area of contact, the combined VM-PM thickness was measured by drawing a line from the outer edge of the PM segmentation to the inner edge of the VM segmentation (see Fig. 3-5B, red lines within the orange box). To calculate the extent of the VM-PM contact, a line was drawn and measured across the full length of the contact site, between the VM and PM, in each virtual slice (see Fig. 3-5B, yellow line). The VM-PM contact length measurements, from each virtual slice, were then used to estimate the total VM-PM contact area. This was calculated by taking the contact length in each virtual slice and multiplying by the thickness of the slice. Then, the sum of all contact areas from all slices was calculated. The calculated contact area was then superimposed over a rendering of the PM at the site of contact (see Fig. 3-5D; Fig. 3-7, second row). A spline fitting was applied using a custom macro in Mathematica (see Supplemental-3) to provide a better estimate of the true VM-PM contact area (see Fig. 3-7, third and fourth rows).

Results

Following this protocol, we were able to collect clear projection images (e.g., Fig. 3-3, left panel), and accordingly, high-resolution electron tomograms, composed of multiple virtual slices (e.g., Fig. 3-3, right panel), of active zones at the *Drosophila* NMJ. To demonstrate the utility of the described protocol, examples tomograms of the *Drosophila* NMJ, segmented objects within the tomogram (presynaptic membrane, synaptic vesicles), and example measurements (membrane thickness, contact area) collected from tomograms are provided in the following sections.

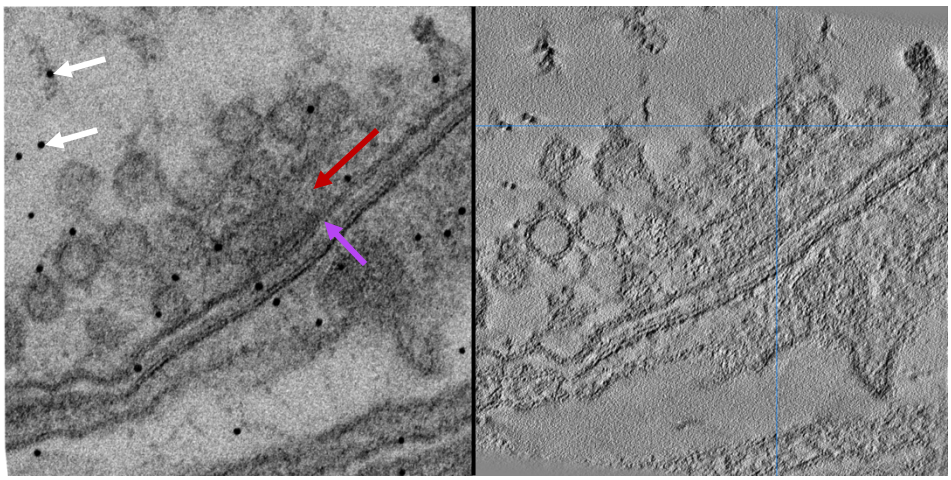

Figure 3-3. *Projection image and tomographic virtual slice at a Drosophila active zone*

Left Panel: A single electron micrograph of a *Drosophila* NMJ active zone in a 70 nm plastic section, taken at 0° tilt. A cloud of vesicles can be seen surrounding the electron-dense T-Bar (red arrow). The T-Bar is closely associated with the presynaptic membrane which possesses "railroad track" staining (purple arrow), stereotypical of phospholipid bilayers. Round, 5 nm gold colloid beads (white arrows) can be seen scattered across the micrograph. Right Panel: A single 0.54 nm thick virtual slice from a 45 nm thick tomogram of the same active zone. The visibility of structures within the virtual slice is not hindered by objects within the thickness of the section as in the left panel.

Tomogram of an Active Zone at a Drosophila NMJ

The tomograms collected using the described protocol contain clear, high resolution (0.54 nm voxel size) examples of the *Drosophila* active zone (e.g., Fig. 3-4). The T-bar, a distinctive characteristic of the *Drosophila* AZM, was highlighted (not segmented) in red to aid in visualization (Fig. 3-4B). In close proximity to the T-bar, there is a visible docked vesicle (Fig. 3-4B,C, green segmentation) in contact with the plasma membrane (Fig. 3-4B,C, blue segmentation). A characteristic cloud of undocked vesicles (e.g., 3-4A,B white arrows; Fig. 3-4B,C, yellow segmentations) can also be seen surrounding the T-bar. Within the example provided, the pre-synaptic and vesicle membranes are distinct, as seen by the "railroad track" staining pattern, typical of lipid bilayers (Fig. 3-4A).

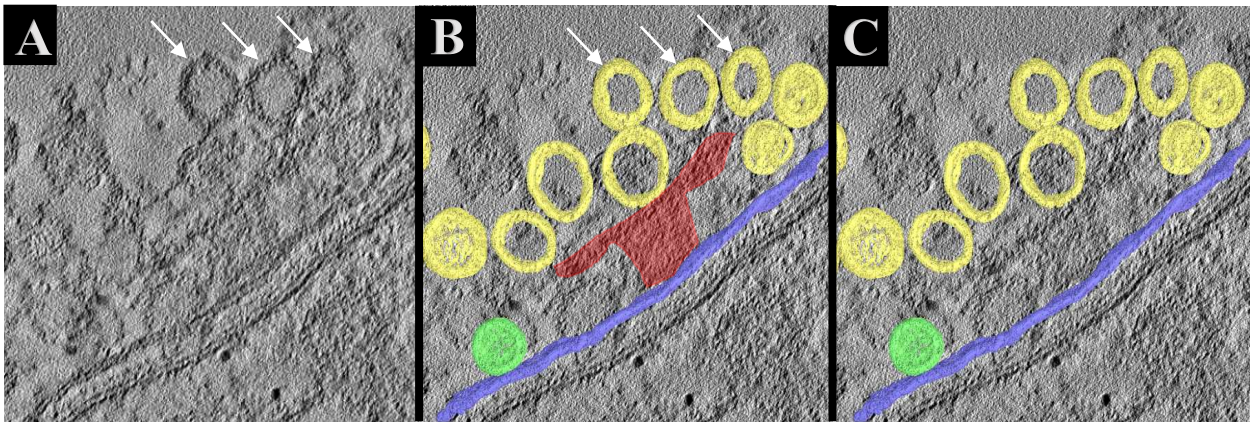

Figure 3-4. *High-Resolution Tomogram of an Active Zone at a Drosophila NMJ*

Panel A: A single 0.54 nm thick virtual slice from a 45 nm thick tomogram. Panel B and Panel C: Object segmentations from all 84 virtual slices in the tomogram are superimposed on the individual slice shown in Panel A. The T-bar is highlighted (not segmented) in red in Panel C for visualization. White arrows indicate stained cross-section of vesicles. Object segmentations include a docked vesicle (green), presynaptic plasma membrane (blue), and undocked vesicles (yellow).

Quantitative Assessment of Morphological Structures Within Tomograms

Measurements on virtual slices were used to quantify membrane thickness of the vesicle membrane (VM; Fig. 3-5B, red lines, one thickened to aid visualization) and the plasma membrane (PM; Fig. 3-5B, red lines) beyond the site of the VM-PM contact. The VM-PM contact was further assessed by: (a) measuring the combined thickness of the VM-PM through the site of contact (Fig. 3-5B, red lines within orange highlighting) and (b) measuring the extent of the VM-PM contact length on each virtual slice (Fig. 3-5B, yellow line) through the volume. VM-PM contact area can then be visualized by mapping the contact length by virtual slice thickness for each slice onto the 3D rendering of the PM in the region of the VM-PM contact site (Fig. 3-5D).

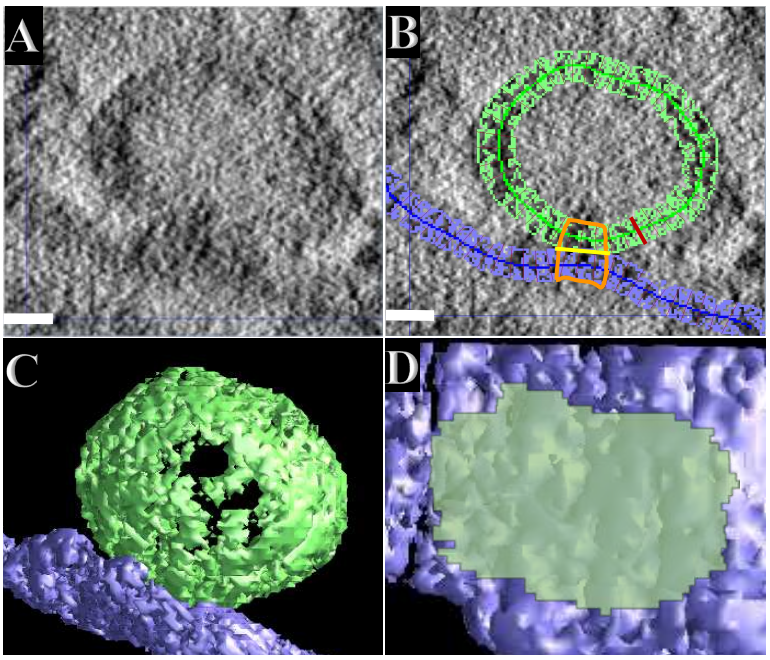

Figure 3-5. *Example Tomographic Measurements*

(A.) A single 0.54 nm virtual slice showing electron dense staining of a docked vesicle and the presynaptic plasma membrane. (B.) Segmentations from this slice are shown for the vesicle (green) and plasma membrane (blue). Membrane thickness measurements (e.g., red line), vesicle membrane plus plasma membrane contact region (orange highlight), and the VM-PM direct contact length (yellow line) are indicated. (C.) 3D rendering of a docked vesicle and PM from 65 virtual slices. (D.) The contact area between the docked vesicle membrane and plasma membrane from multiple (32 in this case) virtual slices is shown. Contact area (green) is superimposed onto 3D PM rendering (blue).

The frequency distribution of membrane thickness measurements was graphed (Fig. 3-6). Shown are the distributions of a) VM thicknesses (Fig. 3-6, green) and PM thickness (Fig. 3-6, blue) beyond the contact site, b) the combined VM-PM thicknesses at the area of contact (Fig. 3-6, orange), and C) a simulated sum of the VM and the PM thickness measurements (Fig. 3-6, white) obtained by randomly adding VM and PM measurements away from the contact area. Because the sample size of VM-PM measurements was low, a bootstrap test was run with a sample size of 10,000 to increase the statistical power of our VM-PM thickness comparisons. The average VM thickness and PM thickness beyond the contact site was 7.2 ± 1.1 nm and 7.7 ±

1.0, respectively, similar to other membrane thicknesses measurements (Jung et al., 2016, Yamamoto, 1963). The average combined VM-PM thickness at the area of contact (Fig. 3-6, orange) was 14.5 ± 1.3 nm, similar to measurements in the frog (Jung et al., 2016). The average simulated sum of the VM and the PM thickness measurements (Fig. 3-6, white) was 14.9 ± 1.5. The average measured VM-PM thickness was not significantly different from the simulated sum ($p = 0.982$). Consistent with the findings in frog, this data suggests that the vesicle and plasma membranes are in direct contact with each other (i.e., no measurable gap between them where VM-PM thickness would be greater than the simulated sum), and are not in a state of hemifusion (where the VM-PM thickness would be less than the simulated sum).

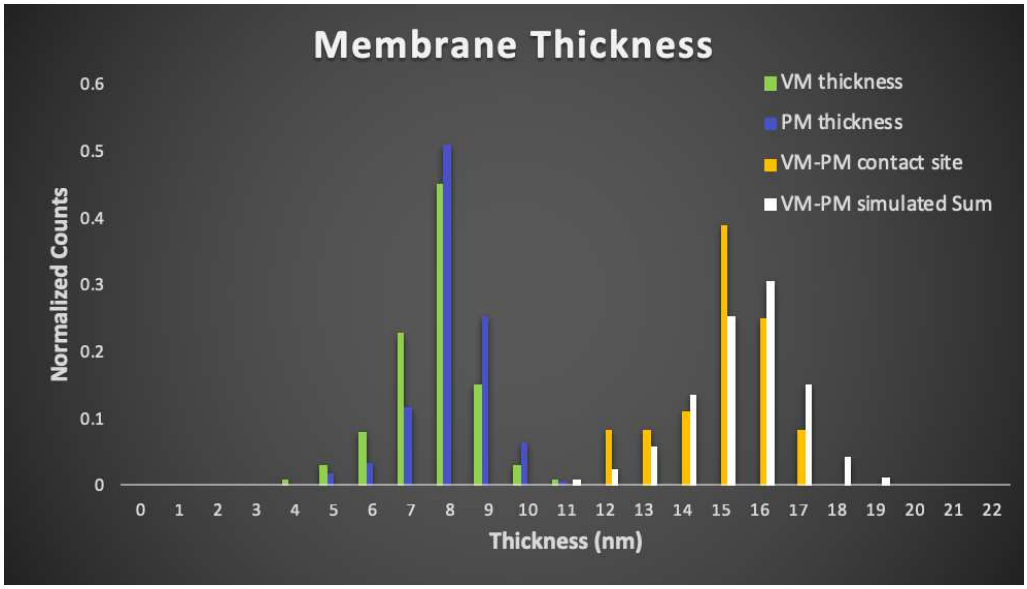

Figure 3-6. *Frequency Distributions of Membrane Thickness Measures*

The thicknesses of the VM (green) and PM (blue) away from the area of contact are graphed. The thicknesses of the VM-PM at the contact site (orange) and the simulated sum (white) of VM and PM thicknesses away from the contact site are graphed.

Once docked vesicles were fully segmented and measurements were taken, the 3D renderings of docked synaptic vesicles and their associated presynaptic membrane were captured as images in EM3D using screenshots (Fig. 3-7, first row). For each docked vesicle, the total

contact area was calculated and superimposed onto the PM rendering (Fig. 3-7, second row). The contact area estimated by this process appears to be jagged, inconsistent with the smooth, elliptical nature of synaptic vesicles. This jagged appearance is most likely an artifact of incomplete staining in individual virtual slices (see discussion). To correct for this, a spline fitting was applied using a custom macro in Mathematica to provide a better estimate of the true VM-PM contact area. The spline fitting for each docked vesicle was then superimposed onto a capture of the presynaptic membrane rendering at the site of contact (Fig. 3-7, third row). The corresponding contact area from Mathematica was recorded for each vesicle (Fig. 3-7, fourth row).

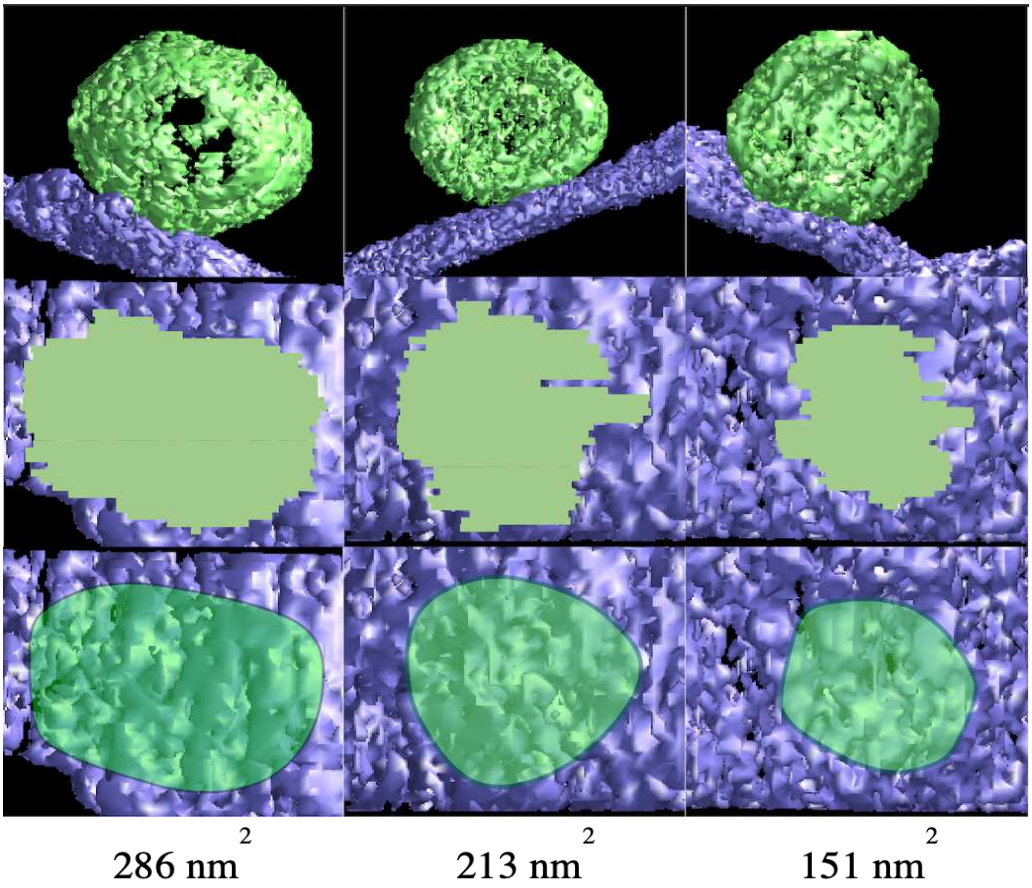

Figure 3-7. *VM-PM Contact Area for Three Docked Vesicles*

First Row: 3D renderings of docked vesicles. Second Row: Contact areas

constructed from contact length measurements in individual virtual slices superimposed onto 3D PM renderings. Third Row: Contact areas smoothed by spline fittings superimposed onto 3D PM renderings. Fourth Row: Contact area calculated from spline fittings, from left to right, are 286 nm^2, 213 nm^2, and 151 nm^2, respectively.

Importantly, the VM-PM contact areas calculated from active zones at the *Drosophila* neuromuscular junctions, to-date, fall within the range of values seen at the frog neuromuscular junction (Jung et al., 2016). Contact area measurements have been used as a correlate to the degree of priming of synaptic vesicles (Jung et al., 2016). In the frog studies, Jung et al. (2016) found that the VM-PM contact areas for docked vesicles had a normal distribution and the vesicles with the largest VM-PM contact area disappeared upon stimulation. Their studies indicated that the extent of contact area correlated to the degree of vesicle priming, with small areas of contact representing minimal vesicle priming (i.e., vesicles unlikely to fuse upon Ca^{2+} influx) and large areas of contact representing maximal priming (i.e., vesicles most likely to fuse). Should further analysis for VM-PM contact areas in *Drosophila* replicate this finding in the frog, we would be able to use the morphological measure of contact area, described here, to directly test putative priming mutants in *Drosophila*, using electron tomography.

These preliminary results demonstrate that this method of electron tomography in *Drosophila*:

1. Provides a way to unequivocally identify which vesicles are in direct contact with the presynaptic membrane and therefore are docked;
2. Makes it possible to obtain morphological measurements of membrane thickness at VM-PM contact sites to directly test for existence of hemi-fusion of membranes at rest and during activity; and,

3. Allows for the quantitative measurement of the VM-PM contact area of docked vesicles to be used as a correlate of synaptic vesicle priming (varying measurements smaller to larger areas) should a normal distribution, as seen in frog, be found (~75 VM-PM areas per genotype needed).

Discussion

In this protocol, we present methods to achieve 2-3 nm spatial resolution at *Drosophila* melanogaster neuromuscular junctions. In addition to the materials and methods (above), it is important to address some aspects of the protocol where special attention should be paid.

First careful attention should be paid during sample preparation and tilt-series acquisition surrounding the following topics:

1. Osmolarity of fixative and stain – the osmolarity of buffers, fixatives and stain should match the physiologic osmolarity of *Drosophila* hemolymph (342-364 mOsms on average; Begg and Cruickshank, 1963; Albers, et al., 2004; Stewart et al., 1994). If the osmolarity of working solutions is outside of the physiologic osmolarity of *Drosophila* hemolymph, the tissue can shrink or expand during fixing/staining which could impact the physical organization of structures within the tissue. For example, hyperosmotic solutions commonly used during chemical fixation result in the collapse of the T-bar onto the plasma membrane (Fouquet et al., 2009), whereas iso-osmotic fixation (Koenig and Ikeda, 1999) preserves the slight gap seen between these structures when prepared by quick-freeze/freeze substitution (Rostaing et al., 2006; Gray et al., 2006; Siksou et al., 2007; Fouquet et al., 2009).
2. Sectioning resin embedded tissue – section thickness must be carefully chosen

to maximize the availability of ROIs within the tilt-series. We chose to work with 70 nm "thin sections" because they appeared to have consistent contrast of staining when visualized by electron microscopy. In 70 nm sections, there was less obstruction by objects within the tissue section than there would be in thicker sections, which improved visualization of thin, filaments closest to the membrane and vesicle. Most importantly for priming studies, 70 nm sections were thick enough to contain many docked vesicles in which the entire area of contact could be visualized, although area of contact was cut off by the edge of the dataset/plastic section for some. Plastic sections that were 300 nm thick, contained more vesicles which was useful for looking at the contact area of docked vesicles. However, in 300 nm plastic sections, active zones were also obstructed by vesicles and electron dense material within the z plane. This obstruction complicated the visualization of active zones in the microscope prior to data-acquisition, hindered resolution in the z plane of tomograms, and introduced "shadow" artifacts within the tomograms.

3. Post-stain – Post-stain solutions should be applied in a timely fashion to maximize contrast and minimize artifacts from staining (such as lead precipitates).
4. Gold Colloid – should be applied to the same side of the grid as the plastic section. Careful attention should be paid to get an even distribution of gold colloid over the grid (see Fig 3-8, middle panel, for example of even gold distribution). Colloid solution should be shaken to break apart any accumulation of gold fiducials within the solution. If gold fiducials were too

sparse over the ROI, obtaining a tilt-series alignment with a low alignment error proved difficult or impossible (see Fig 3-8, left panel, for example of very little gold distribution). Conversely, if fiducials were too dense or aggregated over the ROI, they obstructed the visualization of structures, and could accumulate too much energy from the electron beam and damage the plastic section during imaging.

5. The electron dosage – the electron beam is powerful and as exposure to the beam increases, the plastic section shrinks. The use of a cryo-stage holder that is cooled to liquid nitrogen temperatures is <u>essential</u> to help minimize shrinkage of the plastic section from electron beam exposure. Additionally, the electron dosage should be monitored during tilt-series acquisition to maximize contrast and minimize noise, without exceeding 100 e-/tilt image or compromising the integrity of the plastic section. If the electron dosage is too high, the heavy metal staining can sublime and redeposit within the section, creating an artifact which presents as a "clumpy" appearance to the stain (see Fig 3-9 Left and Middle panels, for examples of artifact). Note that a higher electron dosage, and the "clumpy" appearance of stain due to sublimation, increase the contrast within the micrographs/tomogram (compare Fig 3-9 Left and Middle panels to the Right panel). However, this increase in contrast is at the expense of the resolution of ultrafine structures such as those at the interface of the vesicle and plasma membrane.
6. Beam-Blanking – a beam blanking step is <u>required</u> to allow time for the charge from the electron beam, within the section, to dissipate, thus reducing

the appearance of drift during image capture (see Fig 3-8, right panel, for an example of drift due to not beam blanking). When describing the appearance of drift to others, I have compared it to a mirage on a hot summers' day which gives objects the illusion of movement.

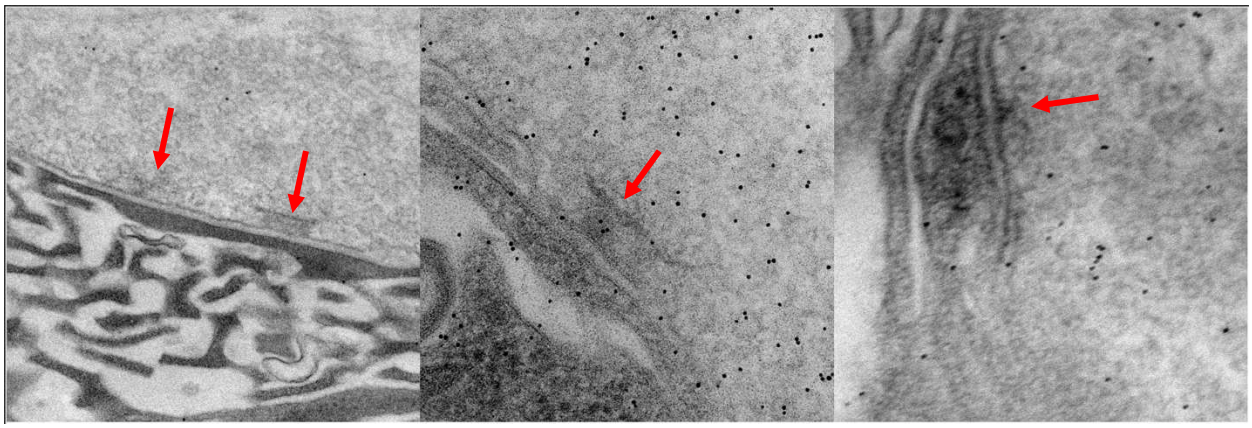

Figure 3-8. *Electron micrographs at Drosophila NMJ Active Zones*

Left Panel: An example electron micrograph of a 300 nm thin plastic section, taken at 29k magnification, with very little gold colloid. Pixel size = 0.619 nm. Middle Panel: An example electron micrograph of a 70 nm thin section, taken at 50k magnification, with good colloid distribution. Pixel size = 0.365 nm. Right Panel: An example electron micrograph of a 70 nm thin section, taken at 50k magnification, with the appearance of drift from not beam blanking. T-Bars indicated by red arrows. Pixel size = 0.365 nm.

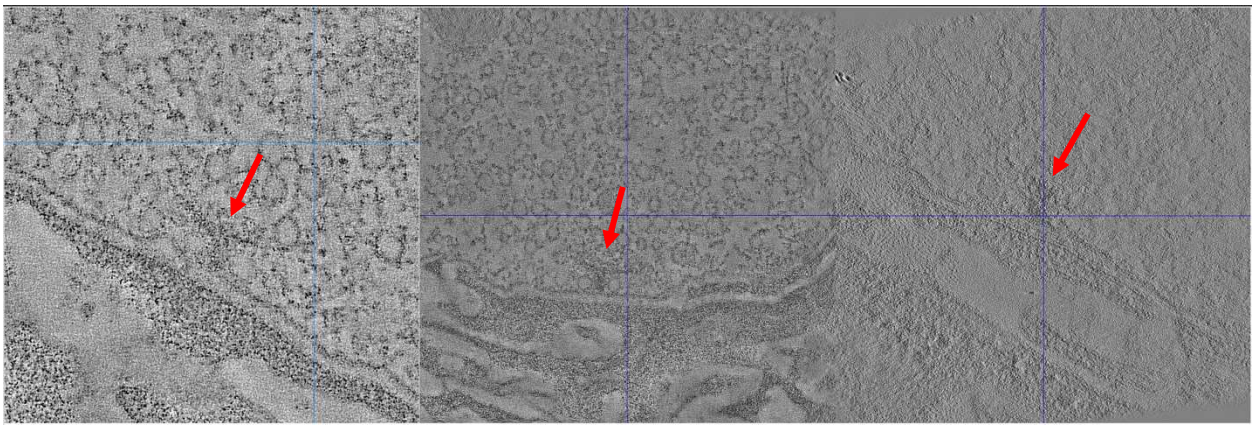

Figure 3-9. *Virtual Slices of Electron Tomograms at Drosophila NMJ Active Zones*

Example tomographic virtual slices with decreasing stain sublimation from left to

right. Left Panel: An example virtual slice, representing 0.619 nm of the volume thickness, contains a T-Bar and has clear "clumpy" stain pattern from sublimation. Middle Panel: An example virtual slice, representing 0.619 nm of the volume thickness, contains a T-Bar and has slight "clumpy" stain pattern from sublimation. Right Panel: An example virtual slice, representing 0.167 nm of the volume thickness, contains a T-Bar and does not exhibit any sublimation of stain. T-Bars indicated by red arrows.

Secondly, careful attention should be paid before, and during, use of EM3D. The EM3D software was specifically designed to analyze the macromolecular architecture at an NMJ and is the only program to date with the capability to segment based on adjusting greyscale (see below). However, there are some caveats to its use. For instance, EM3D has difficulty processing images that are larger than 2k x 2k for alignment and reconstruction. Thus, if projection images within the tilt-series are larger than 2k x 2k, they need to be decimated. There is an option within EM3D to decimate images upon import, but this poses another issue because with decimation, resolution decreases. For example, if you have images that are 4k x 4k with a pixel size of 0.3 nm, and you decimate the tilt series upon import into EM3D, the image resolution will decrease to 2k x 2k with a pixel size of 0.6 nm. To add to its limitations, data exported from EM3D is restricted to a Persistence of Vision Raytracer (.pov) file which is not a widely used (i.e., widely accessible) file format. Lastly, EM3D was only funded from 2003-2007, and Dr. McMahan, whose lab developed and maintained the software, recently retired, so software updates are few and far between (as of October 2023, em3d was last modified on 3/1/2022; http://em3d.org/about.html). Despite EM3D's limitations, it is still the most useful software currently available to assess ultrastructure within the electron tomograms, as discussed below.

While troubleshooting some of the issues mentioned above, I trialed Etomo, a tomographic program in the IMOD software package (https://bio3d.colorado.edu/imod/). Using IMOD and Etomo, I was able to reconstruct tomograms containing sparse, or no fiducials, over

the ROI – something that was not possible using EM3D. However, unlike EM3D, the segmentation tools in Etomo do not base their segmentation of objects on grayscale. Instead, objects are segmented using anchor points and a solid search area around the anchor point. Staining techniques are not perfect and irregularities within heavy metal staining can commonly cause artifacts that appear as "gaps" or "holes" within an object's staining (see Fig 3-10A, yellow arrows for variations in dark staining). To maintain objectivity during segmentation and analysis, it is crucial that an object's segmentation closely matches its staining, and holes within the staining are not included in the object's segmentation (see Fig 3-10B, red arrows, for segmentation that closely outlines staining above the noise threshold). Segmentation within EM3D relies on setting minimum and maximum greyscale, within an adjustable search area, for each object. This feature is extremely advantageous when objects are not clearly defined by consistent, heavy metal staining. Thus, the EM3D user is able to accurately control segmentation to best match the staining as it appears, which is indispensable for maintaining objectivity.

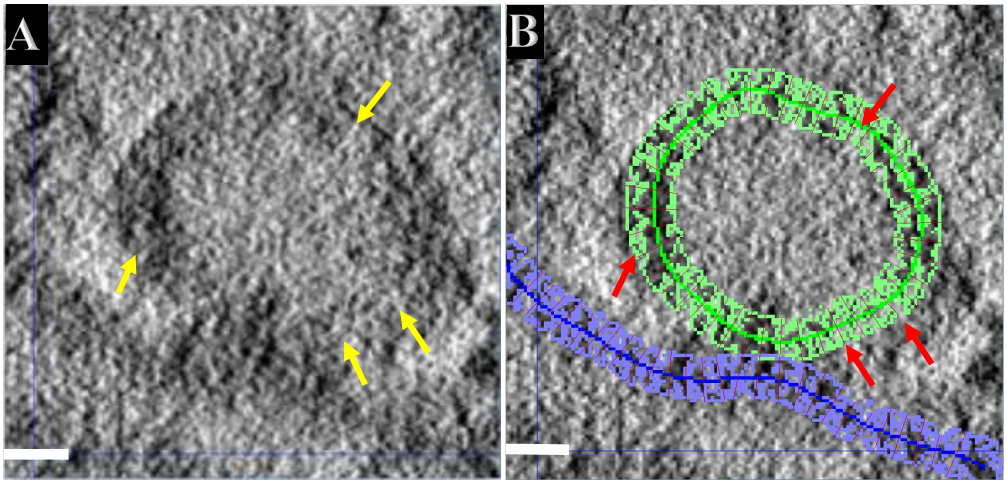

Figure 3-10. *Example Tomographic Measurements*

(A.) A single 0.54 nm virtual slice showing electron dense staining of a docked vesicle and the presynaptic plasma membrane. Staining irregularities resulting in "gaps" or holes" can be visualized (yellow arrows). (B.) Segmentations from this slice are shown outlining electron dense staining for the vesicle (green) and

plasma membrane (blue). Segmentations closely match the object's visible staining and exclude "gaps" or "holes" indistinguishable from noise (red arrows).

Lastly, when analyzing object segmentations and renderings for measurements a couple of things should be kept in mind. When successfully segmented, gaps in an object's staining result in the appearance "holes" within the object's 3D rendering (see Fig 3-5C and Fig 3-7 top row, for renderings of vesicles and membranes with "holes"). Holes in membranes of vesicles and the plasma membrane are not biologically possible and therefore such holes must be artifacts. Conversely, for filaments and undefined structures, gaps in staining/renderings could be biologically relevant and therefore not staining artifacts. Additionally, measurements taken on virtual slices only represent 0.54 nm of tissue, however the spatial resolution is 2-3 nm, thus measurements are taken below the spatial resolution of the tomogram (see Fig 3-5B for measurement examples on one virtual slice). To account for this, we averaged membrane thickness measurements on virtual slices that were 2-3 nm apart in the Z plane.

To account for any artifacts in the VM-PM contact area, caused by staining irregularities in measurements of contact length that were taken on individual virtual slices, we applied a spline fitting to the measurements (see Fig 3-7 second and third row for artifacts from measurements on virtual slices, and spline fittings, respectively). The spline fitting macro that we used in Mathematica smoothed the contact area lengths from each slice into a best-fit elliptical that is more physiologically relevant to vesicles (see Supplemental-3).

Conclusion

To our knowledge, the methods and data presented here are the first to achieve measurements at 2-3 nm resolution (Jiao et al., 2010; Leitinger et al., 2012; Zhan et al., 2016; Bruckner et al., 2017) at a *Drosophila* active zone. By applying this ultra-high level resolution tomography to *Drosophila* synapses, studies that implement this protocol would permit the

structural measurements necessary for the first direct test of molecules hypothesized to enhance vesicle priming. In addition, since *Drosophila* are amenable to transgenic tagging, segmenting the structures of the AZM as well as structures connecting docked vesicles to the presynaptic membrane and T-bars, at 2-3 nm resolution, has the potential to open a whole new field of structural identification of the synaptic molecules critical for intercellular communication in the nervous system. For example, the v-SNAREs and t-SNAREs postulated to mediate vesicle fusion events (Weber et al., 1998; Szule and Coorssen, 2003; Imig et al., 2014; Sudhof, 2014; Sauvola and Littleton, 2021) must be located in structures connecting the vesicle to the presynaptic membrane, yet this has never been shown (Szule et al., 2021; Kusick et al., 2023). Expanding our knowledge of the structure of active zones in *Drosophila* will allow us to capitalize on the powerful capabilities of *Drosophila* genetics to discover functional relationships of the AZM macromolecules at the NMJ. It will also provide insight into the physiological roles of homologous human active zone proteins. The potential avenues for understanding the functional intricacies of the NMJ would be limited only by the human imagination.

Supporting Information

- Supplemental File 1 – Protocol containing sample preparation, fixation, sectioning, and post-staining protocols.
- Supplemental File 2 – Macros used in FIJI and Microsoft Excel.
- Supplemental File 3 – Spline fitting macro for Mathematica.
- Supplemental File 4 – Electron Tomograms of Drosophila NMJ Active zones accessible through the open data publishing platform, Dryad.

CHAPTER 4: DISCUSSION

Many examples within the nervous system highlight the correlation between structure and function. The canonical structure of a neuron supports its function to transmit electrical and chemical information. A chemical synapse's structure allows for the fast, efficient signaling by a neurotransmitter to a post-synaptic cell. The specific lipid and macromolecular composition of synaptic vesicles enables them to dock, and subsequently fuse, with a presynaptic membrane. The overarching goal of my graduate research has been to help unravel the molecular mechanisms of neurotransmitter release by relating structure and function. I accomplished this goal by investigating a functional mutation of the C2B polylysine motif in synaptotagmin (Chapter 2) and by pioneering 2-3 nm resolution tomography in the genetic model, *Drosophila melanogaster* (Chapter 3). Together, my graduate work will permit the structural measurements necessary for the first direct, test of a molecular motif hypothesized to enhance morphological vesicle priming.

In this final chapter, I will discuss my findings, methodology and future directions with emphasis on the investigative power of electron tomography in *Drosophila*. In sum, the spatial dynamics of vesicle docking and priming, and the structure of active zones in *Drosophila* will allow us to capitalize on the powerful capabilities of fly genetics in order to elucidate functional relationships between individual proteins within the AZM macromolecular complexes. It will also provide insight to the physiology of human NMJs through protein homologs.

C_2B Polylysine Motif's Postulated Role in Synaptic Vesicle Priming

Previous research in Dr. Noreen Reist's lab demonstrated that a mutation in synaptotagmin, of the C_2B polylysine motif, results in decreased transmitter release (Mackler et

al., 2001). The decrease in evoked neurotransmitter release could be due to a deficit in any step of the synaptic vesicle cycle. However, findings from Loewen, Lee et al., (2006) suggest that the polylysine motif is implicated in a Ca^{2+}-independent step of the vesicle cycle: endocytosis, docking and/or priming. A pull-down assay in Chapter 2 demonstrates that the polylysine mutant does not affect synaptotagmin's C_2B-mediated interaction with the clathrin adapter protein AP-2, which is inconsistent with a role in endocytosis. Further, Loewen, Lee et al., (2006) found no change in the rate of membrane retrieval in the mutant effectively ruling out a role in endocytosis.

Using standard electron microscopy, I have shown that the number of docked synaptic vesicles is not changed in the polylysine mutant, effectively excluding a deficit in synaptic vesicle docking (Chapter 2). Thus, our current hypothesis is that the C_2B polylysine motif of synaptotagmin enhances synaptic vesicle priming.

Synaptotagmin's documented interactions with inositol phosphates pose a likely mechanism for synaptotagmin's role in priming (Bai et al., 2004; Li et al., 2006, Osborne et al., 2007, Voleti et al., 2017; Wang et al., 2017, Zhu et al., 2022; Mizutani et al., 1997; Rickman et al., 1994). Specifically, the C2B polylysine motif has been documented to (a) mediate the interaction between sytnaptotagmin and PIP2, proposed to facilitate the close apposition of vesicle and target membranes (Bai et al., 2004); and (b) mediate synaptotagmin's interaction with syntaxin/SNAP-25 complex proposed to facilitate priming (Rickman et al., 2004). Future studies will aim to elucidate the polylysine motif's role in vesicle priming and how this relates to the functional interactions of synaptotagmin.

Defining Synaptic Vesicle Docking and Priming

Ideally, any future studies investigating morphological docking and priming would

consider the limitations of standard electron microscopy and account for the physical relationship between vesicles and the presynaptic membrane. When using electron microscopy to assess whether a synaptic vesicle is docked, multiple things should be considered:

1. What is the plastic section thickness?
2. What is the average vesicle diameter?
3. Are the electron-dense AZM projections visible?
4. Is the vesicle visibly connected to the AZM?
5. If the AZM is visible, is the structure known? – Is the entirety of the AZM captured?
6. Is there a discernable gap between the vesicle and the membrane?
7. If there is a discernable gap, is there a visible filament below the vesicle, tethering the vesicle to the plasma membrane?
8. How far away from the AZM, laterally, is a vesicle considered docked?

Taking these points into considerations, and addressing them, when investigating morphological docking could clarify confusions around the spatial variability between vesicles and their associated membrane and therefore would aid in the determination vesicle docking.

Using the enhanced spatial resolution of electron tomography, work in Dr. U.J. McMahan's lab has developed a technique to measure vesicle priming at the frog NMJ (Jung et al., 2016). By measuring the contact area between the vesicle membrane and presynaptic membrane (VM-PM contact area) of docked vesicles, they have shown that this area of contact has a normal distribution (see Fig. 4-1 at rest). Importantly, the vesicles with the largest VM-PM contact area disappear upon stimulation shifting the entire histogram to smaller VM-PM contact areas (see Fig. 4-1 during stimulation). Thus, their data indicates that priming of docked vesicles

is in a state of dynamic equilibrium that can be measured by the VM-PM contact area: the higher the VM-PM contact area, the more "primed" (or likely to fuse upon a Ca^{2+} signal) the vesicle (Jung et al., 2016). Their work was the first, with a sufficient level of spatial resolution (2 nm), to allow this discovery that vesicle priming is dynamic and in equilibrium.

As part of my graduate research, I spent the Spring semester of 2018 as a visiting scholar in Dr. McMahan's lab at Texas A&M. While there, I learned how to do electron tomography in *Drosophila* with the level of resolution that the McMahan lab has previously demonstrated in frog. I also learned how to objectively segment structures using their EM3D software (as presented in Chapter 3). After returning to Colorado State University, I learned that there was only one electron microscope in all of Northern Colorado capable of the high degree of tilt with a cryo-specimen holder. So, I established a collaboration with the Electron Microscopy facility at the University of Colorado, Boulder. Using tomograms of *Drosophila* active zones, collected at the University of Colorado, I have since demonstrated the feasibility of assessing morphological vesicle docking and priming at *Drosophila* active zones. Now, sufficient numbers of tomographic datasets are required [estimated at ~30 per genotype based on the studies in frog (Jung et al., 2016] to construct VM-PM contact area histograms for docked vesicles in C_2B polylysine mutants and controls (see Aim 1 below).

Aim 1: The C_2B Polylysine Motif of Synaptotagmin Promotes Maximal Priming of Docked Synaptic Vesicles

Using the methodology, outlined in Chapter 3, the hypothesis that the C_2B polylysine motif within synaptotagmin enhances synaptic vesicle priming. To directly test this hypothesis, the VM-PM contact areas, of docked synaptic vesicles, could be measured at the larval NMJ in controls and in C_2B mutants to create distribution histograms (see Fig. 4-1). Based on the studies in frog (Jung et al., 2016), analysis of the VM-PM contact area for ~75 docked vesicles per

genotype would be required to accurately compare their frequency histograms. Based on preliminary observations in *Drosophila*, 2–5 docked synaptic vesicles could be visualized per tomographic dataset, or 60–150 docked vesicles total per genotype. Thus, the estimated number of tomographic datasets needed to create distribution histograms is approximately 30 (24–36) tomographic datasets per genotype.

Potential Results and Interpretations

(A) If the histograms of VM-PM contact area are the same in the mutants and the controls, this would indicate that the C_2B polylysine motif does not enhance the priming of docked synaptic vesicles, refuting the hypothesis. In this case, the decrease in transmitter release seen in the mutants must result from another, as yet unknown, variable. (B) If the population of largest contact area docked vesicles seen in the control VM-PM contact area histogram is missing from the histogram of the mutants, this would support the hypothesis that the C_2B polylysine motif plays a crucial role in promoting maximal vesicle priming. (C) If the overall histogram for the mutants is significantly shifted toward smaller VM-PM contact areas, this would also indicate a role in promoting priming. (D) If the histograms exhibit some other significant difference, this could suggest that role of the C_2B polylysine motif is more complex than simply promoting maximal priming. However, further interpretations would require knowledge of the specific differences.

Potential Pitfalls

(A) If a difference in priming exists between mutants and controls, but is relatively small, or if I cannot segment as many docked vesicles as predicted, I may see a trend toward smaller contact areas in the mutants that fails to reach significance. In that case, a more extensive study would be warranted. We could also use a statistical bootstrap test as a way to estimate summary

statistics of the data. (B) The VM-PM contact area histogram for *Drosophila* might not show a normal distribution like frog. In this case, one would need to see the specific shape of the distribution before they could interpret this result. However, this is unlikely as all of the key synaptic proteins as well as the identified functions of synaptotagmin are highly conserved from *Drosophila* through mammals (Matthew et al., 1981; Sudhof et al., 1989; Perin et al., 1991); all of the functions of synaptotagmin identified first in *Drosophila* have later been shown to be conserved in mice or rats (Geppert et al., 1994; Lloyd et al., 2000).

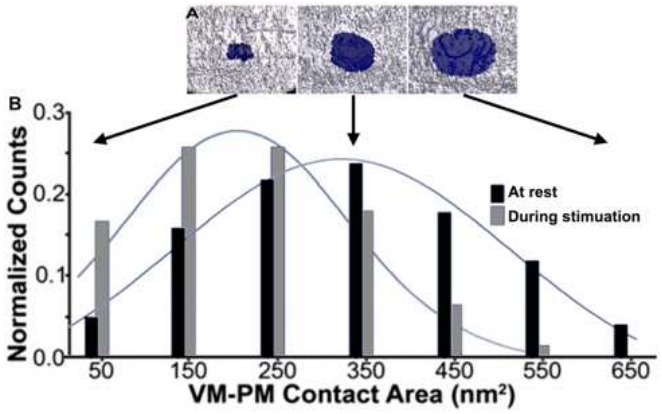

Figure 4-1: *Correlation Between VM-PM Contact Area and Extent of Vesicle Priming*

Top: Examples of VM-PM contact areas overlaid on plasma membrane renderings. Bottom: VM-PM contact area at rest has a normal frequency distribution that is shifted to smaller contact areas by stimulation, and the resulting fusion of maximally-primed vesicles (Fig. adapted from reference Jung et al., 2016).

Aim 2: Determine the ultrastructure of Active Zone Material in *Drosophila* using High-Resolution Electron Tomography

As physical interactions among AZM proteins are known to be required for neurotransmitter release, determining the distribution of proteins and protein-protein appositions within the AZM is needed to decipher the molecular mechanisms of vesicle fusion. The

McMahan lab has generated 3D renderings in frog, showing the structure of the AZM at 2 nm resolution (see Fig. 4-2A). However, frogs are not amenable for genetic tagging, so protein identification has not been possible. While the McMahan group has generated partial AZM renderings in mouse (structures analogous to those in yellow and brown only in Fig. 4-4A), the entire AZM has not been segmented and transgenic mouse studies are expensive. *Drosophila*, on the other hand, is a genetic system that is cheap and rapid. Further, I have just established the ultra high-resolution electron (2-3 nm) tomography of the *Drosophila* AZM that would be required for these studies. Currently, a clear 3D reconstruction of the AZM (compare Fig. 4-4B to 4-4A) has not been accomplished. However, tomograms I've already collected at *Drosophila* active zones, using methodology presented in Chapter 3, and tomograms from controls (as part of Aim 1), could be used to start defining common AZM structures of *Drosophila*. My graduate work enables the investigation of AZM structure, at a level of resolution previously unavailable in *Drosophila*, thereby paving the way for an ultra-high resolution characterization of AZM ultrastructure, and identification of individual proteins.

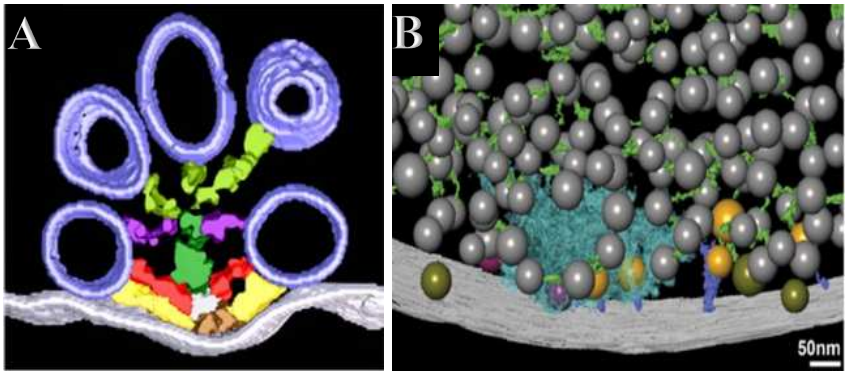

Figure 4-2. *Schematic 3D Reconstructions of the AZM at the Frog and Fly NMJs by Electron Tomography*

(A.) Frog: vesicles (blue spheres) and AZM (yellow, brown, white, green, red, and purple structures) have a well-characterized arrangement. (B.) *Drosophila*: vesicles (gray and gold spheres) are shown surrounding a convoluted AZM (light blue). As tomography in *Drosophila* is not yet as advanced as in frog, the

organization of macromolecules composing the AZM remains unknown. Adapted from Szule et al. (2012) and Bruckner et al. (2017), respectively.

Potential Results and Interpretations

As the molecules that dock, prime, and fuse vesicles are conserved in *Drosophila* through mammals, I anticipate that the synaptic ultra-structure of components connecting vesicles to the plasma membrane will have similarities to that in frog (as already seen in mouse; Nagwaney et al., 2009). In addition, since standard EM already reveals significant differences in the overall AZM structure across these species, I would expect to find novel structures as well.

Preliminary Results

As discussed in Chapter 1, active zones can almost universally be identified by their three distinct features: (1) the aggregation of electron dense material at the presynaptic membrane; (2) a tight cluster of synaptic vesicles; and (3) the presence of intramembranous particles. Interestingly enough, I have consistently observed intramembranous particles and electron dense filaments connecting the vesicle to the plasma membrane in high-resolution tomograms I collected at *Drosophila* active zones (see Fig 4-3).

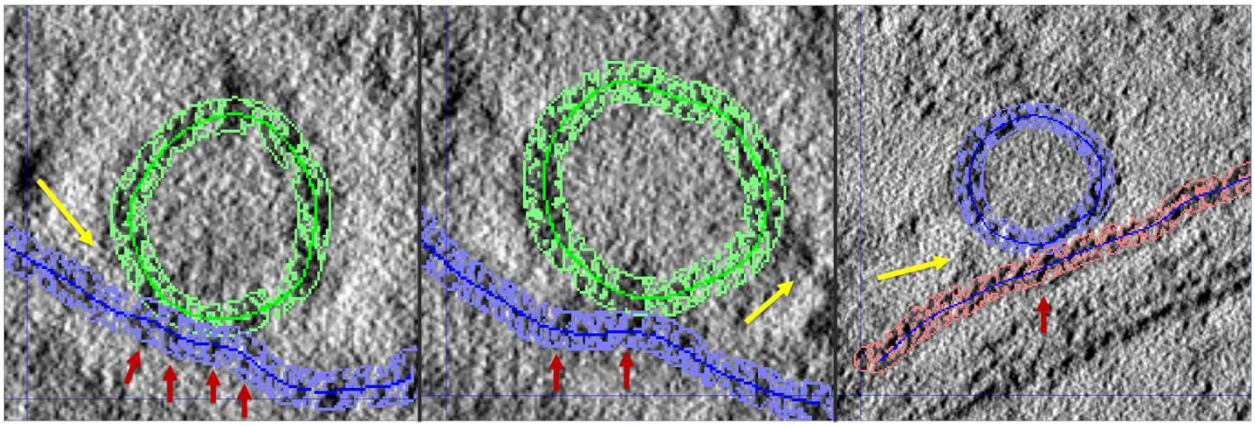

Figure 4-3. *Virtual slices with superimposed segmentations, of vesicle and plasma membranes, from high-resolution electron tomograms, at Drosophila Active zones.*

Virtual slices, representing 0.54 nm thickness of the tomogram, are shown for three docked vesicles with the vesicle and plasma membrane segmentations

super-imposed. Vesicles (green, and purple, elliptical structures) can be seen in contact with the plasma membrane (purple, and salmon, planar structures). Electron-dense filaments can be seen connecting the vesicle and associated plasma membrane (yellow arrows). Electron-dense structures, consistent with intramembranous particles, can be seen between the vesicle and plasma membrane, at the area of contact (red arrows).

Similar intramembranous particles have been previously observed, by electron microscopy and freeze fracture, adjacent to docked synaptic vesicles (Nagwaney et al., 2009; Harlow et al., 2013; Cole et al., 2016) under docked synaptic vesicles (Cole et al., 2016; Li et al., 2019; Radhakrishan et al., 2021), and near, or under presynaptic densities (Feeney et al., 1998; Rostaing et al., 2006; Jiao et al., 2012; Zhan et al., 2016; Bruckner et al., 2017; Fouquet et al., 2009). In most instances, the intramembranous particles observed by electron microscopy/tomography and freeze-fracture are thought to include calcium channels (Heuser et al., 1979; Feeney et al., 1998; Atwood and Karanuthi, 2002; Fouquet et al., 2009; Slater, 2015; Szule, 2021). However, they are also hypothesized to comprise part of the SNARE complex (Slater, 2015; Cole et al., 2016; Li et al., 2019; Szule, 2021; Radhakris et al., 2021).

Similar to the filaments I have observed (Fig 4-3B, yellow arrows), other labs have documented the presence of electron dense filaments that connect vesicles to the plasma membrane (Nagwaney et al., 2009; Harlow et al., 2013; Cole et al., 2016; Jiao et al., 2012; Zhan et al., 2016; Bruckner et al., 2017). The electron dense filaments are hypothesized to be comprised of SNARE complex proteins; scaffolding and/or tethering proteins, Depending on both the vesicle's and filament's positioning in reference to the plasma membrane (Fernandez-Busnadiego et al., 2013; Imig et al., 2014; Helmprobst et al., 2015; Zhan et al., 2016; Bruckner et al., 2017; Chakrabarti et al., 2019; Szule, 2021).

It is important to note that some argue that only high-pressure freeze and freeze-substitution (HFP/FS) methods should be used to visualize vesicle docking and electron dense

structures using electron microscopy (Smith and Reese, 1980; Landis et al., 1988; Fouquet et al. 2009; Rostaing et al., 2006; Helmprobst et al., 2015). However, Jung et al., 2016, compared chemical fixation and HPF/FS techniques and confirmed there was no difference in the appearance or sizes of active zone material. Additionally, I have noted the presence of IMPs, under the T-bar pedestal, in my own preliminary electron tomograms from *Drosophila* L3 larvae that were chemically fixed and stained. It is important to note that, during sample preparation, I paid careful attention to the osmolarity of chemical fixatives, so that they remained in the physiological range of *Drosophila* hemolymph (as discussed in Chapter 3). As a confirmation that my chemical fixation protocol does not cause a collapse of the T-bar onto the presynaptic membrane, as reported for chemical fixation by Fouquet et al. 2009, the slight gap between the T-bar and presynaptic membrane is preserved in my preparations – as also seen by Koenig and Ikeda, 1999.

Potential Pitfalls

Structural irregularities: Since electron tomographic analysis depends on the averaging of repeating structural components oriented to the same cardinal plane (Harlow et al., 2001; Nagwaney et al., 2009; Szule et al., 2012; Harlow et al., 2013), if the organization of *Drosophila* AZM is not as stereotypically regular as that of frog, our analysis could become more complicated. However, we know from standard EM that there is a repeating structure, the T-bar. So, some regularities exist. If the degree of regularity is less, one would need to increase the number of tomograms collected to get a more reliable averaging of structures. Regardless, any advances in describing the AZM ultrastructure of *Drosophila* at 2 nm resolution will open the door for genetic tagging studies to precisely localize molecular components required for synaptic transmission which is impossible in frog and costly in mouse. However, it is important to note

that most immuno-labeling techniques are not practical for use in identifying AZM structures due to their small size (10's of nanometers). The use of antibodies (~150 kDa) would introduce a gap between the antigen and tag that is larger than the structures needed to be identified. Genetic tagging techniques, such as miniSOG provide a promising, versatile, label for protein localization using electron microscopy/tomography.

Conclusion

To my knowledge, the data I have already collected and analyzed, during my graduate work, are the first example tomographic datasets with 2-3 nm spatial resolution at a *Drosophila* active zone. By extending the McMahan lab's ultra high-resolution tomography to *Drosophila* synapses, the methods presented in Chapter 3 would permit the structural measurements necessary for the first direct test of a molecular motif hypothesized to enhance vesicle priming, as presented in Chapter 2. In addition, since *Drosophila* are amenable to transgenic tagging, segmenting the structures connecting docked vesicles, presynaptic membrane, and T-bars, within high-resolution tomograms, has the potential to open a whole new field of structural identification of synaptic molecules critical for intercellular communication in the nervous system.

REFERENCES

Abdulreda, M. H., Bhalla, A., Rico, F., Berggren, P. O., Chapman, E. R., & Moy, V. T. (2009). Pulling force generated by interacting SNAREs facilitates membrane hemifusion. Integr Biol (Camb), 1(4), 301-310. https://doi.org/10.1039/b900685k

Ackermann, F., Waites, C. L., & Garner, C. C. (2015). Presynaptic active zones in invertebrates and vertebrates. EMBO Rep, 16(8), 923-938. https://doi.org/10.15252/embr.201540434

Ahmad, M., Polepalli, J. S., Goswami, D., Yang, X., Kaeser-Woo, Y. J., Sudhof, T. C., & Malenka, R. C. (2012). Postsynaptic complexin controls AMPA receptor exocytosis during LTP. Neuron, 73(2), 260-267. https://doi.org/10.1016/j.neuron.2011.11.020

Ahmari, S. E., Buchanan, J., & Smith, S. J. (2000). Assembly of presynaptic active zones from cytoplasmic transport packets. Nat Neurosci, 3(5), 445-451. https://doi.org/10.1038/74814

Akbergenova, Y., Cunningham, K. L., Zhang, Y. V., Weiss, S., & Littleton, J. T. (2018). Characterization of developmental and molecular factors underlying release heterogeneity at *Drosophila* synapses. Elife, 7. https://doi.org/10.7554/eLife.38268

Albers, M. A., & Bradley, T. J. (2004). Osmotic regulation in adult *Drosophila* melanogaster during dehydration and rehydration. J Exp Biol, 207(Pt 13), 2313-2321. https://doi.org/10.1242/jeb.01024

Aldahabi, M., Balint, F., Holderith, N., Lorincz, A., Reva, M., & Nusser, Z. (2022). Different priming states of synaptic vesicles underlie distinct release probabilities at hippocampal excitatory synapses. Neuron, 110(24), 4144-4161 e4147. https://doi.org/10.1016/j.neuron.2022.09.035

Arac, D., Chen, X., Khant, H. A., Ubach, J., Ludtke, S. J., Kikkawa, M., Johnson, A. E., Chiu, W., Sudhof, T. C., & Rizo, J. (2006). Close membrane-membrane proximity induced by Ca(2+)-dependent multivalent binding of synaptotagmin-1 to phospholipids. Nat Struct Mol Biol, 13(3), 209-217. https://doi.org/10.1038/nsmb1056

Atlas, D. (2022). Revisiting the molecular basis of synaptic transmission. Prog Neurobiol, 216, 102312. https://doi.org/10.1016/j.pneurobio.2022.102312

Atwood, H. L. (2006). Neuroscience. Gatekeeper at the synapse. Science, 312(5776), 1008-1009. https://doi.org/10.1126/science.1128445

Atwood, H. L., & Karunanithi, S. (2002). Diversification of synaptic strength: presynaptic elements. Nat Rev Neurosci, 3(7), 497-516. https://doi.org/10.1038/nrn876

Bacaj, T., Wu, D., Burre, J., Malenka, R. C., Liu, X., & Sudhof, T. C. (2015). Synaptotagmin-1 and -7 Are Redundantly Essential for Maintaining the Capacity of the Readily-Releasable Pool of Synaptic Vesicles. PLoS Biol, 13(10), e1002267. https://doi.org/10.1371/journal.pbio.1002267

Bacaj, T., Wu, D., Yang, X., Morishita, W., Zhou, P., Xu, W., Malenka, R. C., & Sudhof, T. C. (2013). Synaptotagmin-1 and synaptotagmin-7 trigger synchronous and asynchronous phases of neurotransmitter release. Neuron, 80(4), 947-959. https://doi.org/10.1016/j.neuron.2013.10.026

Bai, H., Xue, R., Bao, H., Zhang, L., Yethiraj, A., Cui, Q., & Chapman, E. R. (2016). Different states of synaptotagmin regulate evoked versus spontaneous release. Nat Commun, 7, 10971. https://doi.org/10.1038/ncomms10971

Bai, J., & Chapman, E. R. (2004). The C2 domains of synaptotagmin--partners in exocytosis. Trends Biochem Sci, 29(3), 143-151. https://doi.org/10.1016/j.tibs.2004.01.008

Bai, J., Tucker, W. C., & Chapman, E. R. (2004). PIP2 increases the speed of response of synaptotagmin and steers its membrane-penetration activity toward the plasma membrane. Nat Struct Mol Biol, 11(1), 36-44. https://doi.org/10.1038/nsmb709

Bai, J., Wang, C. T., Richards, D. A., Jackson, M. B., & Chapman, E. R. (2004). Fusion pore dynamics are regulated by synaptotagmin*t-SNARE interactions. Neuron, 41(6), 929-942. https://doi.org/10.1016/s0896-6273(04)00117-5

Banerjee, A., Imig, C., Balakrishnan, K., Kershberg, L., Lipstein, N., Uronen, R. L., Wang, J., Cai, X., Benseler, F., Rhee, J. S., Cooper, B. H., Liu, C., Wojcik, S. M., Brose, N., & Kaeser, P. S. (2022). Molecular and functional architecture of striatal dopamine release sites. Neuron, 110(2), 248-265 e249. https://doi.org/10.1016/j.neuron.2021.10.028

Bao, H., Goldschen-Ohm, M., Jeggle, P., Chanda, B., Edwardson, J. M., & Chapman, E. R. (2016). Exocytotic fusion pores are composed of both lipids and proteins. Nat Struct Mol Biol, 23(1), 67-73. https://doi.org/10.1038/nsmb.3141

Barcena, M., & Koster, A. J. (2009). Electron tomography in life science. Semin Cell Dev Biol, 20(8), 920-930. https://doi.org/10.1016/j.semcdb.2009.07.008

Barker, L. A., Dowdall, M. J., & Whittaker, V. P. (1972). Choline metabolism in the cerebral cortex of guinea pigs. Stable-bound acetylcholine. Biochem J, 130(4), 1063-1075. https://doi.org/10.1042/bj1301063

Bendahmane, M., Bohannon, K. P., Bradberry, M. M., Rao, T. C., Schmidtke, M. W., Abbineni, P. S., Chon, N. L., Tran, S., Lin, H., Chapman, E. R., Knight, J. D., & Anantharam, A. (2018). The synaptotagmin C2B domain calcium-binding loops modulate the rate of fusion pore expansion. Mol Biol Cell, 29(7), 834-845. https://doi.org/10.1091/mbc.E17-11-0623

Bennett, M. K., Calakos, N., Kreiner, T., & Scheller, R. H. (1992). Synaptic vesicle membrane proteins interact to form a multimeric complex. J Cell Biol, 116(3), 761-775. https://doi.org/10.1083/jcb.116.3.761

Betz, W. J., & Bewick, G. S. (1992). Optical analysis of synaptic vesicle recycling at the frog neuromuscular junction. Science, 255(5041), 200-203. https://doi.org/10.1126/science.1553547

Betz, W. J., Bewick, G. S., & Ridge, R. M. (1992). Intracellular movements of fluorescently labeled synaptic vesicles in frog motor nerve terminals during nerve stimulation. Neuron, 9(5), 805-813. https://doi.org/10.1016/0896-6273(92)90235-6

Betz, W. J., & Richards, D. A. (2000). What goes out must come in. Nat Neurosci, 3(7), 636-637. https://doi.org/10.1038/76579

Blundell, J., Kaeser, P. S., Sudhof, T. C., & Powell, C. M. (2010). RIM1alpha and interacting proteins involved in presynaptic plasticity mediate prepulse inhibition and additional behaviors linked to schizophrenia. J Neurosci, 30(15), 5326-5333. https://doi.org/10.1523/JNEUROSCI.0328-10.2010

Bommert, K., Charlton, M. P., DeBello, W. M., Chin, G. J., Betz, H., & Augustine, G. J. (1993). Inhibition of neurotransmitter release by C2-domain peptides implicates synaptotagmin in exocytosis. Nature, 363(6425), 163-165. https://doi.org/10.1038/363163a0

Borden, C. R., Stevens, C. F., Sullivan, J. M., & Zhu, Y. (2005). Synaptotagmin mutants Y311N and K326/327A alter the calcium dependence of neurotransmission. Mol Cell Neurosci, 29(3), 462-470. https://doi.org/10.1016/j.mcn.2005.03.015

Bouazza-Arostegui, B., Camacho, M., Brockmann, M. M., Zobel, S., & Rosenmund, C. (2022). Deconstructing Synaptotagmin-1's Distinct Roles in Synaptic Vesicle Priming and

Neurotransmitter Release. J Neurosci, 42(14), 2856-2871. https://doi.org/10.1523/JNEUROSCI.1945-21.2022

Bowers, M. R. (2020). Reevaulating the functional role of the C2A domain of synatptotagmin in neurotransmitter release (Publication Number 28026417) [Dissertation, Colorado State University]. Colorado State University. Libraries. https://hdl.handle.net/10217/211818

Bowers, M. R., & Reist, N. E. (2020). Synaptotagmin: Mechanisms of an electrostatic switch. Neurosci Lett, 722, 134834. https://doi.org/10.1016/j.neulet.2020.134834

Bowers, M. R., & Reist, N. E. (2020). The C2A domain of synaptotagmin is an essential component of the calcium sensor for synaptic transmission. PLoS One, 15(2), e0228348. https://doi.org/10.1371/journal.pone.0228348

Brand, A. H., & Perrimon, N. (1993). Targeted gene expression as a means of altering cell fates and generating dominant phenotypes. Development, 118(2), 401-415. https://doi.org/10.1242/dev.118.2.401

Brewer, K. D., Bacaj, T., Cavalli, A., Camilloni, C., Swarbrick, J. D., Liu, J., Zhou, A., Zhou, P., Barlow, N., Xu, J., Seven, A. B., Prinslow, E. A., Voleti, R., Häussinger, D., Bonvin, A. M., Tomchick, D. R., Vendruscolo, M., Graham, B., Südhof, T. C., & Rizo, J. (2015). Dynamic binding mode of a Synaptotagmin-1-SNARE complex in solution. Nat Struct Mol Biol, 22(7), 555-564. https://doi.org/10.1038/nsmb.3035

Broadie, K. S. (1996). Regulation of the synaptic vesicle cycle in *Drosophila*. Biochem Soc Trans, 24(3), 639-645. https://doi.org/10.1042/bst0240639

Brockmann, M. M., Zarebidaki, F., Camacho, M., Grauel, M. K., Trimbuch, T., Sudhof, T. C., & Rosenmund, C. (2020). A Trio of Active Zone Proteins Comprised of RIM-BPs, RIMs,

and Munc13s Governs Neurotransmitter Release. Cell Rep, 32(5), 107960. https://doi.org/10.1016/j.celrep.2020.107960

Brodin, L., & Shupliakov, O. (2006). Giant reticulospinal synapse in lamprey: molecular links between active and periactive zones. Cell Tissue Res, 326(2), 301-310. https://doi.org/10.1007/s00441-006-0216-2

Brose, N., Brunger, A., Cafiso, D., Chapman, E. R., Diao, J., Hughson, F. M., Jackson, M. B., Jahn, R., Lindau, M., Ma, C., Rizo, J., Shin, Y. K., Sollner, T. H., Tamm, L., Yoon, T. Y., & Zhang, Y. (2019). Synaptic vesicle fusion: today and beyond. Nat Struct Mol Biol, 26(8), 663-668. https://doi.org/10.1038/s41594-019-0277-z

Brose, N., Petrenko, A. G., Sudhof, T. C., & Jahn, R. (1992). Synaptotagmin - a Calcium Sensor on the Synaptic Vesicle Surface. Science, 256(5059), 1021-1025. https://doi.org/DOI 10.1126/science.1589771

Bruckner, J. J., Gratz, S. J., Slind, J. K., Geske, R. R., Cummings, A. M., Galindo, S. E., Donohue, L. K., & O'Connor-Giles, K. M. (2012). Fife, a *Drosophila* Piccolo-RIM homolog, promotes active zone organization and neurotransmitter release. J Neurosci, 32(48), 17048-17058. https://doi.org/10.1523/jneurosci.3267-12.2012

Bruckner, J. J., Zhan, H., Gratz, S. J., Rao, M., Ukken, F., Zilberg, G., & O'Connor-Giles, K. M. (2017). Fife organizes synaptic vesicles and calcium channels for high-probability neurotransmitter release. J Cell Biol, 216(1), 231-246. https://doi.org/10.1083/jcb.201601098

Bruckner, J. J., Zhan, H., & O'Connor-Giles, K. M. (2015). Advances in imaging ultrastructure yield new insights into presynaptic biology. Front Cell Neurosci, 9, 196. https://doi.org/10.3389/fncel.2015.00196

Brunger, A. T., Choi, U. B., Lai, Y., Leitz, J., & Zhou, Q. (2018). Molecular Mechanisms of Fast Neurotransmitter Release. Annu Rev Biophys, 47, 469-497. https://doi.org/10.1146/annurev-biophys-070816-034117

Bulgari, D., Deitcher, D. L., Schmidt, B. F., Carpenter, M. A., Szent-Gyorgyi, C., Bruchez, M. P., & Levitan, E. S. (2019). Activity-evoked and spontaneous opening of synaptic fusion pores. Proc Natl Acad Sci U S A, 116(34), 17039-17044. https://doi.org/10.1073/pnas.1905322116

Butola, T., Alvanos, T., Hintze, A., Koppensteiner, P., Kleindienst, D., Shigemoto, R., Wichmann, C., & Moser, T. (2021). RIM-Binding Protein 2 Organizes Ca(2+) Channel Topography and Regulates Release Probability and Vesicle Replenishment at a Fast Central Synapse. J Neurosci, 41(37), 7742-7767. https://doi.org/10.1523/JNEUROSCI.0586-21.2021

Calloway, N., Gouzer, G., Xue, M., & Ryan, T. A. (2015). The active-zone protein Munc13 controls the use-dependence of presynaptic voltage-gated calcium channels. Elife, 4. https://doi.org/10.7554/eLife.07728

Cano, R., & Tabares, L. (2016). The Active and Periactive Zone Organization and the Functional Properties of Small and Large Synapses. Front Synaptic Neurosci, 8, 12. https://doi.org/10.3389/fnsyn.2016.00012

Cao, P., Maximov, A., & Sudhof, T. C. (2011). Activity-dependent IGF-1 exocytosis is controlled by the Ca(2+)-sensor synaptotagmin-10. Cell, 145(2), 300-311. https://doi.org/10.1016/j.cell.2011.03.034

Cao, P., Yang, X., & Sudhof, T. C. (2013). Complexin activates exocytosis of distinct secretory vesicles controlled by different synaptotagmins. J Neurosci, 33(4), 1714-1727. https://doi.org/10.1523/JNEUROSCI.4087-12.2013

Ceccarelli, B., Hurlbut, W. P., & Mauro, A. (1973). Turnover of transmitter and synaptic vesicles at the frog neuromuscular junction. J Cell Biol, 57(2), 499-524. https://doi.org/10.1083/jcb.57.2.499

Chakrabarti, R., & Wichmann, C. (2019). Nanomachinery Organizing Release at Neuronal and Ribbon Synapses. Int J Mol Sci, 20(9). https://doi.org/10.3390/ijms20092147

Chang, C. W., Hui, E., Bai, J., Bruns, D., Chapman, E. R., & Jackson, M. B. (2015). A structural role for the synaptobrevin 2 transmembrane domain in dense-core vesicle fusion pores. J Neurosci, 35(14), 5772-5780. https://doi.org/10.1523/jneurosci.3983-14.2015

Chang, S., Trimbuch, T., & Rosenmund, C. (2018). Synaptotagmin-1 drives synchronous Ca(2+)-triggered fusion by C(2)B-domain-mediated synaptic-vesicle-membrane attachment. Nat Neurosci, 21(1), 33-40. https://doi.org/10.1038/s41593-017-0037-5

Chang, W. P., & Sudhof, T. C. (2009). SV2 renders primed synaptic vesicles competent for Ca2+ -induced exocytosis. J Neurosci, 29(4), 883-897. https://doi.org/10.1523/JNEUROSCI.4521-08.2009

Chapman, E. R. (2002). Synaptotagmin: a Ca(2+) sensor that triggers exocytosis? Nat Rev Mol Cell Biol, 3(7), 498-508. https://doi.org/10.1038/nrm855

Chapman, E. R. (2008). How does synaptotagmin trigger neurotransmitter release? Annu Rev Biochem, 77, 615-641. https://doi.org/10.1146/annurev.biochem.77.062005.101135

Chapman, E. R. (2018). A Ca(2+) Sensor for Exocytosis. Trends Neurosci, 41(6), 327-330. https://doi.org/10.1016/j.tins.2018.03.012

Chapman, E. R., & Davis, A. F. (1998). Direct interaction of a Ca2+-binding loop of synaptotagmin with lipid bilayers. J Biol Chem, 273(22), 13995-14001. https://doi.org/10.1074/jbc.273.22.13995

Chapman, E. R., Desai, R. C., Davis, A. F., & Tornehl, C. K. (1998). Delineation of the oligomerization, AP-2 binding, and synprint binding region of the C2B domain of synaptotagmin. J Biol Chem, 273(49), 32966-32972. https://doi.org/10.1074/jbc.273.49.32966

Chen, S., Gendelman, H. K., Roche, J. P., Alsharif, P., & Graf, E. R. (2015). Mutational Analysis of Rab3 Function for Controlling Active Zone Protein Composition at the *Drosophila* Neuromuscular Junction. PLoS One, 10(8), e0136938. https://doi.org/10.1371/journal.pone.0136938

Chen, Y., Wang, Y. H., Zheng, Y., Li, M., Wang, B., Wang, Q. W., Fu, C. L., Liu, Y. N., Li, X., & Yao, J. (2021). Synaptotagmin-1 interacts with PI(4,5)P2 to initiate synaptic vesicle docking in hippocampal neurons. Cell Rep, 34(11), 108842. https://doi.org/10.1016/j.celrep.2021.108842

Chicka, M. C., & Chapman, E. R. (2009). Concurrent binding of complexin and synaptotagmin to liposome-embedded SNARE complexes. Biochemistry, 48(4), 657-659. https://doi.org/10.1021/bi801962d

Chicka, M. C., Hui, E., Liu, H., & Chapman, E. R. (2008). Synaptotagmin arrests the SNARE complex before triggering fast, efficient membrane fusion in response to Ca2+. Nat Struct Mol Biol, 15(8), 827-835. https://doi.org/10.1038/nsmb.1463

Chieregatti, E., Chicka, M. C., Chapman, E. R., & Baldini, G. (2004). SNAP-23 functions in docking/fusion of granules at low Ca2+. Mol Biol Cell, 15(4), 1918-1930. https://doi.org/10.1091/mbc.e03-09-0684

Clarke, G. L., Chen, J., & Nishimune, H. (2012). Presynaptic Active Zone Density during Development and Synaptic Plasticity. Front Mol Neurosci, 5, 12. https://doi.org/10.3389/fnmol.2012.00012

Cohen, R., Elferink, L. A., & Atlas, D. (2003). The C2A domain of synaptotagmin alters the kinetics of voltagegated Ca2+ channels Ca(v)1.2 (Lc-type) and Ca(v)2.3 (R-type). Journal of Biological Chemistry, 278(11), 9258-9266. https://doi.org/10.1074/jbc.M210270200

Cole, A. A., Chen, X., & Reese, T. S. (2016). A Network of Three Types of Filaments Organizes Synaptic Vesicles for Storage, Mobilization, and Docking. J Neurosci, 36(11), 3222-3230. https://doi.org/10.1523/jneurosci.2939-15.2016

Courtney, K. C., Vevea, J. D., Li, Y., Wu, Z., Zhang, Z., & Chapman, E. R. (2021). Synaptotagmin 1 oligomerization via the juxtamembrane linker regulates spontaneous and evoked neurotransmitter release. Proc Natl Acad Sci U S A, 118(48). https://doi.org/10.1073/pnas.2113859118

Courtney, N. A., Bao, H., Briguglio, J. S., & Chapman, E. R. (2019). Synaptotagmin 1 clamps synaptic vesicle fusion in mammalian neurons independent of complexin. Nat Commun, 10(1), 4076. https://doi.org/10.1038/s41467-019-12015-w

Couteaux, R., & Pecot-Dechavassine, M. (1970). [Synaptic vesicles and pouches at the level of "active zones" of the neuromuscular junction]. C R Acad Hebd Seances Acad Sci D,

271(25), 2346-2349. https://www.ncbi.nlm.nih.gov/pubmed/4995202 (Vesicules synaptiques et poches au niveau des "zones actives" de la jonction neuromusculaire.)

Cruickshank, M. B. a. (1962). A Partial Analysis of *Drosophila* Larval Haemolymph. Proceedings of the Royal Society of Edinburgh, 68(3), 215-236. https://www.cambridge.org/core/journals/proceedings-of-the-royal-society-of-edinburgh-section-b-biological-sciences/article/abs/xvia-partial-analysis-of-*Drosophila*-larval-haemolymph/2CBF2CFF6CBE513E19A5FF39D77F149C

Dani, A., Huang, B., Bergan, J., Dulac, C., & Zhuang, X. (2010). Superresolution imaging of chemical synapses in the brain. Neuron, 68(5), 843-856. https://doi.org/10.1016/j.neuron.2010.11.021

Davletov, B., Sontag, J. M., Hata, Y., Petrenko, A. G., Fykse, E. M., Jahn, R., & Sudhof, T. C. (1993). Phosphorylation of Synaptotagmin-I by Casein Kinase-Ii. Journal of Biological Chemistry, 268(9), 6816-6822. <Go to ISI>://WOS:A1993KT36800105

Davletov, B. A., & Sudhof, T. C. (1993). A single C2 domain from synaptotagmin I is sufficient for high affinity Ca2+/phospholipid binding. J Biol Chem, 268(35), 26386-26390. https://www.ncbi.nlm.nih.gov/pubmed/8253763

Dawson-Scully, K., Lin, Y., Imad, M., Zhang, J., Marin, L., Horne, J. A., Meinertzhagen, I. A., Karunanithi, S., Zinsmaier, K. E., & Atwood, H. L. (2007). Morphological and functional effects of altered cysteine string protein at the *Drosophila* larval neuromuscular junction. Synapse, 61(1), 1-16. https://doi.org/10.1002/syn.20335

Desai, R. C., Vyas, B., Earles, C. A., Littleton, J. T., Kowalchyck, J. A., Martin, T. F., & Chapman, E. R. (2000). The C2B domain of synaptotagmin is a Ca(2+)-sensing module

essential for exocytosis. J Cell Biol, 150(5), 1125-1136. https://doi.org/10.1083/jcb.150.5.1125

DiAntonio, A., Burgess, R. W., Chin, A. C., Deitcher, D. L., Scheller, R. H., & Schwarz, T. L. (1993). Identification and characterization of *Drosophila* genes for synaptic vesicle proteins. J Neurosci, 13(11), 4924-4935. https://doi.org/10.1523/JNEUROSCI.13-11-04924.1993

DiAntonio, A., Parfitt, K. D., & Schwarz, T. L. (1993). Synaptic transmission persists in synaptotagmin mutants of *Drosophila*. Cell, 73(7), 1281-1290. https://doi.org/10.1016/0092-8674(93)90356-u

Diao, J., Burre, J., Vivona, S., Cipriano, D. J., Sharma, M., Kyoung, M., Sudhof, T. C., & Brunger, A. T. (2013). Native alpha-synuclein induces clustering of synaptic-vesicle mimics via binding to phospholipids and synaptobrevin-2/VAMP2. Elife, 2, e00592. https://doi.org/10.7554/eLife.00592

Dresbach, T., Qualmann, B., Kessels, M. M., Garner, C. C., & Gundelfinger, E. D. (2001). The presynaptic cytomatrix of brain synapses. Cell Mol Life Sci, 58(1), 94-116. https://doi.org/10.1007/pl00000781

Dresbach, T., Torres, V., Wittenmayer, N., Altrock, W. D., Zamorano, P., Zuschratter, W., Nawrotzki, R., Ziv, N. E., Garner, C. C., & Gundelfinger, E. D. (2006). Assembly of active zone precursor vesicles: obligatory trafficking of presynaptic cytomatrix proteins Bassoon and Piccolo via a trans-Golgi compartment. J Biol Chem, 281(9), 6038-6047. https://doi.org/10.1074/jbc.M508784200

Dreyer, F., Peper, K., Akert, K., Sandri, C., & Moor, H. (1973). Ultrastructure of the "active zone" in the frog neuromuscular junction. Brain Res, 62(2), 373-380. https://doi.org/10.1016/0006-8993(73)90699-9

Ehmann, N., van de Linde, S., Alon, A., Ljaschenko, D., Keung, X. Z., Holm, T., Rings, A., DiAntonio, A., Hallermann, S., Ashery, U., Heckmann, M., Sauer, M., & Kittel, R. J. (2014). Quantitative super-resolution imaging of Bruchpilot distinguishes active zone states. Nat Commun, 5, 4650. https://doi.org/10.1038/ncomms5650

Engel, A. G. (2008). The neuromuscular junction. Handb Clin Neurol, 91, 103-148. https://doi.org/10.1016/S0072-9752(07)01503-5

Evans, C. S., He, Z., Bai, H., Lou, X., Jeggle, P., Sutton, R. B., Edwardson, J. M., & Chapman, E. R. (2016). Functional analysis of the interface between the tandem C2 domains of synaptotagmin-1. Mol Biol Cell, 27(6), 979-989. https://doi.org/10.1091/mbc.E15-07-0503

Feeney, C. J., Karunanithi, S., Pearce, J., Govind, C. K., & Atwood, H. L. (1998). Motor nerve terminals on abdominal muscles in larval flesh flies, Sarcophaga bullata: comparisons with *Drosophila*. J Comp Neurol, 402(2), 197-209. https://www.ncbi.nlm.nih.gov/pubmed/9845243

Fejtova, A., & Gundelfinger, E. D. (2006). Molecular organization and assembly of the presynaptic active zone of neurotransmitter release. Results Probl Cell Differ, 43, 49-68. https://doi.org/10.1007/400_012

Fergestad, T., & Broadie, K. (2001). Interaction of stoned and synaptotagmin in synaptic vesicle endocytosis. J Neurosci, 21(4), 1218-1227. https://doi.org/10.1523/JNEUROSCI.21-04-01218.2001

Fernandez-Alfonso, T., & Ryan, T. A. (2004). The kinetics of synaptic vesicle pool depletion at CNS synaptic terminals. Neuron, 41(6), 943-953. https://doi.org/10.1016/s0896-6273(04)00113-8

Fernandez-Busnadiego, R., Asano, S., Oprisoreanu, A. M., Sakata, E., Doengi, M., Kochovski, Z., Zurner, M., Stein, V., Schoch, S., Baumeister, W., & Lucic, V. (2013). Cryo-electron tomography reveals a critical role of RIM1alpha in synaptic vesicle tethering. J Cell Biol, 201(5), 725-740. https://doi.org/10.1083/jcb.201206063

Fernandez-Chacon, R., Shin, O. H., Konigstorfer, A., Matos, M. F., Meyer, A. C., Garcia, J., Gerber, S. H., Rizo, J., Sudhof, T. C., & Rosenmund, C. (2002). Structure/function analysis of Ca2+ binding to the C2A domain of synaptotagmin 1. J Neurosci, 22(19), 8438-8446. https://doi.org/10.1523/JNEUROSCI.22-19-08438.2002

Fouquet, W., Owald, D., Wichmann, C., Mertel, S., Depner, H., Dyba, M., Hallermann, S., Kittel, R. J., Eimer, S., & Sigrist, S. J. (2009). Maturation of active zone assembly by *Drosophila* Bruchpilot. J Cell Biol, 186(1), 129-145. https://doi.org/10.1083/jcb.200812150

Frazier, A. A., Roller, C. R., Havelka, J. J., Hinderliter, A., & Cafiso, D. S. (2003). Membrane-bound orientation and position of the synaptotagmin I C2A domain by site-directed spin labeling. Biochemistry, 42(1), 96-105. https://doi.org/10.1021/bi0268145

Fukuda, M., Moreira, J. E., Lewis, F. M., Sugimori, M., Niinobe, M., Mikoshiba, K., & Llinás, R. (1995). Role of the C2B domain of synaptotagmin in vesicular release and recycling as determined by specific antibody injection into the squid giant synapse preterminal. Proc Natl Acad Sci U S A, 92(23), 10708-10712. https://doi.org/10.1073/pnas.92.23.10708

Fulterer, A., Andlauer, T. F. M., Ender, A., Maglione, M., Eyring, K., Woitkuhn, J., Lehmann, M., Matkovic-Rachid, T., Geiger, J. R. P., Walter, A. M., Nagel, K. I., & Sigrist, S. J. (2018). Active Zone Scaffold Protein Ratios Tune Functional Diversity across Brain Synapses. Cell Rep, 23(5), 1259-1274. https://doi.org/10.1016/j.celrep.2018.03.126

Gaffaney, J. D., Dunning, F. M., Wang, Z., Hui, E., & Chapman, E. R. (2008). Synaptotagmin C2B domain regulates Ca2+-triggered fusion in vitro: critical residues revealed by scanning alanine mutagenesis. J Biol Chem, 283(46), 31763-31775. https://doi.org/10.1074/jbc.M803355200

Galbraith, C. G., & Galbraith, J. A. (2011). Super-resolution microscopy at a glance. J Cell Sci, 124(Pt 10), 1607-1611. https://doi.org/10.1242/jcs.080085

Gan, Q., & Watanabe, S. (2018). Synaptic Vesicle Endocytosis in Different Model Systems. Front Cell Neurosci, 12, 171. https://doi.org/10.3389/fncel.2018.00171

Geppert, M., Goda, Y., Hammer, R. E., Li, C., Rosahl, T. W., Stevens, C. F., & Sudhof, T. C. (1994). Synaptotagmin I: a major Ca2+ sensor for transmitter release at a central synapse. Cell, 79(4), 717-727. https://doi.org/10.1016/0092-8674(94)90556-8

Gerber, S. H., & Sudhof, T. C. (2002). Molecular determinants of regulated exocytosis. Diabetes, 51 Suppl 1, S3-11. https://doi.org/10.2337/diabetes.51.2007.s3

Ghelani, T., & Sigrist, S. J. (2018). Coupling the Structural and Functional Assembly of Synaptic Release Sites. Front Neuroanat, 12, 81. https://doi.org/10.3389/fnana.2018.00081

Glebov, O. O., Jackson, R. E., Winterflood, C. M., Owen, D. M., Barker, E. A., Doherty, P., Ewers, H., & Burrone, J. (2017). Nanoscale Structural Plasticity of the Active Zone Matrix Modulates Presynaptic Function. Cell Rep, 18(11), 2715-2728. https://doi.org/10.1016/j.celrep.2017.02.064

Goel, P., Li, X., & Dickman, D. (2019). Estimation of the Readily Releasable Synaptic Vesicle Pool at the *Drosophila* Larval Neuromuscular Junction. Bio Protoc, 9(1). https://doi.org/10.21769/BioProtoc.3127

Gong, J., Lai, Y., Li, X., Wang, M., Leitz, J., Hu, Y., Zhang, Y., Choi, U. B., Cipriano, D., Pfuetzner, R. A., Sudhof, T. C., Yang, X., Brunger, A. T., & Diao, J. (2016). C-terminal domain of mammalian complexin-1 localizes to highly curved membranes. Proc Natl Acad Sci U S A, 113(47), E7590-E7599. https://doi.org/10.1073/pnas.1609917113

Gonzalez-Gaitan, M., & Jackle, H. (1997). Role of *Drosophila* alpha-adaptin in presynaptic vesicle recycling. Cell, 88(6), 767-776. https://doi.org/10.1016/s0092-8674(00)81923-6

Grass, I., Thiel, S., Honing, S., & Haucke, V. (2004). Recognition of a basic AP-2 binding motif within the C2B domain of synaptotagmin is dependent on multimerization. Journal of Biological Chemistry, 279(52), 54872-54880. https://doi.org/10.1074/jbc.M409995200

Gratz, S. J., Goel, P., Bruckner, J. J., Hernandez, R. X., Khateeb, K., Macleod, G. T., Dickman, D., & O'Connor-Giles, K. M. (2019). Endogenous Tagging Reveals Differential Regulation of Ca(2+) Channels at Single Active Zones during Presynaptic Homeostatic Potentiation and Depression. J Neurosci, 39(13), 2416-2429. https://doi.org/10.1523/jneurosci.3068-18.2019

Gruget, C., Bello, O., Coleman, J., Krishnakumar, S. S., Perez, E., Rothman, J. E., Pincet, F., & Donaldson, S. H. (2020). Synaptotagmin-1 membrane binding is driven by the C2B domain and assisted cooperatively by the C2A domain. Scientific Reports, 10(1). https://doi.org/ARTN 18011

10.1038/s41598-020-74923-y

Guan, Z., Bykhovskaia, M., Jorquera, R. A., Sutton, R. B., Akbergenova, Y., & Littleton, J. T. (2017). A synaptotagmin suppressor screen indicates SNARE binding controls the timing and Ca(2+) cooperativity of vesicle fusion. Elife, 6. https://doi.org/10.7554/eLife.28409

Gundelfinger, E. D., Reissner, C., & Garner, C. C. (2015). Role of Bassoon and Piccolo in Assembly and Molecular Organization of the Active Zone. Front Synaptic Neurosci, 7, 19. https://doi.org/10.3389/fnsyn.2015.00019

Gundelfinger, E. D., & tom Dieck, S. (2000). Molecular organization of excitatory chemical synapses in the mammalian brain. Naturwissenschaften, 87(12), 513-523. https://doi.org/10.1007/s001140050770

Gustavsson, N., Seah, T., Lao, Y., Radda, G. K., Sudhof, T. C., & Han, W. (2011). Delayed onset of hyperglycaemia in a mouse model with impaired glucagon secretion demonstrates that dysregulated glucagon secretion promotes hyperglycaemia and type 2 diabetes. Diabetologia, 54(2), 415-422. https://doi.org/10.1007/s00125-010-1950-2

Gustavsson, N., Wang, X., Wang, Y., Seah, T., Xu, J., Radda, G. K., Sudhof, T. C., & Han, W. (2010). Neuronal calcium sensor synaptotagmin-9 is not involved in the regulation of glucose homeostasis or insulin secretion. PLoS One, 5(11), e15414. https://doi.org/10.1371/journal.pone.0015414

Gustavsson, N., Wei, S. H., Hoang, D. N., Lao, Y., Zhang, Q., Radda, G. K., Rorsman, P., Sudhof, T. C., & Han, W. (2009). Synaptotagmin-7 is a principal Ca2+ sensor for Ca2+ -induced glucagon exocytosis in pancreas. J Physiol, 587(Pt 6), 1169-1178. https://doi.org/10.1113/jphysiol.2008.168005

Hammarlund, M., Palfreyman, M. T., Watanabe, S., Olsen, S., & Jorgensen, E. M. (2007). Open syntaxin docks synaptic vesicles. PLoS Biol, 5(8), e198. https://doi.org/10.1371/journal.pbio.0050198

Han, K. A., Um, J. W., & Ko, J. (2019). Intracellular protein complexes involved in synapse assembly in presynaptic neurons. Adv Protein Chem Struct Biol, 116, 347-373. https://doi.org/10.1016/bs.apcsb.2018.11.008

Han, X., Wang, C. T., Bai, J., Chapman, E. R., & Jackson, M. B. (2004). Transmembrane segments of syntaxin line the fusion pore of Ca2+-triggered exocytosis. Science, 304(5668), 289-292. https://doi.org/10.1126/science.1095801

Harlow, M., Ress, D., Koster, A., Marshall, R. M., Schwarz, M., & McMahan, U. J. (1998). Dissection of active zones at the neuromuscular junction by EM tomography. J Physiol Paris, 92(2), 75-78. https://doi.org/10.1016/S0928-4257(98)80141-1

Harlow, M. L., Ress, D., Stoschek, A., Marshall, R. M., & McMahan, U. J. (2001). The architecture of active zone material at the frog's neuromuscular junction. Nature, 409(6819), 479-484. https://doi.org/10.1038/35054000

Harlow, M. L., Szule, J. A., Xu, J., Jung, J. H., Marshall, R. M., & McMahan, U. J. (2013). Alignment of synaptic vesicle macromolecules with the macromolecules in active zone material that direct vesicle docking. PLoS One, 8(7), e69410. https://doi.org/10.1371/journal.pone.0069410

Harris, K. M., & Weinberg, R. J. (2012). Ultrastructure of synapses in the mammalian brain. Cold Spring Harb Perspect Biol, 4(5). https://doi.org/10.1101/cshperspect.a005587

Harris, N., Fetter, R. D., Brasier, D. J., Tong, A., & Davis, G. W. (2018). Molecular Interface of Neuronal Innate Immunity, Synaptic Vesicle Stabilization, and Presynaptic Homeostatic

Plasticity. Neuron, 100(5), 1163-1179 e1164. https://doi.org/10.1016/j.neuron.2018.09.048

Hata, Y., & Takai, Y. (1999). Roles of postsynaptic density-95/synapse-associated protein 90 and its interacting proteins in the organization of synapses. Cell Mol Life Sci, 56(5-6), 461-472. https://doi.org/10.1007/s000180050445

Haucke, V., & De Camilli, P. (1999). AP-2 recruitment to synaptotagmin stimulated by tyrosine-based endocytic motifs. Science, 285(5431), 1268-1271. https://doi.org/10.1126/science.285.5431.1268

Haucke, V., Wenk, M. R., Chapman, E. R., Farsad, K., & De Camilli, P. (2000). Dual interaction of synaptotagmin with mu2- and alpha-adaptin facilitates clathrin-coated pit nucleation. EMBO J, 19(22), 6011-6019. https://doi.org/10.1093/emboj/19.22.6011

Helmprobst, F., Frank, M., & Stigloher, C. (2015). Presynaptic architecture of the larval zebrafish neuromuscular junction. J Comp Neurol, 523(13), 1984-1997. https://doi.org/10.1002/cne.23775

Heuser, J., & Lennon, A. M. (1973). Morphological evidence for exocytosis of acetylcholine during formation of synaptosomes from Torpedo electric organ. J Physiol, 233(1), 39P-41P. https://www.ncbi.nlm.nih.gov/pubmed/4759116

Heuser, J. E., & Reese, T. S. (1973). Evidence for recycling of synaptic vesicle membrane during transmitter release at the frog neuromuscular junction. J Cell Biol, 57(2), 315-344. https://doi.org/10.1083/jcb.57.2.315

Hilton, B. J., Husch, A., Schaffran, B., Lin, T. C., Burnside, E. R., Dupraz, S., Schelski, M., Kim, J., Muller, J. A., Schoch, S., Imig, C., Brose, N., & Bradke, F. (2022). An active

vesicle priming machinery suppresses axon regeneration upon adult CNS injury. Neuron, 110(1), 51-69 e57. https://doi.org/10.1016/j.neuron.2021.10.007

Homan, A. E., & Meriney, S. D. (2018). Active zone structure-function relationships at the neuromuscular junction. Synapse, 72(11), e22057. https://doi.org/10.1002/syn.22057

Hughes, B. W., Kusner, L. L., & Kaminski, H. J. (2006). Molecular architecture of the neuromuscular junction. Muscle Nerve, 33(4), 445-461. https://doi.org/10.1002/mus.20440

Hui, E., Bai, J., Wang, P., Sugimori, M., Llinas, R. R., & Chapman, E. R. (2005). Three distinct kinetic groupings of the synaptotagmin family: candidate sensors for rapid and delayed exocytosis. Proc Natl Acad Sci U S A, 102(14), 5210-5214. https://doi.org/10.1073/pnas.0500941102

Hui, E., Gaffaney, J. D., Wang, Z., Johnson, C. P., Evans, C. S., & Chapman, E. R. (2011). Mechanism and function of synaptotagmin-mediated membrane apposition. Nat Struct Mol Biol, 18(7), 813-821. https://doi.org/10.1038/nsmb.2075

Hui, E., Johnson, C. P., Yao, J., Dunning, F. M., & Chapman, E. R. (2009). Synaptotagmin-mediated bending of the target membrane is a critical step in Ca(2+)-regulated fusion. Cell, 138(4), 709-721. https://doi.org/10.1016/j.cell.2009.05.049

Imig, C., Min, S. W., Krinner, S., Arancillo, M., Rosenmund, C., Sudhof, T. C., Rhee, J., Brose, N., & Cooper, B. H. (2014). The morphological and molecular nature of synaptic vesicle priming at presynaptic active zones. Neuron, 84(2), 416-431. https://doi.org/10.1016/j.neuron.2014.10.009

Imoto, Y., Raychaudhuri, S., Ma, Y., Fenske, P., Sandoval, E., Itoh, K., Blumrich, E. M., Matsubayashi, H. T., Mamer, L., Zarebidaki, F., Sohl-Kielczynski, B., Trimbuch, T.,

Nayak, S., Iwasa, J. H., Liu, J., Wu, B., Ha, T., Inoue, T., Jorgensen, E. M., . . . Watanabe, S. (2022). Dynamin is primed at endocytic sites for ultrafast endocytosis. Neuron, 110(17), 2815-2835 e2813. https://doi.org/10.1016/j.neuron.2022.06.010

Inkson, B. J. (2016). Scanning electron microscopy (SEM) and transmission electron microscopy (TEM) for materials characterization. In Materials Characterization Using Nondestructive Evaluation (NDE) Methods (pp. 17-43). https://doi.org/10.1016/b978-0-08-100040-3.00002-x

Jackson, M. B., & Chapman, E. R. (2006). Fusion pores and fusion machines in Ca2+-triggered exocytosis. Annu Rev Biophys Biomol Struct, 35, 135-160. https://doi.org/10.1146/annurev.biophys.35.040405.101958

Jackson, M. B., & Chapman, E. R. (2008). The fusion pores of Ca2+ -triggered exocytosis. Nat Struct Mol Biol, 15(7), 684-689. https://doi.org/10.1038/nsmb.1449

Jahn, R., Lang, T., & Sudhof, T. C. (2003). Membrane fusion. Cell, 112(4), 519-533. https://doi.org/10.1016/s0092-8674(03)00112-0

Jahne, S., Rizzoli, S. O., & Helm, M. S. (2015). The structure and function of presynaptic endosomes. Exp Cell Res, 335(2), 172-179. https://doi.org/10.1016/j.yexcr.2015.04.017

Jan, L. Y., & Jan, Y. N. (1976). Properties of the larval neuromuscular junction in *Drosophila* melanogaster. J Physiol, 262(1), 189-214. https://doi.org/10.1113/jphysiol.1976.sp011592

Jarousse, N., & Kelly, R. B. (2001). The AP-2 binding site of synaptotagmin 1 is not an internalization signal but a regulator of endocytosis. Journal of Cell Biology, 154(4), 857-866. https://doi.org/DOI 10.1083/jcb.200103040

Jarousse, N., Wilson, J. D., Arac, D., Rizo, J., & Kelly, R. B. (2003). Endocytosis of synaptotagmin 1 is mediated by a novel, tryptophan-containing motif. Traffic, 4(7), 468-478. https://doi.org/DOI 10.1034/j.1600-0854.2003.00101.x

Jiao, W., Masich, S., Franzen, O., & Shupliakov, O. (2010). Two pools of vesicles associated with the presynaptic cytosolic projection in *Drosophila* neuromuscular junctions. J Struct Biol, 172(3), 389-394. https://doi.org/10.1016/j.jsb.2010.07.007

John, A., Ng-Cordell, E., Hanna, N., Brkic, D., & Baker, K. (2021). The neurodevelopmental spectrum of synaptic vesicle cycling disorders. J Neurochem, 157(2), 208-228. https://doi.org/10.1111/jnc.15135

Jorgensen, E. M., Hartwieg, E., Schuske, K., Nonet, M. L., Jin, Y., & Horvitz, H. R. (1995). Defective recycling of synaptic vesicles in synaptotagmin mutants of Caenorhabditis elegans. Nature, 378(6553), 196-199. https://doi.org/10.1038/378196a0

Jung, J. H. (2019). Synaptic Vesicles Having Large Contact Areas with the Presynaptic Membrane are Preferentially Hemifused at Active Zones of Frog Neuromuscular Junctions Fixed during Synaptic Activity. Int J Mol Sci, 20(11). https://doi.org/10.3390/ijms20112692

Jung, J. H., & Doniach, S. (2017). A stochastic model of active zone material mediated synaptic vesicle docking and priming at resting active zones. Sci Rep, 7(1), 278. https://doi.org/10.1038/s41598-017-00360-z

Jung, J. H., Kirk, L. M., Bourne, J. N., & Harris, K. M. (2021). Shortened tethering filaments stabilize presynaptic vesicles in support of elevated release probability during LTP in rat hippocampus. Proc Natl Acad Sci U S A, 118(17). https://doi.org/10.1073/pnas.2018653118

Jung, J. H., & Szule, J. (2017). Automatic Optimization Method for Segmentation and Surface Model Generation in Electron Tomography. IEEE Life Sciences Letters, 3(2), 5-8. https://doi.org/10.1109/lls.2017.2756886

Jung, J. H., Szule, J. A., Marshall, R. M., & McMahan, U. J. (2016). Variable priming of a docked synaptic vesicle. Proc Natl Acad Sci U S A, 113(8), E1098-1107. https://doi.org/10.1073/pnas.1523054113

Jung, J. H., Szule, J. A., Stouder, K., Marshall, R. M., & McMahan, U. J. (2018). Active Zone Material-Directed Orientation, Docking, and Fusion of Dense Core Vesicles Alongside Synaptic Vesicles at Neuromuscular Junctions. Front Neuroanat, 12, 72. https://doi.org/10.3389/fnana.2018.00072

Kaeser, P. S., Kwon, H. B., Chiu, C. Q., Deng, L., Castillo, P. E., & Sudhof, T. C. (2008). RIM1alpha and RIM1beta are synthesized from distinct promoters of the RIM1 gene to mediate differential but overlapping synaptic functions. J Neurosci, 28(50), 13435-13447. https://doi.org/10.1523/JNEUROSCI.3235-08.2008

Kaeser-Woo, Y. J., Yang, X., & Sudhof, T. C. (2012). C-terminal complexin sequence is selectively required for clamping and priming but not for Ca2+ triggering of synaptic exocytosis. J Neurosci, 32(8), 2877-2885. https://doi.org/10.1523/JNEUROSCI.3360-11.2012

Kaeser-Woo, Y. J., Younts, T. J., Yang, X., Zhou, P., Wu, D., Castillo, P. E., & Sudhof, T. C. (2013). Synaptotagmin-12 phosphorylation by cAMP-dependent protein kinase is essential for hippocampal mossy fiber LTP. J Neurosci, 33(23), 9769-9780. https://doi.org/10.1523/JNEUROSCI.5814-12.2013

Karmakar, S., Sharma, L. G., Roy, A., Patel, A., & Pandey, L. M. (2019). Neuronal SNARE complex: A protein folding system with intricate protein-protein interactions, and its common neuropathological hallmark, SNAP-25. Neurochem Int, 122, 196-207. https://doi.org/10.1016/j.neuint.2018.12.001

Kasatkina, L. A., Gumenyuk, V. P., Sturm, E. M., Heinemann, A., Bernas, T., & Trikash, I. O. (2018). Modulation of neurosecretion and approaches for its multistep analysis. Biochim Biophys Acta Gen Subj, 1862(12), 2701-2713. https://doi.org/10.1016/j.bbagen.2018.08.004

Katz, B. (1970). Quantal mechanism of neural transmitter release. Science, 173(3992), 123-126. https://doi.org/10.1126/science.173.3992.123

Katz, B. (2003). Neural transmitter release: from quantal secretion to exocytosis and beyond. J Neurocytol, 32(5-8), 437-446. https://doi.org/10.1023/B:NEUR.0000020603.84188.03

Katz, B., & Miledi, R. (1964). Further Observations on the Distribution of Actylcholine-Reactive Sites in Skeletal Muscle. J Physiol, 170(2), 379-388. https://doi.org/10.1113/jphysiol.1964.sp007338

Katz, B., & Miledi, R. (1965). The Measurement of Synaptic Delay, and the Time Course of Acetylcholine Release at the Neuromuscular Junction. Proc R Soc Lond B Biol Sci, 161, 483-495. https://doi.org/10.1098/rspb.1965.0016

Katz, B., & Miledi, R. (1965). Propagation of Electric Activity in Motor Nerve Terminals. Proc R Soc Lond B Biol Sci, 161, 453-482. https://doi.org/10.1098/rspb.1965.0015

Katz, B., & Miledi, R. (1967). The timing of calcium action during neuromuscular transmission. J Physiol, 189(3), 535-544. https://doi.org/10.1113/jphysiol.1967.sp008183

Katz, B., & Miledi, R. (1970). Further study of the role of calcium in synaptic transmission. J Physiol, 207(3), 789-801. https://doi.org/10.1113/jphysiol.1970.sp009095

Katz, B., & Miledi, R. (1970). Membrane noise produced by acetylcholine. Nature, 226(5249), 962-963. https://doi.org/10.1038/226962a0

Kawasaki, F., Collins, S. C., & Ordway, R. W. (2002). Synaptic calcium-channel function in *Drosophila*: analysis and transformation rescue of temperature-sensitive paralytic and lethal mutations of cacophony. J Neurosci, 22(14), 5856-5864. https://doi.org/10.1523/JNEUROSCI.22-14-05856.2002

Kittel, R. J., Wichmann, C., Rasse, T. M., Fouquet, W., Schmidt, M., Schmid, A., Wagh, D. A., Pawlu, C., Kellner, R. R., Willig, K. I., Hell, S. W., Buchner, E., Heckmann, M., & Sigrist, S. J. (2006). Bruchpilot promotes active zone assembly, Ca2+ channel clustering, and vesicle release. Science, 312(5776), 1051-1054. https://doi.org/10.1126/science.1126308

Knight, D., Iliadi, K., Charlton, M. P., Atwood, H. L., & Boulianne, G. L. (2007). Presynaptic plasticity and associative learning are impaired in a *Drosophila* presenilin null mutant. Dev Neurobiol, 67(12), 1598-1613. https://doi.org/10.1002/dneu.20532

Ko, J., Yoon, C., Piccoli, G., Chung, H. S., Kim, K., Lee, J. R., Lee, H. W., Kim, H., Sala, C., & Kim, E. (2006). Organization of the presynaptic active zone by ERC2/CAST1-dependent clustering of the tandem PDZ protein syntenin-1. J Neurosci, 26(3), 963-970. https://doi.org/10.1523/jneurosci.4475-05.2006

Kobbersmed, J. R., Grasskamp, A. T., Jusyte, M., Bohme, M. A., Ditlevsen, S., Sorensen, J. B., & Walter, A. M. (2020). Rapid regulation of vesicle priming explains synaptic facilitation

despite heterogeneous vesicle:Ca(2+) channel distances. Elife, 9. https://doi.org/10.7554/eLife.51032

Kochubey, O., & Schneggenburger, R. (2011). Synaptotagmin increases the dynamic range of synapses by driving Ca(2)+-evoked release and by clamping a near-linear remaining Ca(2)+ sensor. Neuron, 69(4), 736-748. https://doi.org/10.1016/j.neuron.2011.01.013

Koenig, J. H., & Ikeda, K. (1989). Disappearance and reformation of synaptic vesicle membrane upon transmitter release observed under reversible blockage of membrane retrieval. J Neurosci, 9(11), 3844-3860. https://doi.org/10.1523/JNEUROSCI.09-11-03844.1989

Koenig, J. H., & Ikeda, K. (1996). Synaptic vesicles have two distinct recycling pathways. J Cell Biol, 135(3), 797-808. https://doi.org/10.1083/jcb.135.3.797

Koenig, J. H., & Ikeda, K. (1999). Contribution of active zone subpopulation of vesicles to evoked and spontaneous release. J Neurophysiol, 81(4), 1495-1505. https://doi.org/10.1152/jn.1999.81.4.1495

Koenig, J. H., Kosaka, T., & Ikeda, K. (1989). The relationship between the number of synaptic vesicles and the amount of transmitter released. J Neurosci, 9(6), 1937-1942. https://doi.org/10.1523/JNEUROSCI.09-06-01937.1989

Kusick, G. F., Ogunmowo, T. H., & Watanabe, S. (2022). Transient docking of synaptic vesicles: Implications and mechanisms. Curr Opin Neurobiol, 74, 102535. https://doi.org/10.1016/j.conb.2022.102535

Lagache, T., Grassart, A., Dallongeville, S., Faklaris, O., Sauvonnet, N., Dufour, A., Danglot, L., & Olivo-Marin, J. C. (2018). Mapping molecular assemblies with fluorescence microscopy and object-based spatial statistics. Nat Commun, 9(1), 698. https://doi.org/10.1038/s41467-018-03053-x

Laghaei, R., Ma, J., Tarr, T. B., Homan, A. E., Kelly, L., Tilvawala, M. S., Vuocolo, B. S., Rajasekaran, H. P., Meriney, S. D., & Dittrich, M. (2018). Transmitter release site organization can predict synaptic function at the neuromuscular junction. J Neurophysiol, 119(4), 1340-1355. https://doi.org/10.1152/jn.00168.2017

Landis, D. M., Hall, A. K., Weinstein, L. A., & Reese, T. S. (1988). The organization of cytoplasm at the presynaptic active zone of a central nervous system synapse. Neuron, 1(3), 201-209. https://doi.org/10.1016/0896-6273(88)90140-7

Lazarevic, V., Pothula, S., Andres-Alonso, M., & Fejtova, A. (2013). Molecular mechanisms driving homeostatic plasticity of neurotransmitter release. Front Cell Neurosci, 7, 244. https://doi.org/10.3389/fncel.2013.00244

Lee, J., Guan, Z., Akbergenova, Y., & Littleton, J. T. (2013). Genetic analysis of synaptotagmin C2 domain specificity in regulating spontaneous and evoked neurotransmitter release. J Neurosci, 33(1), 187-200. https://doi.org/10.1523/JNEUROSCI.3214-12.2013

Leitinger, G., Masich, S., Neumüller, J., Pabst, M. A., Pavelka, M., Rind, F. C., Shupliakov, O., Simmons, P. J., & Kolb, D. (2012). Structural organization of the presynaptic density at identified synapses in the locust central nervous system. J Comp Neurol, 520(2), 384-400. https://doi.org/10.1002/cne.22744

Lepicard, S., Franco, B., de Bock, F., & Parmentier, M. L. (2014). A presynaptic role of microtubule-associated protein 1/Futsch in *Drosophila*: regulation of active zone number and neurotransmitter release. J Neurosci, 34(20), 6759-6771. https://doi.org/10.1523/jneurosci.4282-13.2014

Li, C., Ullrich, B., Zhang, J. Z., Anderson, R. G., Brose, N., & Sudhof, T. C. (1995). Ca(2+)-dependent and -independent activities of neural and non-neural synaptotagmins. Nature, 375(6532), 594-599. https://doi.org/10.1038/375594a0

Li, L., Shin, O. H., Rhee, J. S., Araç, D., Rah, J. C., Rizo, J., Südhof, T., & Rosenmund, C. (2006). Phosphatidylinositol phosphates as co-activators of Ca2+ binding to C2 domains of synaptotagmin 1. J Biol Chem, 281(23), 15845-15852. https://doi.org/10.1074/jbc.M600888200

Li, W., Geng, C., & Liu, B. (2018). Visualization of synaptic vesicle dynamics with fluorescence proteins. Folia Neuropathol, 56(1), 21-29. https://doi.org/10.5114/fn.2018.74656

Li, X., Radhakrishnan, A., Grushin, K., Kasula, R., Chaudhuri, A., Gomathinayagam, S., Krishnakumar, S. S., Liu, J., & Rothman, J. E. (2019). Symmetrical organization of proteins under docked synaptic vesicles. FEBS Lett, 593(2), 144-153. https://doi.org/10.1002/1873-3468.13316

Li, X., Wu, Y., Su, Y., Rey-Suarez, I., Matthaeus, C., Updegrove, T. B., Wei, Z., Zhang, L., Sasaki, H., Li, Y., Guo, M., Giannini, J. P., Vishwasrao, H. D., Chen, J., Lee, S. J., Shao, L., Liu, H., Ramamurthi, K. S., Taraska, J. W., . . . Shroff, H. (2023). Three-dimensional structured illumination microscopy with enhanced axial resolution. Nat Biotechnol. https://doi.org/10.1038/s41587-022-01651-1

Li, Z., Burrone, J., Tyler, W. J., Hartman, K. N., Albeanu, D. F., & Murthy, V. N. (2005). Synaptic vesicle recycling studied in transgenic mice expressing synaptopHluorin. Proc Natl Acad Sci U S A, 102(17), 6131-6136. https://doi.org/10.1073/pnas.0501145102

Lin, K. H., Taschenberger, H., & Neher, E. (2022). A sequential two-step priming scheme reproduces diversity in synaptic strength and short-term plasticity. Proc Natl Acad Sci U S A, 119(34), e2207987119. https://doi.org/10.1073/pnas.2207987119

Littleton, J. T. (2006). Mixing and matching during synaptic vesicle endocytosis. Neuron, 51(2), 149-151. https://doi.org/10.1016/j.neuron.2006.07.002

Littleton, J. T., Bai, J., Vyas, B., Desai, R., Baltus, A. E., Garment, M. B., Carlson, S. D., Ganetzky, B., & Chapman, E. R. (2001). synaptotagmin mutants reveal essential functions for the C2B domain in Ca2+-triggered fusion and recycling of synaptic vesicles in vivo. J Neurosci, 21(5), 1421-1433. https://doi.org/10.1523/JNEUROSCI.21-05-01421.2001

Littleton, J. T., Bellen, H. J., & Perin, M. S. (1993). Expression of synaptotagmin in *Drosophila* reveals transport and localization of synaptic vesicles to the synapse. Development, 118(4), 1077-1088. https://doi.org/10.1242/dev.118.4.1077

Littleton, J. T., Chapman, E. R., Kreber, R., Garment, M. B., Carlson, S. D., & Ganetzky, B. (1998). Temperature-sensitive paralytic mutations demonstrate that synaptic exocytosis requires SNARE complex assembly and disassembly. Neuron, 21(2), 401-413. https://doi.org/10.1016/s0896-6273(00)80549-8

Littleton, J. T., Stern, M., Perin, M., & Bellen, H. J. (1994). Calcium dependence of neurotransmitter release and rate of spontaneous vesicle fusions are altered in *Drosophila* synaptotagmin mutants. Proc Natl Acad Sci U S A, 91(23), 10888-10892. https://doi.org/10.1073/pnas.91.23.10888

Littleton, J. T., Stern, M., Schulze, K., Perin, M., & Bellen, H. J. (1993). Mutational analysis of *Drosophila* synaptotagmin demonstrates its essential role in Ca(2+)-activated

neurotransmitter release. Cell, 74(6), 1125-1134. https://doi.org/10.1016/0092-8674(93)90733-7

Liu, C., & Kaeser, P. S. (2019). Nanoscale Location Matters: Emerging Principles of Ca(2+) Channel Organization at the Presynaptic Active Zone. Neuron, 104(4), 627-629. https://doi.org/10.1016/j.neuron.2019.10.015

Liu, S., Hoess, P., & Ries, J. (2022). Super-Resolution Microscopy for Structural Cell Biology. Annu Rev Biophys, 51, 301-326. https://doi.org/10.1146/annurev-biophys-102521-112912

Liu, T., Wang, T., Chapman, E. R., & Weisshaar, J. C. (2008). Productive hemifusion intermediates in fast vesicle fusion driven by neuronal SNAREs. Biophys J, 94(4), 1303-1314. https://doi.org/10.1529/biophysj.107.107896

Liu, Z., Chen, Z., Shang, C., Yan, F., Shi, Y., Zhang, J., Qu, B., Han, H., Wang, Y., Li, D., Sudhof, T. C., & Cao, P. (2017). IGF1-Dependent Synaptic Plasticity of Mitral Cells in Olfactory Memory during Social Learning. Neuron, 95(1), 106-122 e105. https://doi.org/10.1016/j.neuron.2017.06.015

Liu, Z., Zhu, Y., Zhang, L., Jiang, W., Liu, Y., Tang, Q., Cai, X., Li, J., Wang, L., Tao, C., Yin, X., Li, X., Hou, S., Jiang, D., Liu, K., Zhou, X., Zhang, H., Liu, M., Fan, C., & Tian, Y. (2023). Structural and functional imaging of brains. Sci China Chem, 66(2), 324-366. https://doi.org/10.1007/s11426-022-1408-5

Llinas, R. R., Sugimori, M., Moran, K. A., Moreira, J. E., & Fukuda, M. (2004). Vesicular reuptake inhibition by a synaptotagmin I C2B domain antibody at the squid giant synapse. Proc Natl Acad Sci U S A, 101(51), 17855-17860. https://doi.org/10.1073/pnas.0408200101

Lloyd, T. E., Verstreken, P., Ostrin, E. J., Phillippi, A., Lichtarge, O., & Bellen, H. J. (2000). A genome-wide search for synaptic vesicle cycle proteins in *Drosophila*. Neuron, 26(1), 45-50. https://doi.org/10.1016/s0896-6273(00)81136-8

Loewen, C. A., Lee, S. M., Shin, Y. K., & Reist, N. E. (2006). C2B polylysine motif of synaptotagmin facilitates a Ca2+-independent stage of synaptic vesicle priming in vivo. Molecular Biology of the Cell, 17(12), 5211-5226. https://doi.org/10.1091/mbc.E06-07-0622

Loewen, C. A., Mackler, J. M., & Reist, N. E. (2001). *Drosophila* synaptotagmin I null mutants survive to early adulthood. Genesis, 31(1), 30-36. https://doi.org/10.1002/gene.10002

Loewen, C. A., Royer, S. M., & Reist, N. E. (2006). *Drosophila* synaptotagmin I null mutants show severe alterations in vesicle populations but calcium-binding motif mutants do not. J Comp Neurol, 496(1), 1-12. https://doi.org/10.1002/cne.20868

Long, B. R., Robinson, D. C., & Zhong, H. (2014). Subdiffractive microscopy: techniques, applications, and challenges. Wiley Interdiscip Rev Syst Biol Med, 6(2), 151-168. https://doi.org/10.1002/wsbm.1259

Lucic, V., Forster, F., & Baumeister, W. (2005). Structural studies by electron tomography: from cells to molecules. Annu Rev Biochem, 74, 833-865. https://doi.org/10.1146/annurev.biochem.73.011303.074112

Lunardi, N., Oklopcic, A., Prillaman, M., Erisir, A., & Jevtovic-Todorovic, V. (2015). Early Exposure to General Anesthesia Disrupts Spatial Organization of Presynaptic Vesicles in Nerve Terminals of the Developing Rat Subiculum. Mol Neurobiol, 52(2), 942-951. https://doi.org/10.1007/s12035-015-9246-7

Luo, F., Bacaj, T., & Sudhof, T. C. (2015). Synaptotagmin-7 Is Essential for Ca2+-Triggered Delayed Asynchronous Release But Not for Ca2+-Dependent Vesicle Priming in Retinal Ribbon Synapses. J Neurosci, 35(31), 11024-11033. https://doi.org/10.1523/JNEUROSCI.0759-15.2015

Luo, F., & Sudhof, T. C. (2017). Synaptotagmin-7-Mediated Asynchronous Release Boosts High-Fidelity Synchronous Transmission at a Central Synapse. Neuron, 94(4), 826-839 e823. https://doi.org/10.1016/j.neuron.2017.04.020

Mace, K. E., Biela, L. M., Sares, A. G., & Reist, N. E. (2009). Synaptotagmin I stabilizes synaptic vesicles via its C(2)A polylysine motif. Genesis, 47(5), 337-345. https://doi.org/10.1002/dvg.20502

Macintosh, B. R., Jones, D., Devrome, A. N., & Rassier, D. E. (2007). Prediction of summation in incompletely fused tetanic contractions of rat muscle. J Biomech, 40(5), 1066-1072. https://doi.org/10.1016/j.jbiomech.2006.04.009

Mackler, J. M., Drummond, J. A., Loewen, C. A., Robinson, I. M., & Reist, N. E. (2002). The C(2)B Ca(2+)-binding motif of synaptotagmin is required for synaptic transmission in vivo. Nature, 418(6895), 340-344. https://doi.org/10.1038/nature00846

Mackler, J. M., & Reist, N. E. (2001). Mutations in the second C2 domain of synaptotagmin disrupt synaptic transmission at *Drosophila* neuromuscular junctions. J Comp Neurol, 436(1), 4-16. https://www.ncbi.nlm.nih.gov/pubmed/11413542

Macleod, G. T., Marin, L., Charlton, M. P., & Atwood, H. L. (2004). Synaptic vesicles: test for a role in presynaptic calcium regulation. J Neurosci, 24(10), 2496-2505. https://doi.org/10.1523/jneurosci.5372-03.2004

Madziva, M. T., Bai, J., Bhalla, A., Chapman, E. R., & Edwardson, J. M. (2005). Effects of synaptotagmin reveal two distinct mechanisms of agonist-stimulated internalization of the M4 muscarinic acetylcholine receptor. Br J Pharmacol, 144(6), 761-771. https://doi.org/10.1038/sj.bjp.0706035

Maidorn, M., Rizzoli, S. O., & Opazo, F. (2016). Tools and limitations to study the molecular composition of synapses by fluorescence microscopy. Biochem J, 473(20), 3385-3399. https://doi.org/10.1042/BCJ20160366

Matthew, W. D., Tsavaler, L., & Reichardt, L. F. (1981). Identification of a synaptic vesicle-specific membrane protein with a wide distribution in neuronal and neurosecretory tissue. J Cell Biol, 91(1), 257-269. https://doi.org/10.1083/jcb.91.1.257

Maus, L., Lee, C., Altas, B., Sertel, S. M., Weyand, K., Rizzoli, S. O., Rhee, J., Brose, N., Imig, C., & Cooper, B. H. (2020). Ultrastructural Correlates of Presynaptic Functional Heterogeneity in Hippocampal Synapses. Cell Rep, 30(11), 3632-3643 e3638. https://doi.org/10.1016/j.celrep.2020.02.083

Maximov, A., Tang, J., Yang, X., Pang, Z. P., & Sudhof, T. C. (2009). Complexin controls the force transfer from SNARE complexes to membranes in fusion. Science, 323(5913), 516-521. https://doi.org/10.1126/science.1166505

McMahan, U. J., & Wallace, B. G. (1989). Molecules in basal lamina that direct the formation of synaptic specializations at neuromuscular junctions. Dev Neurosci, 11(4-5), 227-247. https://doi.org/10.1159/000111903

McMahon, H. T., & Sudhof, T. C. (1995). Synaptic core complex of synaptobrevin, syntaxin, and SNAP-25 forms high affinity alpha-SNAP binding site. J Biol Chem, 270(5), 2213-2217. https://doi.org/10.1074/jbc.270.5.2213

Meinertzhagen, I. A., & Sorra, K. E. (2001). Synaptic organization in the fly's optic lamina: few cells, many synapses and divergent microcircuits. Prog Brain Res, 131, 53-69. https://doi.org/10.1016/s0079-6123(01)31007-5

Meriney, S. D., & Dittrich, M. (2013). Organization and function of transmitter release sites at the neuromuscular junction. J Physiol, 591(13), 3159-3165. https://doi.org/10.1113/jphysiol.2012.248625

Michel, K., Muller, J. A., Oprisoreanu, A. M., & Schoch, S. (2015). The presynaptic active zone: A dynamic scaffold that regulates synaptic efficacy. Exp Cell Res, 335(2), 157-164. https://doi.org/10.1016/j.yexcr.2015.02.011

Millar, A. G., Bradacs, H., Charlton, M. P., & Atwood, H. L. (2002). Inverse relationship between release probability and readily releasable vesicles in depressing and facilitating synapses. J Neurosci, 22(22), 9661-9667. https://doi.org/10.1523/jneurosci.22-22-09661.2002

Millar, A. G., Zucker, R. S., Ellis-Davies, G. C., Charlton, M. P., & Atwood, H. L. (2005). Calcium sensitivity of neurotransmitter release differs at phasic and tonic synapses. J Neurosci, 25(12), 3113-3125. https://doi.org/10.1523/jneurosci.4717-04.2005

Min, D., Kim, K., Hyeon, C., Cho, Y. H., Shin, Y. K., & Yoon, T. Y. (2013). Mechanical unzipping and rezipping of a single SNARE complex reveals hysteresis as a force-generating mechanism. Nat Commun, 4, 1705. https://doi.org/10.1038/ncomms2692

Mizutani, A., Fukuda, M., Niinobe, M., & Mikoshiba, K. (1997). Regulation of AP-2-synaptotagmin interaction by inositol high polyphosphates. Biochemical and Biophysical Research Communications, 240(1), 128-131. https://doi.org/DOI 10.1006/bbrc.1997.7578

Mochida, S., Fukuda, M., Niinobe, M., Kobayashi, H., & Mikoshiba, K. (1997). Roles of synaptotagmin C2 domains in neurotransmitter secretion and inositol high-polyphosphate binding at mammalian cholinergic synapses. Neuroscience, 77(4), 937-943. https://doi.org/10.1016/s0306-4522(96)00572-6

Nagwaney, S., Harlow, M. L., Jung, J. H., Szule, J. A., Ress, D., Xu, J., Marshall, R. M., & McMahan, U. J. (2009). Macromolecular connections of active zone material to docked synaptic vesicles and presynaptic membrane at neuromuscular junctions of mouse. J Comp Neurol, 513(5), 457-468. https://doi.org/10.1002/cne.21975

Nalefski, E. A., & Falke, J. J. (1996). The C2 domain calcium-binding motif: structural and functional diversity. Protein Sci, 5(12), 2375-2390. https://doi.org/10.1002/pro.5560051201

Nalefski, E. A., Wisner, M. A., Chen, J. Z., Sprang, S. R., Fukuda, M., Mikoshiba, K., & Falke, J. J. (2001). C2 domains from different Ca2+ signaling pathways display functional and mechanistic diversity. Biochemistry, 40(10), 3089-3100. https://doi.org/10.1021/bi001968a

Neher, E., & Brose, N. (2018). Dynamically Primed Synaptic Vesicle States: Key to Understand Synaptic Short-Term Plasticity. Neuron, 100(6), 1283-1291. https://doi.org/10.1016/j.neuron.2018.11.024

Nelson, J. C., Stavoe, A. K., & Colón-Ramos, D. A. (2013). The actin cytoskeleton in presynaptic assembly. Cell Adh Migr, 7(4), 379-387. https://doi.org/10.4161/cam.24803

Nestvogel, D. B., Merino, R. M., Leon-Pinzon, C., Schottdorf, M., Lee, C., Imig, C., Brose, N., & Rhee, J. S. (2020). The Synaptic Vesicle Priming Protein CAPS-1 Shapes the

Adaptation of Sensory Evoked Responses in Mouse Visual Cortex. Cell Rep, 30(10), 3261-3269 e3264. https://doi.org/10.1016/j.celrep.2020.02.045

Nishiki, T., & Augustine, G. J. (2004). Dual roles of the C2B domain of synaptotagmin I in synchronizing Ca2+-dependent neurotransmitter release. J Neurosci, 24(39), 8542-8550. https://doi.org/10.1523/JNEUROSCI.2545-04.2004

Nishiki, T., & Augustine, G. J. (2004). Synaptotagmin I synchronizes transmitter release in mouse hippocampal neurons. J Neurosci, 24(27), 6127-6132. https://doi.org/10.1523/JNEUROSCI.1563-04.2004

Nishimune, H. (2012). Molecular mechanism of active zone organization at vertebrate neuromuscular junctions. Mol Neurobiol, 45(1), 1-16. https://doi.org/10.1007/s12035-011-8216-y

Nishimune, H. (2012). Active zones of mammalian neuromuscular junctions: formation, density, and aging. Ann N Y Acad Sci, 1274(1), 24-32. https://doi.org/10.1111/j.1749-6632.2012.06836.x

Nonet, M. L., Holgado, A. M., Brewer, F., Serpe, C. J., Norbeck, B. A., Holleran, J., Wei, L., Hartwieg, E., Jorgensen, E. M., & Alfonso, A. (1999). UNC-11, a Caenorhabditis elegans AP180 homologue, regulates the size and protein composition of synaptic vesicles. Mol Biol Cell, 10(7), 2343-2360. https://doi.org/10.1091/mbc.10.7.2343

Nyenhuis, S. B., Thapa, A., & Cafiso, D. S. (2019). Phosphatidylinositol 4,5 Bisphosphate Controls the cis and trans Interactions of Synaptotagmin 1. Biophys J, 117(2), 247-257. https://doi.org/10.1016/j.bpj.2019.06.016

O'Connor-Giles, K. M., & Ganetzky, B. (2008). Satellite signaling at synapses. Fly (Austin), 2(5), 259-261. https://doi.org/10.4161/fly.7133

Osborne, S. L., Wallis, T. P., Jimenez, J. L., Gorman, J. J., & Meunier, F. A. (2007). Identification of secretory granule phosphatidylinositol 4,5-bisphosphate-interacting proteins using an affinity pulldown strategy. Mol Cell Proteomics, 6(7), 1158-1169. https://doi.org/10.1074/mcp.M600430-MCP200

Osborne, S. L., Wallis, T. P., Jimenez, J. L., Gorman, J. J., & Meunier, F. A. (2007). Identification of secretory granule phosphatidylinositol 4,5-bisphosphateinteracting proteins using an affinity pulldown strategy. Molecular & Cellular Proteomics, 6(7), 1158-1169. https://doi.org/10.1074/mcp.M600430-MCP200

Owald, D., & Sigrist, S. J. (2009). Assembling the presynaptic active zone. Curr Opin Neurobiol, 19(3), 311-318. https://doi.org/10.1016/j.conb.2009.03.003

Paddock, B. E., Striegel, A. R., Hui, E., Chapman, E. R., & Reist, N. E. (2008). Ca2+-dependent, phospholipid-binding residues of synaptotagmin are critical for excitation-secretion coupling in vivo. J Neurosci, 28(30), 7458-7466. https://doi.org/10.1523/jneurosci.0197-08.2008

Paddock, B. E., Wang, Z., Biela, L. M., Chen, K., Getzy, M. D., Striegel, A., Richmond, J. E., Chapman, E. R., Featherstone, D. E., & Reist, N. E. (2011). Membrane penetration by synaptotagmin is required for coupling calcium binding to vesicle fusion in vivo. J Neurosci, 31(6), 2248-2257. https://doi.org/10.1523/jneurosci.3153-09.2011

Padmanabhan, P., Bademosi, A. T., Kasula, R., Lauwers, E., Verstreken, P., & Meunier, F. A. (2020). Need for speed: Super-resolving the dynamic nanoclustering of syntaxin-1 at exocytic fusion sites. Neuropharmacology, 169, 107554. https://doi.org/10.1016/j.neuropharm.2019.02.036

Pang, Z. P., Bacaj, T., Yang, X., Zhou, P., Xu, W., & Sudhof, T. C. (2011). Doc2 supports spontaneous synaptic transmission by a Ca(2+)-independent mechanism. Neuron, 70(2), 244-251. https://doi.org/10.1016/j.neuron.2011.03.011

Pang, Z. P., & Sudhof, T. C. (2010). Cell biology of Ca2+-triggered exocytosis. Curr Opin Cell Biol, 22(4), 496-505. https://doi.org/10.1016/j.ceb.2010.05.001

Pang, Z. P., Xu, W., Cao, P., & Sudhof, T. C. (2010). Calmodulin suppresses synaptotagmin-2 transcription in cortical neurons. J Biol Chem, 285(44), 33930-33939. https://doi.org/10.1074/jbc.M110.150151

Parfitt, K., Reist, N., Li, J., Burgess, R., Deitcher, D., DiAntonio, A., & Schwarz, T. L. (1995). *Drosophila* genetics and the functions of synaptic proteins. Cold Spring Harb Symp Quant Biol, 60, 371-377. https://doi.org/10.1101/sqb.1995.060.01.041

Park, Y., Hernandez, J. M., van den Bogaart, G., Ahmed, S., Holt, M., Riedel, D., & Jahn, R. (2012). Controlling synaptotagmin activity by electrostatic screening. Nat Struct Mol Biol, 19(10), 991-997. https://doi.org/10.1038/nsmb.2375

Patrizio, A., & Specht, C. G. (2016). Counting numbers of synaptic proteins: absolute quantification and single molecule imaging techniques. Neurophotonics, 3(4), 041805. https://doi.org/10.1117/1.NPh.3.4.041805

Pennycook, S. J. (2003). Transmission Electron Microscopy: Overview and Challenges AIP Conference Proceedings,

Perin, M. S., Fried, V. A., Mignery, G. A., Jahn, R., & Sudhof, T. C. (1990). Phospholipid binding by a synaptic vesicle protein homologous to the regulatory region of protein kinase C. Nature, 345(6272), 260-263. https://doi.org/10.1038/345260a0

Perin, M. S., Johnston, P. A., Ozcelik, T., Jahn, R., Francke, U., & Sudhof, T. C. (1991). Structural and functional conservation of synaptotagmin (p65) in *Drosophila* and humans. J Biol Chem, 266(1), 615-622. https://www.ncbi.nlm.nih.gov/pubmed/1840599

Petrenko, A. G., Perin, M. S., Davletov, B. A., Ushkaryov, Y. A., Geppert, M., & Sudhof, T. C. (1991). Binding of synaptotagmin to the alpha-latrotoxin receptor implicates both in synaptic vesicle exocytosis. Nature, 353(6339), 65-68. https://doi.org/10.1038/353065a0

Petzoldt, A. G., Lutzkendorf, J., & Sigrist, S. J. (2016). Mechanisms controlling assembly and plasticity of presynaptic active zone scaffolds. Curr Opin Neurobiol, 39, 69-76. https://doi.org/10.1016/j.conb.2016.04.009

Pofantis, E., Neher, E., & Dresbach, T. (2021). Regulation of a subset of release-ready vesicles by the presynaptic protein Mover. Proc Natl Acad Sci U S A, 118(3). https://doi.org/10.1073/pnas.2022551118

Poskanzer, K. E., Fetter, R. D., & Davis, G. W. (2006). Discrete residues in the c(2)b domain of synaptotagmin I independently specify endocytic rate and synaptic vesicle size. Neuron, 50(1), 49-62. https://doi.org/10.1016/j.neuron.2006.02.021

Prokop, A., & Meinertzhagen, I. A. (2006). Development and structure of synaptic contacts in *Drosophila*. Semin Cell Dev Biol, 17(1), 20-30. https://doi.org/10.1016/j.semcdb.2005.11.010

Pyle, J. L., Kavalali, E. T., Piedras-Renteria, E. S., & Tsien, R. W. (2000). Rapid reuse of readily releasable pool vesicles at hippocampal synapses. Neuron, 28(1), 221-231. https://doi.org/10.1016/s0896-6273(00)00098-2

Qin, N., Chen, Z., & Xue, R. (2022). A two-subpopulation model that reflects heterogeneity of large dense core vesicles in exocytosis. Cell Cycle, 21(5), 531-546. https://doi.org/10.1080/15384101.2022.2026576

Quinones-Frias, M. C., & Littleton, J. T. (2021). Function of *Drosophila* Synaptotagmins in membrane trafficking at synapses. Cell Mol Life Sci, 78(9), 4335-4364. https://doi.org/10.1007/s00018-021-03788-9

Radhakrishnan, A., Li, X., Grushin, K., Krishnakumar, S. S., Liu, J., & Rothman, J. E. (2021). Symmetrical arrangement of proteins under release-ready vesicles in presynaptic terminals. Proc Natl Acad Sci U S A, 118(5). https://doi.org/10.1073/pnas.2024029118

Reist, N. E., Buchanan, J., Li, J., DiAntonio, A., Buxton, E. M., & Schwarz, T. L. (1998). Morphologically docked synaptic vesicles are reduced in synaptotagmin mutants of *Drosophila*. J Neurosci, 18(19), 7662-7673. https://doi.org/10.1523/JNEUROSCI.18-19-07662.1998

Reshetniak, S., & Rizzoli, S. O. (2019). Interrogating Synaptic Architecture: Approaches for Labeling Organelles and Cytoskeleton Components. Front Synaptic Neurosci, 11, 23. https://doi.org/10.3389/fnsyn.2019.00023

Ress, D., Harlow, M. L., Schwarz, M., Marshall, R. M., & McMahan, U. J. (1999). Automatic acquisition of fiducial markers and alignment of images in tilt series for electron tomography. J Electron Microsc (Tokyo), 48(3), 277-287. https://doi.org/10.1093/oxfordjournals.jmicro.a023679

Ress, D. B., Harlow, M. L., Marshall, R. M., & McMahan, U. J. (2004). Methods for generating high-resolution structural models from electron microscope tomography data. Structure, 12(10), 1763-1774. https://doi.org/10.1016/j.str.2004.07.022

Rey, S. A., Smith, C. A., Fowler, M. W., Crawford, F., Burden, J. J., & Staras, K. (2015). Ultrastructural and functional fate of recycled vesicles in hippocampal synapses. Nat Commun, 6, 8043. https://doi.org/10.1038/ncomms9043

Richards, D. A., Bai, J., & Chapman, E. R. (2005). Two modes of exocytosis at hippocampal synapses revealed by rate of FM1-43 efflux from individual vesicles. J Cell Biol, 168(6), 929-939. https://doi.org/10.1083/jcb.200407148

Richards, D. A., Guatimosim, C., & Betz, W. J. (2000). Two endocytic recycling routes selectively fill two vesicle pools in frog motor nerve terminals. Neuron, 27(3), 551-559. https://doi.org/10.1016/s0896-6273(00)00065-9

Rickman, C., Archer, D. A., Meunier, F. A., Craxton, M., Fukuda, M., Burgoyne, R. D., & Davletov, B. (2004). Synaptotagmin interaction with the syntaxin/SNAP-25 dimer is mediated by an evolutionarily conserved motif and is sensitive to inositol hexakisphosphate. J Biol Chem, 279(13), 12574-12579. https://doi.org/10.1074/jbc.M310710200

Rigoard, P., Buffenoir, K., Bauche, S., Giot, J. P., Koenig, J., Hantai, D., Lapierre, F., & Wager, M. (2009). [Structural and molecular organization, development and maturation of the neuromuscular junction]. Neurochirurgie, 55 Suppl 1, S34-42. https://doi.org/10.1016/j.neuchi.2008.03.012 (Organisation structurale, moleculaire, formation et maturation de la jonction neuromusculaire.)

Rizo, J. (2022). Molecular Mechanisms Underlying Neurotransmitter Release. Annu Rev Biophys, 51, 377-408. https://doi.org/10.1146/annurev-biophys-111821-104732

Rizo, J., Sari, L., Qi, Y., Im, W., & Lin, M. M. (2022). All-atom molecular dynamics simulations of Synaptotagmin-SNARE-complexin complexes bridging a vesicle and a flat lipid bilayer. Elife, 11. https://doi.org/10.7554/eLife.76356

Rizo, J., & Sudhof, T. C. (1998). C2-domains, structure and function of a universal Ca2+-binding domain. J Biol Chem, 273(26), 15879-15882. https://doi.org/10.1074/jbc.273.26.15879

Rizo, J., & Sudhof, T. C. (2012). The membrane fusion enigma: SNAREs, Sec1/Munc18 proteins, and their accomplices--guilty as charged? Annu Rev Cell Dev Biol, 28, 279-308. https://doi.org/10.1146/annurev-cellbio-101011-155818

Rizo, J., & Xu, J. (2015). The Synaptic Vesicle Release Machinery. Annu Rev Biophys, 44, 339-367. https://doi.org/10.1146/annurev-biophys-060414-034057

Robinow, S., & White, K. (1988). The locus elav of *Drosophila* melanogaster is expressed in neurons at all developmental stages. Dev Biol, 126(2), 294-303. https://doi.org/10.1016/0012-1606(88)90139-x

Rostaing, P., Real, E., Siksou, L., Lechaire, J. P., Boudier, T., Boeckers, T. M., Gertler, F., Gundelfinger, E. D., Triller, A., & Marty, S. (2006). Analysis of synaptic ultrastructure without fixative using high-pressure freezing and tomography. Eur J Neurosci, 24(12), 3463-3474. https://doi.org/10.1111/j.1460-9568.2006.05234.x

Rothman, J. E. (1996). The protein machinery of vesicle budding and fusion. Protein Sci, 5(2), 185-194. https://doi.org/10.1002/pro.5560050201

Rothman, J. E., Grushin, K., Bera, M., & Pincet, F. (2023). Turbocharging synaptic transmission. FEBS Lett, 597(18), 2233-2249. https://doi.org/10.1002/1873-3468.14718

Rothman, J. E., Krishnakumar, S. S., Grushin, K., & Pincet, F. (2017). Hypothesis - buttressed rings assemble, clamp, and release SNAREpins for synaptic transmission. FEBS Lett, 591(21), 3459-3480. https://doi.org/10.1002/1873-3468.12874

Ryan, T. A., Reuter, H., & Smith, S. J. (1997). Optical detection of a quantal presynaptic membrane turnover. Nature, 388(6641), 478-482. https://doi.org/10.1038/41335

Ryan, T. A., Reuter, H., Wendland, B., Schweizer, F. E., Tsien, R. W., & Smith, S. J. (1993). The kinetics of synaptic vesicle recycling measured at single presynaptic boutons. Neuron, 11(4), 713-724. https://doi.org/10.1016/0896-6273(93)90081-2

Saludes, J. P., Morton, L. A., Ghosh, N., Beninson, L. A., Chapman, E. R., Fleshner, M., & Yin, H. (2012). Detection of highly curved membrane surfaces using a cyclic peptide derived from synaptotagmin-I. ACS Chem Biol, 7(10), 1629-1635. https://doi.org/10.1021/cb3002705

Saraswati, S., Adolfsen, B., & Littleton, J. T. (2007). Characterization of the role of the Synaptotagmin family as calcium sensors in facilitation and asynchronous neurotransmitter release. Proc Natl Acad Sci U S A, 104(35), 14122-14127. https://doi.org/10.1073/pnas.0706711104

Sauvola, C. W., & Littleton, J. T. (2021). SNARE Regulatory Proteins in Synaptic Vesicle Fusion and Recycling. Front Mol Neurosci, 14, 733138. https://doi.org/10.3389/fnmol.2021.733138

Scheefhals, N., & MacGillavry, H. D. (2018). Functional organization of postsynaptic glutamate receptors. Mol Cell Neurosci, 91, 82-94. https://doi.org/10.1016/j.mcn.2018.05.002

Schermelleh, L., Ferrand, A., Huser, T., Eggeling, C., Sauer, M., Biehlmaier, O., & Drummen, G. P. C. (2019). Super-resolution microscopy demystified. Nat Cell Biol, 21(1), 72-84. https://doi.org/10.1038/s41556-018-0251-8

Schiavo, G., Benfenati, F., Poulain, B., Rossetto, O., Polverino de Laureto, P., DasGupta, B. R., & Montecucco, C. (1992). Tetanus and botulinum-B neurotoxins block neurotransmitter release by proteolytic cleavage of synaptobrevin. Nature, 359(6398), 832-835. https://doi.org/10.1038/359832a0

Schiavo, G., Gmachl, M. J., Stenbeck, G., Sollner, T. H., & Rothman, J. E. (1995). A possible docking and fusion particle for synaptic transmission. Nature, 378(6558), 733-736. https://doi.org/10.1038/378733a0

Schiavo, G., Gu, Q. M., Prestwich, G. D., Sollner, T. H., & Rothman, J. E. (1996). Calcium-dependent switching of the specificity of phosphoinositide binding to synaptotagmin. Proc Natl Acad Sci U S A, 93(23), 13327-13332. https://doi.org/10.1073/pnas.93.23.13327

Schiavo, G., Stenbeck, G., Rothman, J. E., & Sollner, T. H. (1997). Binding of the synaptic vesicle v-SNARE, synaptotagmin, to the plasma membrane t-SNARE, SNAP-25, can explain docked vesicles at neurotoxin-treated synapses. Proc Natl Acad Sci U S A, 94(3), 997-1001. https://doi.org/10.1073/pnas.94.3.997

Schikorski, T. (2014). Readily releasable vesicles recycle at the active zone of hippocampal synapses. Proc Natl Acad Sci U S A, 111(14), 5415-5420. https://doi.org/10.1073/pnas.1321541111

Schoch, S., & Gundelfinger, E. D. (2006). Molecular organization of the presynaptic active zone. Cell Tissue Res, 326(2), 379-391. https://doi.org/10.1007/s00441-006-0244-y

Sclip, A., Bacaj, T., Giam, L. R., & Sudhof, T. C. (2016). Extended Synaptotagmin (ESyt) Triple Knock-Out Mice Are Viable and Fertile without Obvious Endoplasmic Reticulum Dysfunction. PLoS One, 11(6), e0158295. https://doi.org/10.1371/journal.pone.0158295

Segovia, M., Ales, E., Montes, M. A., Bonifas, I., Jemal, I., Lindau, M., Maximov, A., Sudhof, T. C., & Alvarez de Toledo, G. (2010). Push-and-pull regulation of the fusion pore by synaptotagmin-7. Proc Natl Acad Sci U S A, 107(44), 19032-19037. https://doi.org/10.1073/pnas.1014070107

Shahin, V., Datta, D., Hui, E., Henderson, R. M., Chapman, E. R., & Edwardson, J. M. (2008). Synaptotagmin perturbs the structure of phospholipid bilayers. Biochemistry, 47(7), 2143-2152. https://doi.org/10.1021/bi701879g

Sheng, M., & Kim, E. (2011). The postsynaptic organization of synapses. Cold Spring Harb Perspect Biol, 3(12). https://doi.org/10.1101/cshperspect.a005678

Shields, M. C., Bowers, M. R., Fulcer, M. M., Bollig, M. K., Rock, P. J., Sutton, B. R., Vrailas-Mortimer, A. D., Lochmuller, H., Whittaker, R. G., Horvath, R., & Reist, N. E. (2017). *Drosophila* studies support a role for a presynaptic synaptotagmin mutation in a human congenital myasthenic syndrome. PLoS One, 12(9), e0184817. https://doi.org/10.1371/journal.pone.0184817

Shields, M. C., Bowers, M. R., Kramer, H. L., Fulcer, M. M., Perinet, L. C., Metz, M. J., & Reist, N. E. (2020). The role of the C2A domain of synaptotagmin 1 in asynchronous neurotransmitter release. PLoS One, 15(5), e0232991. https://doi.org/10.1371/journal.pone.0232991

Shimojo, M., Madara, J., Pankow, S., Liu, X., Yates, J., 3rd, Sudhof, T. C., & Maximov, A. (2019). Synaptotagmin-11 mediates a vesicle trafficking pathway that is essential for

development and synaptic plasticity. Genes Dev, 33(5-6), 365-376. https://doi.org/10.1101/gad.320077.118

Shin, O. H., Xu, J., Rizo, J., & Sudhof, T. C. (2009). Differential but convergent functions of Ca2+ binding to synaptotagmin-1 C2 domains mediate neurotransmitter release. Proc Natl Acad Sci U S A, 106(38), 16469-16474. https://doi.org/10.1073/pnas.0908798106

Shon, M. J., Kim, H., & Yoon, T. Y. (2018). Focused clamping of a single neuronal SNARE complex by complexin under high mechanical tension. Nat Commun, 9(1), 3639. https://doi.org/10.1038/s41467-018-06122-3

Shu, X., Lev-Ram, V., Deerinck, T. J., Qi, Y., Ramko, E. B., Davidson, M. W., Jin, Y., Ellisman, M. H., & Tsien, R. Y. (2011). A genetically encoded tag for correlated light and electron microscopy of intact cells, tissues, and organisms. PLoS Biol, 9(4), e1001041. https://doi.org/10.1371/journal.pbio.1001041

Sigrist, S. J., & Schmitz, D. (2011). Structural and functional plasticity of the cytoplasmic active zone. Curr Opin Neurobiol, 21(1), 144-150. https://doi.org/10.1016/j.conb.2010.08.012

Slater, C. R. (2015). The functional organization of motor nerve terminals. Prog Neurobiol, 134, 55-103. https://doi.org/10.1016/j.pneurobio.2015.09.004

Smith, J. E., & Reese, T. S. (1980). Use of aldehyde fixatives to determine the rate of synaptic transmitter release. J Exp Biol, 89, 19-29. https://doi.org/10.1242/jeb.89.1.19

Sollner, T. H., & Rothman, J. E. (1996). Molecular machinery mediating vesicle budding, docking and fusion. Cell Struct Funct, 21(5), 407-412. https://doi.org/10.1247/csf.21.407

Stewart, B. A., Atwood, H. L., Renger, J. J., Wang, J., & Wu, C. F. (1994). Improved stability of *Drosophila* larval neuromuscular preparations in haemolymph-like physiological solutions. J Comp Physiol A, 175(2), 179-191. https://doi.org/10.1007/BF00215114

Stigloher, C., Zhan, H., Zhen, M., Richmond, J., & Bessereau, J. L. (2011). The presynaptic dense projection of the Caenorhabditis elegans cholinergic neuromuscular junction localizes synaptic vesicles at the active zone through SYD-2/liprin and UNC-10/RIM-dependent interactions. J Neurosci, 31(12), 4388-4396. https://doi.org/10.1523/JNEUROSCI.6164-10.2011

Striegel, A. R., Biela, L. M., Evans, C. S., Wang, Z., Delehoy, J. B., Sutton, R. B., Chapman, E. R., & Reist, N. E. (2012). Calcium binding by synaptotagmin's C2A domain is an essential element of the electrostatic switch that triggers synchronous synaptic transmission. J Neurosci, 32(4), 1253-1260. https://doi.org/10.1523/jneurosci.4652-11.2012

Sudhof, T. C. (2004). The synaptic vesicle cycle. Annu Rev Neurosci, 27, 509-547. https://doi.org/10.1146/annurev.neuro.26.041002.131412

Sudhof, T. C. (2012). Calcium control of neurotransmitter release. Cold Spring Harb Perspect Biol, 4(1), a011353. https://doi.org/10.1101/cshperspect.a011353

Sudhof, T. C. (2013). A molecular machine for neurotransmitter release: synaptotagmin and beyond. Nat Med, 19(10), 1227-1231. https://doi.org/10.1038/nm.3338

Sudhof, T. C. (2014). The molecular machinery of neurotransmitter release (Nobel lecture). Angew Chem Int Ed Engl, 53(47), 12696-12717. https://doi.org/10.1002/anie.201406359

Südhof, T. C. (2012). The presynaptic active zone. Neuron, 75(1), 11-25. https://doi.org/10.1016/j.neuron.2012.06.012

Südhof, T. C. (2013). Neurotransmitter release: the last millisecond in the life of a synaptic vesicle. Neuron, 80(3), 675-690. https://doi.org/10.1016/j.neuron.2013.10.022

Sudhof, T. C., & Malenka, R. C. (2008). Understanding synapses: past, present, and future. Neuron, 60(3), 469-476. https://doi.org/10.1016/j.neuron.2008.10.011

Sudhof, T. C., & Rizo, J. (2011). Synaptic vesicle exocytosis. Cold Spring Harb Perspect Biol, 3(12). https://doi.org/10.1101/cshperspect.a005637

Sudhof, T. C., & Rothman, J. E. (2009). Membrane fusion: grappling with SNARE and SM proteins. Science, 323(5913), 474-477. https://doi.org/10.1126/science.1161748

Sutton, R. B., Davletov, B. A., Berghuis, A. M., Sudhof, T. C., & Sprang, S. R. (1995). Structure of the first C2 domain of synaptotagmin I: a novel Ca2+/phospholipid-binding fold. Cell, 80(6), 929-938. https://doi.org/10.1016/0092-8674(95)90296-1

Sutton, R. B., Ernst, J. A., & Brunger, A. T. (1999). Crystal structure of the cytosolic C2A-C2B domains of synaptotagmin III. Implications for Ca(+2)-independent snare complex interaction. J Cell Biol, 147(3), 589-598. https://doi.org/10.1083/jcb.147.3.589

Szule, J. A. (2021). Hypothesis Relating the Structure, Biochemistry and Function of Active Zone Material Macromolecules at a Neuromuscular Junction. Front Synaptic Neurosci, 13, 798225. https://doi.org/10.3389/fnsyn.2021.798225

Szule, J. A., & Coorssen, J. R. (2003). Revisiting the role of SNAREs in exocytosis and membrane fusion. Biochim Biophys Acta, 1641(2-3), 121-135. https://doi.org/10.1016/s0167-4889(03)00095-8

Szule, J. A., Harlow, M. L., Jung, J. H., De-Miguel, F. F., Marshall, R. M., & McMahan, U. J. (2012). Regulation of synaptic vesicle docking by different classes of macromolecules in active zone material. PLoS One, 7(3), e33333. https://doi.org/10.1371/journal.pone.0033333

Szule, J. A., Jarvis, S. E., Hibbert, J. E., Spafford, J. D., Braun, J. E., Zamponi, G. W., Wessel, G. M., & Coorssen, J. R. (2003). Calcium-triggered membrane fusion proceeds independently of specific presynaptic proteins. J Biol Chem, 278(27), 24251-24254. https://doi.org/10.1074/jbc.C300197200

Szule, J. A., Jung, J. H., & McMahan, U. J. (2015). The structure and function of 'active zone material' at synapses. Philos Trans R Soc Lond B Biol Sci, 370(1672). https://doi.org/10.1098/rstb.2014.0189

Takahashi, H., Shahin, V., Henderson, R. M., Takeyasu, K., & Edwardson, J. M. (2010). Interaction of Synaptotagmin with Lipid Bilayers, Analyzed by Single-Molecule Force Spectroscopy. Biophysical Journal, 99(8), 2550-2558. https://doi.org/10.1016/j.bpj.2010.08.047

Tamura, T., Hou, J., Reist, N. E., & Kidokoro, Y. (2007). Nerve-evoked synchronous release and high K+ -induced quantal events are regulated separately by synaptotagmin I at *Drosophila* neuromuscular junctions. J Neurophysiol, 97(1), 540-549. https://doi.org/10.1152/jn.00905.2006

Tan, C., de Nola, G., Qiao, C., Imig, C., Born, R. T., Brose, N., & Kaeser, P. S. (2022). Munc13 supports fusogenicity of non-docked vesicles at synapses with disrupted active zones. Elife, 11. https://doi.org/10.7554/eLife.79077

Tan, C., Wang, S. S. H., de Nola, G., & Kaeser, P. S. (2022). Rebuilding essential active zone functions within a synapse. Neuron, 110(9), 1498-1515 e1498. https://doi.org/10.1016/j.neuron.2022.01.026

Tang, X., Xie, C. L., Wang, Y., & Wang, X. C. (2017). Localization of Rab3A-binding site on C2A domain of synaptotagmin I to reveal its regulatory mechanism. International Journal

of Biological Macromolecules, 96, 736-742. https://doi.org/10.1016/j.ijbiomac.2016.12.074

Thomas, D. M., & Elferink, L. A. (1998). Functional analysis of the C2A domain of synaptotagmin 1: Implications for calcium-regulated secretion. Journal of Neuroscience, 18(10), 3511-3520. <Go to ISI>://WOS:000073484300003

Tucker, W. C., & Chapman, E. R. (2002). Role of synaptotagmin in Ca2+-triggered exocytosis. Biochem J, 366(Pt 1), 1-13. https://doi.org/10.1042/bj20020776

Tucker, W. C., Weber, T., & Chapman, E. R. (2004). Reconstitution of Ca2+-regulated membrane fusion by synaptotagmin and SNAREs. Science, 304(5669), 435-438. https://doi.org/10.1126/science.1097196

Ubach, J., Lao, Y., Fernandez, I., Arac, D., Südhof, T. C., & Rizo, J. (2001). The C2B domain of synaptotagmin I is a Ca2+-binding module. Biochemistry, 40(20), 5854-5860. https://doi.org/10.1021/bi010340c

Ullrich, B., Li, C., Zhang, J. Z., McMahon, H., Anderson, R. G., Geppert, M., & Sudhof, T. C. (1994). Functional properties of multiple synaptotagmins in brain. Neuron, 13(6), 1281-1291. https://doi.org/10.1016/0896-6273(94)90415-4

Valli, J., Garcia-Burgos, A., Rooney, L. M., Vale de Melo, E. O. B., Duncan, R. R., & Rickman, C. (2021). Seeing beyond the limit: A guide to choosing the right super-resolution microscopy technique. J Biol Chem, 297(1), 100791. https://doi.org/10.1016/j.jbc.2021.100791

Van Vactor, D., & Sigrist, S. J. (2017). Presynaptic morphogenesis, active zone organization and structural plasticity in *Drosophila*. Curr Opin Neurobiol, 43, 119-129. https://doi.org/10.1016/j.conb.2017.03.003

Vanlandingham, P. A., Barmchi, M. P., Royer, S., Green, R., Bao, H., Reist, N., & Zhang, B. (2014). AP180 couples protein retrieval to clathrin-mediated endocytosis of synaptic vesicles. Traffic, 15(4), 433-450. https://doi.org/10.1111/tra.12153

Vevea, J. D., & Chapman, E. R. (2020). Acute disruption of the synaptic vesicle membrane protein synaptotagmin 1 using knockoff in mouse hippocampal neurons. Elife, 9. https://doi.org/10.7554/eLife.56469

Voglmaier, S. M., Kam, K., Yang, H., Fortin, D. L., Hua, Z. L., Nicoll, R. A., & Edwards, R. H. (2006). Distinct endocytic pathways control the rate and extent of synaptic vesicle protein recycling. Neuron, 51(1), 71-84. https://doi.org/10.1016/j.neuron.2006.05.027

Voleti, R., Tomchick, D. R., Sudhof, T. C., & Rizo, J. (2017). Exceptionally tight membrane-binding may explain the key role of the synaptotagmin-7 C(2)A domain in asynchronous neurotransmitter release. Proc Natl Acad Sci U S A, 114(40), E8518-E8527. https://doi.org/10.1073/pnas.1710708114

von Poser, C., Zhang, J. Z., Mineo, C., Ding, W., Ying, Y., Sudhof, T. C., & Anderson, R. G. (2000). Synaptotagmin regulation of coated pit assembly. J Biol Chem, 275(40), 30916-30924. https://doi.org/10.1074/jbc.M005559200

Vrselja, Z., Daniele, S. G., Silbereis, J., Talpo, F., Morozov, Y. M., Sousa, A. M. M., Tanaka, B. S., Skarica, M., Pletikos, M., Kaur, N., Zhuang, Z. W., Liu, Z., Alkawadri, R., Sinusas, A. J., Latham, S. R., Waxman, S. G., & Sestan, N. (2019). Restoration of brain circulation and cellular functions hours post-mortem. Nature, 568(7752), 336-343. https://doi.org/10.1038/s41586-019-1099-1

Wagner, N. (2017). Ultrastructural comparison of the *Drosophila* larval and adult ventral abdominal neuromuscular junction. J Morphol, 278(7), 987-996. https://doi.org/10.1002/jmor.20692

Walter, A. M., Bohme, M. A., & Sigrist, S. J. (2018). Vesicle release site organization at synaptic active zones. Neurosci Res, 127, 3-13. https://doi.org/10.1016/j.neures.2017.12.006

Wan, W., & Briggs, J. A. (2016). Cryo-Electron Tomography and Subtomogram Averaging. Methods Enzymol, 579, 329-367. https://doi.org/10.1016/bs.mie.2016.04.014

Wang, C. T., Bai, J., Chang, P. Y., Chapman, E. R., & Jackson, M. B. (2006). Synaptotagmin-Ca2+ triggers two sequential steps in regulated exocytosis in rat PC12 cells: fusion pore opening and fusion pore dilation. J Physiol, 570(Pt 2), 295-307. https://doi.org/10.1113/jphysiol.2005.097378

Wang, C. T., Grishanin, R., Earles, C. A., Chang, P. Y., Martin, T. F., Chapman, E. R., & Jackson, M. B. (2001). Synaptotagmin modulation of fusion pore kinetics in regulated exocytosis of dense-core vesicles. Science, 294(5544), 1111-1115. https://doi.org/10.1126/science.1064002

Wang, C. T., Lu, J. C., Bai, J., Chang, P. Y., Martin, T. F., Chapman, E. R., & Jackson, M. B. (2003). Different domains of synaptotagmin control the choice between kiss-and-run and full fusion. Nature, 424(6951), 943-947. https://doi.org/10.1038/nature01857

Wang, J., Li, F., Bello, O. D., Sindelar, C. V., Pincet, F., Krishnakumar, S. S., & Rothman, J. E. (2017). Circular oligomerization is an intrinsic property of synaptotagmin. Elife, 6. https://doi.org/ARTN e27441

10.7554/eLife.27441

Wang, P., Wang, C. T., Bai, J., Jackson, M. B., & Chapman, E. R. (2003). Mutations in the effector binding loops in the C2A and C2B domains of synaptotagmin I disrupt exocytosis in a nonadditive manner. J Biol Chem, 278(47), 47030-47037. https://doi.org/10.1074/jbc.M306728200

Wang, S., & Ma, C. (2022). Neuronal SNARE complex assembly guided by Munc18-1 and Munc13-1. FEBS Open Bio, 12(11), 1939-1957. https://doi.org/10.1002/2211-5463.13394

Wang, X., Gong, J., Zhu, L., Wang, S., Yang, X., Xu, Y., Yang, X., & Ma, C. (2020). Munc13 activates the Munc18-1/syntaxin-1 complex and enables Munc18-1 to prime SNARE assembly. EMBO J, 39(16), e103631. https://doi.org/10.15252/embj.2019103631

Wang, Z., Liu, H., Gu, Y., & Chapman, E. R. (2011). Reconstituted synaptotagmin I mediates vesicle docking, priming, and fusion. J Cell Biol, 195(7), 1159-1170. https://doi.org/10.1083/jcb.201104079

Wang, Z.-W. (2008). <978-1-59745-481-0.pdf>. Humana Press. https://doi.org/10.1007/978-1-59745-481-0

Watanabe, S., & Boucrot, E. (2017). Fast and ultrafast endocytosis. Curr Opin Cell Biol, 47, 64-71. https://doi.org/10.1016/j.ceb.2017.02.013

Watanabe, S., Davis, M. W., Kusick, G. F., Iwasa, J., & Jorgensen, E. M. (2020). SynapsEM: Computer-Assisted Synapse Morphometry. Front Synaptic Neurosci, 12, 584549. https://doi.org/10.3389/fnsyn.2020.584549

Watanabe, S., Liu, Q., Davis, M. W., Hollopeter, G., Thomas, N., Jorgensen, N. B., & Jorgensen, E. M. (2013). Ultrafast endocytosis at Caenorhabditis elegans neuromuscular junctions. Elife, 2, e00723. https://doi.org/10.7554/eLife.00723

Watanabe, S., Rost, B. R., Camacho-Perez, M., Davis, M. W., Sohl-Kielczynski, B., Rosenmund, C., & Jorgensen, E. M. (2013). Ultrafast endocytosis at mouse hippocampal synapses. Nature, 504(7479), 242-247. https://doi.org/10.1038/nature12809

Weber, T., Zemelman, B. V., McNew, J. A., Westermann, B., Gmachl, M., Parlati, F., Sollner, T. H., & Rothman, J. E. (1998). SNAREpins: minimal machinery for membrane fusion. Cell, 92(6), 759-772. https://doi.org/10.1016/s0092-8674(00)81404-x

Wichmann, C., & Sigrist, S. J. (2010). The active zone T-bar--a plasticity module? J Neurogenet, 24(3), 133-145. https://doi.org/10.3109/01677063.2010.489626

Winther, A. M., Vorontsova, O., Rees, K. A., Nareoja, T., Sopova, E., Jiao, W., & Shupliakov, O. (2015). An Endocytic Scaffolding Protein together with Synapsin Regulates Synaptic Vesicle Clustering in the *Drosophila* Neuromuscular Junction. J Neurosci, 35(44), 14756-14770. https://doi.org/10.1523/JNEUROSCI.1675-15.2015

Wolfes, A. C., & Dean, C. (2020). The diversity of synaptotagmin isoforms. Curr Opin Neurobiol, 63, 198-209. https://doi.org/10.1016/j.conb.2020.04.006

Wu, B., Wei, S., Petersen, N., Ali, Y., Wang, X., Bacaj, T., Rorsman, P., Hong, W., Sudhof, T. C., & Han, W. (2015). Synaptotagmin-7 phosphorylation mediates GLP-1-dependent potentiation of insulin secretion from beta-cells. Proc Natl Acad Sci U S A, 112(32), 9996-10001. https://doi.org/10.1073/pnas.1513004112

Wu, D., Bacaj, T., Morishita, W., Goswami, D., Arendt, K. L., Xu, W., Chen, L., Malenka, R. C., & Sudhof, T. C. (2017). Postsynaptic synaptotagmins mediate AMPA receptor exocytosis during LTP. Nature, 544(7650), 316-321. https://doi.org/10.1038/nature21720

Wu, Y., Gu, Y., Morphew, M. K., Yao, J., Yeh, F. L., Dong, M., & Chapman, E. R. (2012). All three components of the neuronal SNARE complex contribute to secretory vesicle docking. J Cell Biol, 198(3), 323-330. https://doi.org/10.1083/jcb.201106158

Wu, Y., He, Y., Bai, J., Ji, S. R., Tucker, W. C., Chapman, E. R., & Sui, S. F. (2003). Visualization of synaptotagmin I oligomers assembled onto lipid monolayers. Proc Natl Acad Sci U S A, 100(4), 2082-2087. https://doi.org/10.1073/pnas.0435872100

Wu, Z., Ma, L., Courtney, N. A., Zhu, J., Landajuela, A., Zhang, Y., Chapman, E. R., & Karatekin, E. (2022). Polybasic Patches in Both C2 Domains of Synaptotagmin-1 Are Required for Evoked Neurotransmitter Release. J Neurosci, 42(30), 5816-5829. https://doi.org/10.1523/JNEUROSCI.1385-21.2022

Xie, C., Li, J., Guo, T., Yan, Y., Tang, C., Wang, Y., Chen, P., Wang, X., & Liang, S. (2014). Rab3A is a new interacting partner of synaptotagmin I and may modulate synaptic membrane fusion through a competitive mechanism. Biochem Biophys Res Commun, 444(4), 491-495. https://doi.org/10.1016/j.bbrc.2014.01.090

Xu, J., Bacaj, T., Zhou, A., Tomchick, D. R., Sudhof, T. C., & Rizo, J. (2014). Structure and Ca(2)(+)-binding properties of the tandem C(2) domains of E-Syt2. Structure, 22(2), 269-280. https://doi.org/10.1016/j.str.2013.11.011

Xu, J., Pang, Z. P., Shin, O. H., & Sudhof, T. C. (2009). Synaptotagmin-1 functions as a Ca2+ sensor for spontaneous release. Nat Neurosci, 12(6), 759-766. https://doi.org/10.1038/nn.2320

Xu, W., Morishita, W., Buckmaster, P. S., Pang, Z. P., Malenka, R. C., & Sudhof, T. C. (2012). Distinct neuronal coding schemes in memory revealed by selective erasure of fast

synchronous synaptic transmission. Neuron, 73(5), 990-1001. https://doi.org/10.1016/j.neuron.2011.12.036

Xue, M., Craig, T. K., Shin, O. H., Li, L., Brautigam, C. A., Tomchick, D. R., Sudhof, T. C., Rosenmund, C., & Rizo, J. (2010). Structural and mutational analysis of functional differentiation between synaptotagmins-1 and -7. PLoS One, 5(9). https://doi.org/10.1371/journal.pone.0012544

Xue, R., Ruhl, D. A., Briguglio, J. S., Figueroa, A. G., Pearce, R. A., & Chapman, E. R. (2018). Doc2-mediated superpriming supports synaptic augmentation. Proc Natl Acad Sci U S A, 115(24), E5605-e5613. https://doi.org/10.1073/pnas.1802104115

Yakoubi, R., Rollenhagen, A., von Lehe, M., Shao, Y., Sätzler, K., & Lübke, J. H. R. (2019). Quantitative Three-Dimensional Reconstructions of Excitatory Synaptic Boutons in Layer 5 of the Adult Human Temporal Lobe Neocortex: A Fine-Scale Electron Microscopic Analysis. Cereb Cortex, 29(7), 2797-2814. https://doi.org/10.1093/cercor/bhy146

Yang, S. N., Shi, Y., Yang, G., Li, Y., Yu, L., Shin, O. H., Bacaj, T., Sudhof, T. C., Yu, J., & Berggren, P. O. (2012). Inositol hexakisphosphate suppresses excitatory neurotransmission via synaptotagmin-1 C2B domain in the hippocampal neuron. Proc Natl Acad Sci U S A, 109(30), 12183-12188. https://doi.org/10.1073/pnas.1115070109

Yang, X., Cao, P., & Sudhof, T. C. (2013). Deconstructing complexin function in activating and clamping Ca2+-triggered exocytosis by comparing knockout and knockdown phenotypes. Proc Natl Acad Sci U S A, 110(51), 20777-20782. https://doi.org/10.1073/pnas.1321367110

Yang, X., Kaeser-Woo, Y. J., Pang, Z. P., Xu, W., & Sudhof, T. C. (2010). Complexin clamps asynchronous release by blocking a secondary Ca(2+) sensor via its accessory alpha helix. Neuron, 68(5), 907-920. https://doi.org/10.1016/j.neuron.2010.11.001

Yang, X., Pei, J., Kaeser-Woo, Y. J., Bacaj, T., Grishin, N. V., & Sudhof, T. C. (2015). Evolutionary conservation of complexins: from choanoflagellates to mice. EMBO Rep, 16(10), 1308-1317. https://doi.org/10.15252/embr.201540305

Yao, J., Kwon, S. E., Gaffaney, J. D., Dunning, F. M., & Chapman, E. R. (2011). Uncoupling the roles of synaptotagmin I during endo- and exocytosis of synaptic vesicles. Nat Neurosci, 15(2), 243-249. https://doi.org/10.1038/nn.3013

Yao, K. M., & White, K. (1994). Neural specificity of elav expression: defining a *Drosophila* promoter for directing expression to the nervous system. J Neurochem, 63(1), 41-51. https://doi.org/10.1046/j.1471-4159.1994.63010041.x

Yaradanakul, A., Wang, T. M., Lariccia, V., Lin, M. J., Shen, C., Liu, X. R., & Hilgemann, D. W. (2008). Massive Ca-induced membrane fusion and phospholipid changes triggered by reverse Na/Ca exchange in BHK fibroblasts. Journal of General Physiology, 132(1), 29-50. https://doi.org/10.1085/jgp.200709865

Yoshihara, M., Adolfsen, B., & Littleton, J. T. (2003). Is synaptotagmin the calcium sensor? Curr Opin Neurobiol, 13(3), 315-323. https://doi.org/10.1016/s0959-4388(03)00063-1

Yoshihara, M., & Littleton, J. T. (2002). Synaptotagmin I functions as a calcium sensor to synchronize neurotransmitter release. Neuron, 36(5), 897-908. https://doi.org/10.1016/s0896-6273(02)01065-6

Zamorano, P. L., & Garner, C. C. (2001). Unwebbing the presynaptic web. Neuron, 32(1), 3-6. https://doi.org/10.1016/s0896-6273(01)00458-5

Zanazzi, G., & Matthews, G. (2009). The molecular architecture of ribbon presynaptic terminals. Mol Neurobiol, 39(2), 130-148. https://doi.org/10.1007/s12035-009-8058-z

Zarebidaki, F., Camacho, M., Brockmann, M. M., Trimbuch, T., Herman, M. A., & Rosenmund, C. (2020). Disentangling the Roles of RIM and Munc13 in Synaptic Vesicle Localization and Neurotransmission. J Neurosci, 40(49), 9372-9385. https://doi.org/10.1523/JNEUROSCI.1922-20.2020

Zhai, R. G., & Bellen, H. J. (2004). The architecture of the active zone in the presynaptic nerve terminal. Physiology (Bethesda), 19, 262-270. https://doi.org/10.1152/physiol.00014.2004

Zhan, H., Bruckner, J., Zhang, Z., & O'Connor-Giles, K. (2016). Three-dimensional imaging of *Drosophila* motor synapses reveals ultrastructural organizational patterns. J Neurogenet, 30(3-4), 237-246. https://doi.org/10.1080/01677063.2016.1253693

Zhang, B. S., B. (2010). <Zhang, Bing. Electrophysiological recording from *Drosophila* larval body-wall muscles.pdf>. Cold Spring Harbor Protocols. https://doi.org/10/1101/pdb.prot5487

Zhang, J. Z., Davletov, B. A., Sudhof, T. C., & Anderson, R. G. (1994). Synaptotagmin I is a high affinity receptor for clathrin AP-2: implications for membrane recycling. Cell, 78(5), 751-760. https://doi.org/10.1016/s0092-8674(94)90442-1

Zhang, Q. L., Y.; Tsien R. (2009). The Dynamic Control of Kiss-And-Run and Vesicular Reuse Probed with Single Nanoparticles. https://doi.org/10.1126/science.1167373

Zhang, Y., Ma, L., & Bao, H. (2022). Energetics, kinetics, and pathways of SNARE assembly in membrane fusion. Crit Rev Biochem Mol Biol, 57(4), 443-460. https://doi.org/10.1080/10409238.2022.2121804

Zhang, Z., Hui, E., Chapman, E. R., & Jackson, M. B. (2009). Phosphatidylserine regulation of Ca2+-triggered exocytosis and fusion pores in PC12 cells. Mol Biol Cell, 20(24), 5086-5095. https://doi.org/10.1091/mbc.e09-08-0691

Zhang, Z., Hui, E., Chapman, E. R., & Jackson, M. B. (2010). Regulation of exocytosis and fusion pores by synaptotagmin-effector interactions. Mol Biol Cell, 21(16), 2821-2831. https://doi.org/10.1091/mbc.E10-04-0285

Zhang, Z., Wu, Y., Wang, Z., Dunning, F. M., Rehfuss, J., Ramanan, D., Chapman, E. R., & Jackson, M. B. (2011). Release mode of large and small dense-core vesicles specified by different synaptotagmin isoforms in PC12 cells. Mol Biol Cell, 22(13), 2324-2336. https://doi.org/10.1091/mbc.E11-02-0159

Zhou, K., Stawicki, T. M., Goncharov, A., & Jin, Y. (2013). Position of UNC-13 in the active zone regulates synaptic vesicle release probability and release kinetics. Elife, 2, e01180. https://doi.org/10.7554/eLife.01180

Zhou, M., Melin, M. D., Xu, W., & Sudhof, T. C. (2020). Dysfunction of parvalbumin neurons in the cerebellar nuclei produces an action tremor. J Clin Invest, 130(10), 5142-5156. https://doi.org/10.1172/JCI135802

Zhou, Q., Lai, Y., Bacaj, T., Zhao, M., Lyubimov, A. Y., Uervirojnangkoorn, M., Zeldin, O. B., Brewster, A. S., Sauter, N. K., Cohen, A. E., Soltis, S. M., Alonso-Mori, R., Chollet, M., Lemke, H. T., Pfuetzner, R. A., Choi, U. B., Weis, W. I., Diao, J., Sudhof, T. C., & Brunger, A. T. (2015). Architecture of the synaptotagmin-SNARE machinery for neuronal exocytosis. Nature, 525(7567), 62-67. https://doi.org/10.1038/nature14975

Zhou, Q., Zhou, P., Wang, A. L., Wu, D., Zhao, M., Sudhof, T. C., & Brunger, A. T. (2017). The primed SNARE-complexin-synaptotagmin complex for neuronal exocytosis. Nature, 548(7668), 420-425. https://doi.org/10.1038/nature23484

Zhu, J., McDargh, Z. A., Li, F., Krishnakumar, S. S., Rothman, J. E., & O'Shaughnessy, B. (2022). Synaptotagmin rings as high-sensitivity regulators of synaptic vesicle docking and fusion. Proc Natl Acad Sci U S A, 119(38), e2208337119. https://doi.org/10.1073/pnas.2208337119

Zurawski, Z., Page, B., Chicka, M. C., Brindley, R. L., Wells, C. A., Preininger, A. M., Hyde, K., Gilbert, J. A., Cruz-Rodriguez, O., Currie, K. P. M., Chapman, E. R., Alford, S., & Hamm, H. E. (2017). Gβγ directly modulates vesicle fusion by competing with synaptotagmin for binding to neuronal SNARE proteins embedded in membranes. J Biol Chem, 292(29), 12165-12177. https://doi.org/10.1074/jbc.M116.773523

APPENDICES

APPENDIX A: SUPPLEMENTAL-1

PREPARATION OF *DROSOPHILA* L3 LARVAE FOR ELECTRON MICROSCOPY

Overview

The use of electron microscopy tomography and the model system *Drosophila melanogaster* represents a combination of tools with the potential to open a whole new field of structural identification of macromolecular structures critical for intercellular communication. Herein, we provide a suitable protocol for *Drosophila melanogaster* larval sample preparation for imaging neuromuscular junctions using electron microscopy tomography.

Materials and Methods

Lab Safety and MSDS

All fixation, dehydration, and embedding steps within this protocol should be performed in a fume hood wearing appropriate personal protective equipment (PPE). Chemicals used within this protocol are dangerous. In addition to a chemical fume hood, steps of this protocol require a chemical refrigerator (4 °C) and oven (60 °C). The Material Safety and Data Sheet (MSDS) for each chemical should be read prior to use.

Recipes

HL3 (Ca^{2+} Free):
5mM KCl, 70mM NaCl, 20mM $MgCl_2$, 10mM $NaHCO_3$, 5mM HEPES acid (dry), 115 mM Sucrose, 5mM Trehalose – add to nanopure and adjust pH to 7.2 as needed.

Making PEI Coated Grids

PEI support films are stronger and exhibit less beam damage from the electron microscope than traditional Formvar grids. They also don not wrinkle as much when exposed to water. Best of all, prepared films can be stripped off of glass slides up to several weeks after casting, unlike Formvar films that stick irreversibly after a couple of days.

1. Make a PEI solution with a concentration of 0.28% (w/w) **polyetherimide (PEI)** in approximately 500ml **ethylene dichloride (1,2-dichloroethane)**.

   Note: Let the solution stand for at least 24 hours to dissolve – the longer the solution sits, the better the results. “Fresh” PEI solution still contains long strands of undissolved polymer which do not form consistent thin films; overnight is adequate.

2. Plug the internal bottom of the syringe with a small piece of **Kimwipe** and then fill syringe with **molecular sieve** to about the 45ml level. Assemble a **60ml straight tip**

syringe onto a **47mm Swinnex filter holder** containing a **0.22 micron** Millipore **type G5 filter**.

3. Using a stand, place the assembly above a **Coplin Slide Staining Jar** and pour the PEI/ethylene dichloride solution into the syringe, allowing the solution to pass through the molecular sieve, through the Swinnex 0.22-micron filter and into the Coplin Jar to a level just above the slide ridges within the jar.

   Note: The kimwipe collects any dust particulates from the solution. The molecular sieve removes any residual water in the ethylene dichloride solution, and the Millipore filter removes any dust from the molecular sieve. The filter may clog depending on how much of the solution you filter through it. If you notice the solution if no longer filtering, you may have to change Millipore filter.

4. Cap the Coplin Jar containing the filtered PEI solution and place inside a cabinet style desiccator containing fresh desiccant to remove any residual atmospheric moisture.

5. With a kimwipe, wipe clean five [5] **Gold Seal 3010 microscope slides** (only) and place them in a slide grip.

   Note: Wiping microscope slides helps remove oil residue from glass slides.

6. Within the desiccator, dip the slides in the Coplin Jar containing the PEI solution so that solution covers about two-thirds [2/3] of the slides.

7. Remove slides slowly from the Coplin Jar to get an even coat of PEI. Place the whole ends of all five slides on a stack of 4 or 5 large filter papers within the desiccator. This wicks away excess solution and creates a more even film thickness throughout the slide length.

8. Let the slides dry in a desiccator overnight.

   Note: This is critical because if the PEI film is stripped off of the slides too soon, pinholes will form on the still-wet films.

9. Fill a 50 slide Thomas Staining Dish (or similar) with nanopure water to use for the following steps.

10. When the PEI films are dry, score three edges (one end and two longer sides) of the microscope slide with the edge of a razor blade.

    Note: This breaks the continuous PEI film from the edges so it can be stripped off of the microscope slide.

11. Place the microscope slide at about a 30° angle toward a water surface of the Thomas Staining Dish and slowly start submerging the slide while trying to maintain a 30° angle. The film should float from the microscope slide onto the water surface.

12. When the film floats free off the microscope slide, set the slide aside by placing on end.

    Note: **Remember which side of the microscope slide has the remaining film**. This is critical as you will use the remaining film from the other side of the microscope slide to later pick up the film which is now floating.

13. On the floating film, gently place suitable slot grids shiny side down (or notch side up) in a rectangular pattern on the film (4 by 8 grids is usually about right). The thicker, 1 mm x 2 mm slot grids are ideal. For example, EM Sciences Synaptek 2 mm x1 mm notch grids.

    Note: Due to light refracting off of the surface of the water and the PEI film, you'll be able to see the imperfections of the film while it's floating. Be cautious to avoid the imperfections as well as edges that are often distorted or thicker.

14. When the floating film is filled with grids, pick up the film and grids with the microscope slide that you set aside in Step 12 above. With the side of the microscope slide with the PEI coat still intact, touch the edge of the floating film containing the grids at about a 30° angle and push the microscope slide into the water, allowing the film containing grids to stick to the slide.

    Note: Submerge microscope slide quickly to prevent film from wrinkling and grids from accidentally covering each other.

15. Remove the slide from the water and let the microscope slide now containing the PEI coated grids dry, on fresh filter paper, for about 1 hr. Place the slides in another Coplin Jar or face up in a glass petri dish for storage.

    Note: For best film adhesion, put the microscope slide containing grids in the oven for several hours or overnight at 60–70 °C.

16. The PEI coated grids are easily removed from the glass microscope slide just by pushing on them slightly with the point of forceps. This slight pressure will break the film along the outer edges of the grid and free the grid from the slide.

    Note: Move the grid to the edge of the slide to make it easier to grasp the grid with your forceps.

Larvae Dissection and Fixation

1. In ice-cold, Ca^{2+}-free HL3 saline (Stewart et al., 1994) dissect open an L3 larva so that neuromuscular junctions and CNS are well exposed.

2. Immediately after the larva is dissected, draw off the HL3 and pipet ice-cold primary fixative onto the larval fillet. Fix for 60 min at room temperature (RT) in a humidity chamber. Work the fixative in when initially applied, and twice more over the hour of fixation. **Primary fixative: 2.5% glutaraldehyde + 1% acrolein in 0.1M sodium cacodylate buffer (pH 7.2).**

   Notes:
   - A "humidity chamber" is an air-tight container with moist kimwipes on the bottom. This set-up helps prevent the fixatives and sample from drying out in dry climates.
   - To work in fixative, gently puff the primary fix directly onto the sample using a fine pipet tip. Take care to avoid creating bubbles.

3. After 1 hr of fixation, remove primary fixative, and flood the dish with Ca^{2+}-free HL3.

   Note: If dissecting more than one larva, leave the larvae, post-fixative, in Ca^{2+}-free HL3 until all have been dissected and fixed.

4. Wash larva two additional times, in Ca^{2+}-free HL3 for 10 min each wash.

5. Immediately after washing, draw off the HL3, and pipet secondary fixative onto the larval fillet. Fix for 60min at RT in a humidity chamber. Work the fixative in when initially applied, and twice more over the hour of fixation. **Secondary fixative: 0.5% OsO4 + 0.8% KFeCN in 0.1 M sodium cacodylate buffer (pH 7.2)**.

6. Rinse three times with nanopure water, then wash twice in nanopure water for 10 min each.

7. Immediately after washing, draw off the nanopure and incubate in **2-5% uranyl acetate (UA) in nanopure**. Incubate for 1 hr to overnight at 4 °C.

   Note: If larva will be in UA overnight (or any time significantly longer than 1 hour), the dish should be set in a humidity chamber. UA is light sensitive. Thus, the chamber should be wrapped in foil and stored in a dark place to prevent precipitate from forming due to UV light exposure.

8. Draw off the UA and wash three times in nanopure for 10 min each.

Sample Dehydration and Resin Infiltration

9. Remove the nanopure from the samples.

10. Dehydrate the samples in **Ethanol at increasing concentrations (25%, 50%, 75%, 95% and 100%)** with 3 washes of each concentration. Let last wash at each concentration stand for 3 min at room temperature.

11. Carefully remove the samples from the dish and transfer them into individual vials containing **100% Ethanol**. Change 100% Ethanol twice, then let sit in **100% Ethanol** for 30 min at room temperature.

12. Exchange 100% Ethanol for **propylene oxide (PO)**.

13. Use your epoxy resin of choice, we use **EMbed 812** (Electron Microscopy Sciences). To each vial, add an amount of **epoxy resin** approximately equal to the amount of PO already in the vial **(50:50 PO:resin).** Swirl to mix, and then leave on rotator at room temperature for at least 1 hr.

14. Remove the **50:50 PO:resin** and replace with **100% resin**. Leave samples on rotator overnight at room temperature.

Resin Polymerization – Flat Embedding of Samples

15. Transfer 2-3 larva onto a glass microscope slide with frosted side down (away from specimen and resin).

    Notes: Spray non-stick coating to glass slides in advance. It is best to do this step and the following steps on an oven safe tray or dish that is coated in non-stick spray, **TFE Release Agent Dry Lubricant (Miller-stephenson, MS-122N/CO2).** To help minimize damage to the samples during transfer, place a few drops of resin on the microscope slide first. Then transfer the larva onto the drops of resin, using forceps.

16. Place a piece of paper with identifying information for the larva on one end of the microscope slide. Be sure not to place too close to or cover the larva.

    Note: It is best to use pencil to mark the paper. If pen/marker is used, the ink could smear within the resin.

17. Add additional resin on top of the larva to form a thin layer of resin on the microscope slide.

18. Place a piece of **ACLAR embedding film** (e.g., Ted Pella, Inc.) on top of the microscope slide containing the larva in resin.

19. Gently place a second salinized microscope slide on top of the ACLAR film to help keep the larva flat.

20. Polymerize samples in resin overnight at 60 °C.

21. After samples are polymerized, you should be able to remove flat-embedded larva from the microscope slide.

Ultrathin Sectioning

22. Cut the resin-embedded sample out of the flat-embedded setup and mount onto an electron microscopy resin block using more resin.

23. Polymerize for at least 1 hour at 60°C.

    Note: Let the sample containing block to cool before proceeding with Ultrathin Sectioning.

24. Using a double edge razor blade, manually trim all four edges of the tissue block to create a front face that is a trapezoid shape and contains your region of interest.

    Note: After an initial, rough trim, we recommend using a new razor blade to make a more precise trim. This helps prevent: **1**. The tissue block from potentially popping off the chuck, and **2.** A dull razor can introduce metal shavings and unwanted scoring of the block.

25. Transfer the block containing the resin-embedded tissue into an ultramicrotome chuck and secure in place. Trim the front face of the tissue block using a suitable diamond knife, for example a **Diatome 45 degree angle diamond knife** at 6° feed (thickness at 1 μm). Trim until a full, glass-like face has been obtained.

    Notes: It is especially crucial to be able to see your region of interest in case additional trimming is needed.

26. Get to region of interest by the following steps:

    a. Cut 500 nm to 1 μm section(s) at 1mm/sec using a suitable 45° glass knife, at 4° feed, containing a boat filled with filtered nanopure water.

    b. Retrieve section(s) from edge of diamond knife by using an eyelash or dog hair mounted onto a wooden stick.

    c. Collect section(s) from water surface using a **Perfect Loop**.

    d. Transfer section(s) onto a glass microscope slide and then place onto a hot plate to dry.

    e. After water droplet has dried and the plastic section(s) have baked onto the microscope slide, stain section(s) with **Toluidine Blue solution** for 10-30 seconds on hot plate.

       Note: Toluidine Blue stains proteins and nucleic acids, which enables the visualization of structural detail within tissue sections. You do not want Toluidine Blue to completely dry and bake on sections but need to stain long enough to visualize tissue. You may have to adjust staining timeframe depending on the

temperature setting of your hot plate.

f. Remove microscope slide from hot plate and rinse excess Toluidine Blue Stain from slide.

g. Observe sections under a light microscope and assess for region of Interest. If region of interest has not been obtained, repeat steps 26a-g.

27. Once region of interest is located, cut 70nm silver-colored thin sections at 1mm/sec using an ultramicrotome using a diamond knife. Adjust the water level in the knife boat such that the sections float away from the knife edge on the water surface.

    Note: To remove any wrinkles from the sections, it is helpful to spread the plastic sections by waving a heat pen over the boat.

28. Pick up sections on PEI coated slot notch grids using an eyelash or dog hair mounted onto a wooden stick to maneuver the section into place.

29. Place grids in an electron microscope grid holder and set aside to dry.

30. Once dry, grids are ready for post-staining.

    Note: Cutting speeds in this protocol may need to be adjusted depending on the model of ultramicrotome used and the hardness of the resin polymer.

Post-staining Ultrathin Sections

The following steps are to enhance contrast of tissue within plastic embedded thin sections through the application of heavy metals to lipids, proteins, and glycogens.

31. Place a sheet of parafilm on the inside of each of two clean, glass petri dish.

32. In one dish, add 200 μl drops of **2% UA in CO_2 free nanopure** to the parafilm. Add enough drops for the number of grids you intend to post-stain.

    Note: Uranyl Acetate enhances the contrast of tissue embedded in sections by interacting with the proteins and lipid within the tissue. This helps with visualization of the tissue under the electron microscope. UA is light sensitive. Its staining dish should be wrapped in foil and stored in a dark place to prevent precipitate from forming due to UV light exposure.

33. Stain sections by gently placing grids, section side down, onto droplets of 2% UA for 3 min.

34. Remove grids from UA droplets and rinse in CO_2 free nanopure 3 times for 90 s each.

Note: We used 3 separate Wheaton vials containing CO_2 free nanopure for each 90 s rinse. The grids were dunked into each vial such that by breaking the surface tension of the water any debris or precipitates would be forces off of the grid.

35. In the second parafilm coated petri dish, add 200 μl drops of **Lead Citrate** to the parafilm. Add enough drops for the number of grids you intend to post-stain.

    Note: Lead Citrate enhances the contrast of tissue embedded in sections by interacting with proteins and glycogens within the tissue. This helps with visualization of the tissue under the electron microscope. Lead Citrate is also reactive to Carbon Dioxide and will form lead carbonate precipitates if exposed to CO2. Preventative measures can be taken by adding Sodium Hydroxide pellets to the edge of the petri dish.

36. Stain sections by gently placing grids, section side down, onto droplets of 2% UA for 3 min.

37. Remove grids from Lead Citrate droplets and rinse, as above, in CO_2 free nanopure 3 times for 90 s each.

38. 5 or 10 nm gold colloid beads should then be added to the grids using the droplet method as described in Steps 32–33 and 35–36 above.

39. Gently remove grids from droplets of gold colloid.

40. Place grids in an electron microscope grid holder and set aside to dry for a few hours.

41. Once dry, post-stained grids are ready for high resolution imaging using a transmission electron microscope.

    Note: to make CO_2 free nanopure, autoclave nanopure and close lid on container immediately after removing from autoclave.

APPENDIX B: SUPPLEMENTAL-2
MACROS USED IN FIJI AND MICROSOFT EXCEL

The scripts for the macros used in FIJI, to measure membrane thicknesses and synaptic vesicle contact areas, and the macro used in Microsoft Excel to combine measurement Excel files can be found at Zenodo using the DOI: 10.5281/zenodo.10065345

APPENDIX C: SUPPLEMENTAL-3

SPLINE-FITTING MACRO FOR MATHEMETICA

The script for the mathematica macro to create a spline fitting for synaptic vesicle contact areas can be found at Zenodo using the DOI: 10.5281/zenodo.10038700

APPENDIX D: SUPPLEMENTAL-4

HIGH-RESOLUTION ELECTRON TOMOGRAMS OF ACTIVE ZONES AT DROSOPHILA NEUROMUSCULAR JUNCTIONS

Electron Tomographic datasets collected, as described in Chapter 3, can be found at the open data publishing platform Dryad using the DOI: 10.5061/dryad.3xsj3txns